Carbon Fibre Reinforced Polymer Shear Strengthening of Prestressed Concrete I-Girders

By

Rico Joey Massa

August 2018

Department of Civil Engineering & Applied Mechanics

McGill University, Montréal

A thesis submitted to McGill University in partial fulfillment of the requirements of the degree of Master of Engineering

Abstract

Shear resistance deficiencies can arise after the construction of concrete members due to many causes including deterioration, load increases and severe damage. When replacement of these members is undesirable or cost-prohibitive, strengthening and rehabilitation is necessary. One technique which can be used for this purpose is the application of externally bonded fibre reinforced polymers (FRP). This is often used on prestressed concrete I-girders, but few experimental studies have been conducted to understand the behaviour of FRP shear strengthening on these types of members.

This thesis presents the results of beam tests conducted on full-scale precast pretensioned I-girders to study the influence on the shear response of carbon fibre reinforced polymer (CFRP) shear strips. The test program demonstrated that the CFRP strengthening was effective in increasing the shear strength of the webs and in controlling the shear crack widths. The shape of the I-girders makes it difficult to properly anchor the vertical shear strips to prevent debonding which often results in extremely brittle failures. Curved epoxy transitions between the web and the flanges at the re-entrant corners, together with the use of horizontal CFRP strips helped to improve the anchorage of the vertical shear strips. The shear resistance components from the concrete, stirrups and CFRP shear strips were determined experimentally and compared with analytical predictions. The design approach of the 2014 Canadian Highway Bridge Design Code provides conservative estimates of the shear strength of the webs.

Résumé

Des défauts de résistance au cisaillement peuvent se manifester dans des éléments en béton armé à cause de nombreuses raisons, notamment la détérioration, l'augmentation des charges et des dommages graves. Lorsque le remplacement de ces membres est indésirable ou trop coûteux, il devient nécessaire de les renforcer. Une technique de renforcement qui peut être utilisée est l'application d'un système de polymères renforcés de fibres (PRF) encollé sur la surface de ces éléments. Ceci est souvent utilisé sur les poutres en béton précontraint, mais peu d'études expérimentales ont été menées pour comprendre le comportement du renforcement du cisaillement en PRF sur ces types de membres.

Cette mémoire présente les résultats des essais sur des poutres en béton précontraint dans le but d'analyser l'influence des bandes en polymère renforcé de fibres de carbone (PRFC) sur la réponse en cisaillement. Le programme expérimental a démontré que le renforcement en PRFC augmente la résistance au cisaillement des âmes et limite la largeur des fissures de cisaillement. La forme des poutres en *I* empêche l'ancrage solide les bandes de cisaillement verticales et mène à des ruptures extrêmement fragiles. Les transitions d'époxy incurvées aux angles rentrants, combinée avec des bandes de PRFC horizontales, ont amélioré l'ancrage des bandes de cisaillement verticales. Les composantes de résistance au cisaillement du béton, des étriers et des bandes de cisaillement en PRFC ont été déterminées expérimentalement et comparées aux prédictions analytiques. L'approche de conception du « Code canadien sur le calcul des ponts routiers » fournit des estimations prudentes pour la résistance au cisaillement des âmes.

Acknowledgements

The author would like to express his deepest gratitude to Professor Denis Mitchell for his guidance and support throughout this entire process. Great thanks are also reserved for Dr. William Cook, without whom all work within the walls of the Jamieson Structures Laboratory would surely screech to a halt.

Ryan Tack provided valuable assistance during all aspects of the construction and testing of the girders, risking life and appendage in the pursuit of knowledge. The help provided by John Bartczak, Albert Charukhchyan and Omar El Shemy was also invaluable. Besides being a great friend, David Pizzuto was a sounding board during the writing process and provided excellent feedback without making me feel overly dull.

The author also thanks MAPEI Inc. and Hamza Ouziame, M.Ing. for providing the CFRP and other required materials as well as training in the application of the CFRP. The author is grateful to the Centre for Innovation in Infrastructure (CII) and the Jacques Cartier and Champlain Bridges Inc. (JCCBI) for funding the experimental research program. The valuable technical discussions with engineers from CII, PJJCI, MAPEI Inc. and EGP Experts-Conseil en Structures are also acknowledged.

Lastly, the author would like to thank his parents, Giuseppina and Lorenzo, his sister, Lisa and of course, his wonderful girlfriend Elleni who provided the bedrock upon which all his work is founded.

Table of Contents

List of Figures

List of Tables

1 Introduction and Literature Review

1.1 Introduction

The 2016 Canadian Infrastructure Report Card (CIRC, 2016) reports that 26 % of the nation’s bridges are in a condition that requires attention. This includes assets rated to been in fair, poor and very poor condition that have a cumulative replacement value of CAD 13 billion. This replacement cost is prohibitive for many municipalities and the target reinvestment rate required to maintain the aging infrastructure is not being met. A more economically realistic solution over demolition and replacement is to repair and strengthen the bridges for which a call to action is necessary. One technique that can be used for the rehabilitation of bridge infrastructure is the use of fibre reinforced polymer (FRP) composites.

The last two decades has seen an increase in the use of FRP in structural applications. FRP composites can be used to replace traditional steel reinforcement in new concrete structures or in externally bonded applications for the strengthening of existing structures. Externally bonded fibre reinforced polymer is becoming an increasingly popular method to repair and rehabilitate structurally deficient members. In this capacity, FRP has the advantage of having high strength-to-weight and stiffness-to-weight ratios, excellent corrosion resistance, versatility of available geometries and ease of installation. One use of externally-bonded FRP is in the shear strengthening of precast pretensioned bridge I-girders. This is carried out mainly in response to corrosion of the shear reinforcing steel or to increase the shear capacity of the girder to account for a planned increase in the load applied to the girder. A typical method to achieve an increase in shear capacity of an I-girder is to epoxy vertically-oriented FRP strips to the web.

1.2 FRP Composites

1.2.1 Background

FRP is a composite material consisting of fibres imbedded in a polymer matrix. The fibres provide strength and stiffness to the material and are typically made of carbon (CFRP), glass (GFRP) or aramid (AFRP). The polymer matrix serves to protect the fibres, fix their position and provide stress transfer between individual fibres. Resins can be thermoset or thermoplastic and common polymeric resin types include epoxies, vinyl esters and polyesters (ACI 440.R-07, 2007).

FRP composites for structural applications are available in various shapes including bars and plates as well as in fabric form for use in externally bonded applications. In new construction, the FRP reinforcing bars used are generally fabricated using the pultrusion process. In this process, as illustrated in Figure 1.1, the fibres are drawn through a resin bath to be impregnated with resin before passing over a heated die to be cured in the desired shape. The reinforcing bars thus formed can be used in new construction or to reinforce existing structures in a technique called near surface mounting. FRP intended for use in externally bonded applications can be procured in sheet form for hand-layup or as precured laminated bars if the end use does not require a conformable product. FRP sheets are available in various fibre orientations depending on the application. Unidirectional sheets are assumed to be able to carry load only in their principal fibre direction whereas multidirectional sheets can resist loads from multiple directions depending on the orientation of their constitutive plies.

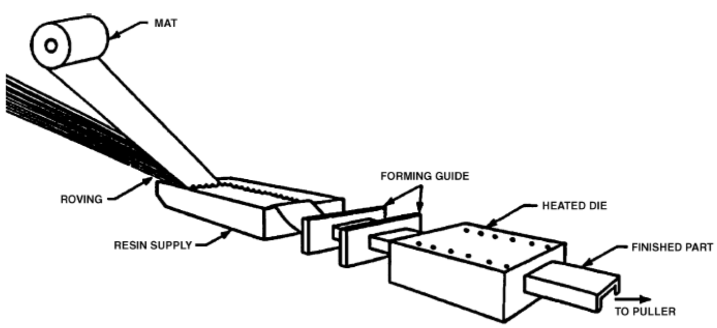

Figure 1.1: Pultrusion process (ACI 440.R-07, 2007)

1.2.2 Material Properties

FRP composites general exhibit a linear elastic stress-strain response in tension. This is indicative of a brittle failure mode and is a disadvantage of FRP when compared to the ductile, yielding response of steel. Hybrid FRP products typically combine carbon fibre with aramid or glass in order to obtain the strength and stiffness of carbon and the greater flexibility of glass or aramid. The resulting hybrid FRP exhibits a stress-strain curve similar to that of steel with a portion resembling steel plastic deformation. Figure 1.2 shows typical stress-strain curves for FRP products as presented in the ACI 440.R-07 (2007). It is difficult to compare mechanical properties among the different FRP manufacturers and their products. Even if the same fibres are used, each manufacturer has their own proprietary manufacturing technique and polymer matrix. For the sake of comparison, Table 1.1 shows the typical material properties for FRP laminates compared to reinforcing steel and is derived from the ACI 440.2R-08 (2008). It should be noted that due to debonding and localized stress concentrations, FRP composites often fail to reach their full rupture stress upon failure.

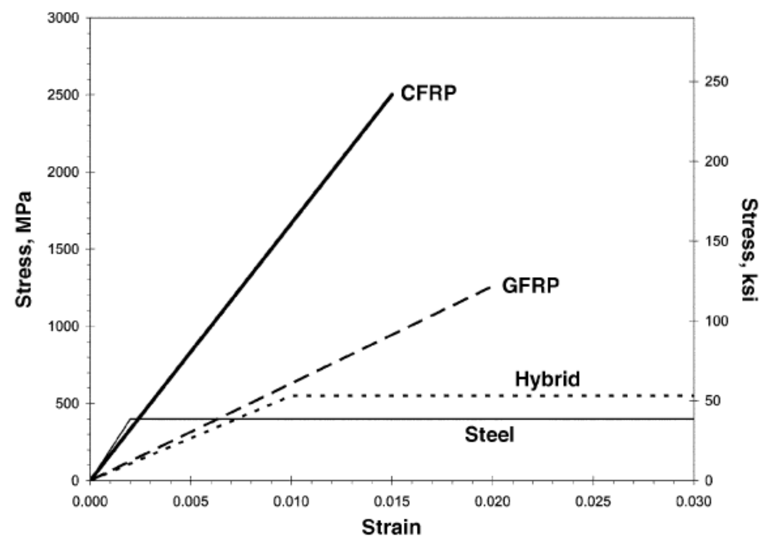

Figure 1.2: Typical stress-strain curves for FRP products compared with steel (ACI 440.R-07, 2007)

Table 1.1: Typical material properties of FRP composites (ACI 440.R-07, 2007)

Material	Density, g/cm³	Tensile Modulus, GPa	Tensile Strength, MPa	Strain to Failure, %
CFRP	1.5 – 1.6	100 – 140	1020 – 2080	1.0 – 1.5
GFRP	1.2 – 2.1	20 – 40	520 – 1400	1.5 – 3.0
AFRP	1.2 – 1.5	48 – 68	700 – 1720	2.0 – 3.0
Steel	7.9	200	400 (yield)	0.2 (yield)

1.2.3 FRP Shear Strengthening Applications

FRP composites can be used to increase the shear strength and performance of structural members. Typically, the laminate or sheet is bonded to the exterior of the member using the hand-layup process. This involves roughening and cleaning the surface, filling voids with epoxy putty, priming the surface and then impregnating the dry FRP sheets in-situ, thereby bonding them to the surface. The ACI 440.2R-08 (2008) – Guide for the Design and Construction of Externally Bonded FRP Systems for Strengthening Concrete Structures, specifies three wrapping schemes for use in the shear strengthening of beams or columns. The wrapping schemes are, in decreasing order of effectiveness: complete wrapping, U-wrapping and side bonding as illustrated in Figure 1.3. Complete wrapping is the most effective in increasing the shear strength of a member but is not always possible due to a lack of access to all sides of the member. U-wrapping is second in effectiveness followed by side bonding. If one of the latter two schemes is used, special care must be taken to address debonding of the FRP sheets. The FRP sheets can be placed continuously along the span, which can prevent the egress of moisture and is thus discouraged. Instead, discrete strips are recommended. Both continuous and discrete strips can be placed with the principal fibre direction parallel to the principal tensile stresses which is more effective, or perpendicular to the longitudinal axis of the member which is easier to install.

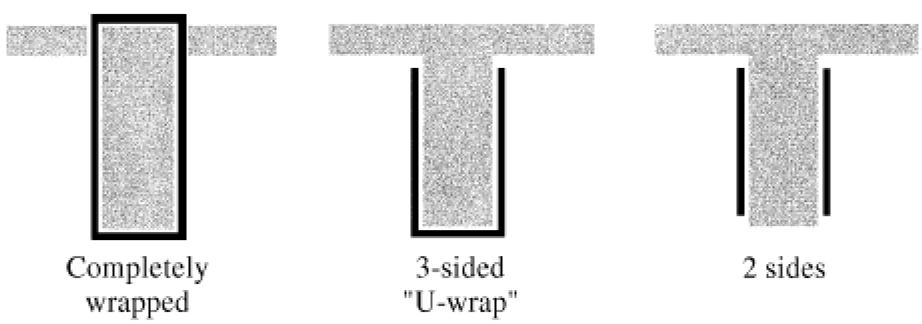

Figure 1.3: Wrapping schemes for shear strengthening using FRP sheets (ACI 440.2R-08, 2008)

FRP shear strengthening of bridge girders has been implemented in the past with good results. The Sainte-Emelie-de-l'Energie Bridge (Figure 1.4a) required a 20 % increase in shear capacity in order to withstand the increase in traffic loads since its construction in 1951. The 21.3

m long single span was reinforced with GFRP strips and the strengthening verified by load testing (Labossière et al., 2000). The Maryland Street Bridge (Figure 1.4b) in Winnipeg was strengthened using vertical CFRP sheets installed on the webs of four of its I-girders. Additional horizontal anchorage strips were then placed at the top and bottom of the web to address the peeling forces introduced by the re-entrant corners where the web meets the flanges. The five-span continuous prestressed concrete structure was constructed in 1969 and required strengthening to sustain increased truck loads (Hutchinson et al., 2003).

Figure 1.4: FRP shear strengthening of bridge girders (a) Sainte-Emelie-de-l'Energie Bridge (Labossière et al., 2000) and (b) Maryland Street Bridge (Hutchinson et al., 2003)

1.3 Previous Experimental Investigations

1.3.1 Rectangular Beams Reinforced in Shear Using Externally-Bonded FRP

The test program conducted by Alzate et al. (2013) consisted of rectangular beams which were 420 mm deep by 250 mm wide. They were reinforced in flexure with 6-20 mm diameter reinforcing bars with a yield strength of 500 MPa. The steel shear reinforcement was made up of 8 mm closed stirrups spaced at 380 mm with a yield strength of 500 MPa. The beam corners were rounded to a 25 mm radius during casting. The beams had concrete compressive strengths of between 20.5 MPa and 37.0 MPa.

The FRP strengthening used was 300 mm wide, unidirectional carbon fibre fabric. Two fabrics from different manufacturers were used. The MBrace CF-130 had a fibre density of 300 g/m^2, thickness of 0.165 mm, tensile strength of 3800 MPa and maximum strain of 1.55 %. It was used on beam series U90C3, U90S3, U45S3 and W90S3. The SikaWrap-530C had a fibre density of 530 g/m^2, thickness of 0.293 mm, tensile strength of 4000 MPa and maximum strain of 1.5 %. It was used on beam series U90C5, U90S5, U45S5 and W90S5. Both fabrics had a Young's modulus of 240 GPa. The surface preparation was done with sandblasting and manual brushing to remove dust and loose debris.

For the purposes of this thesis, the U45S3 and U45S5 beams, having CFRP inclined to 45° with respect to the longitudinal axis of the member will be neglected. The other beams were either U-wrapped (U) or completely wrapped (W), had CFRP strips spaced 500 mm apart (S) or continuously placed (C) and used the 300 g/cm^2 (3) or 530 g/cm^2 (5) fabric.

The completely wrapped beams (W90S3 and W90S5) resulted in an average shear strength that was 2.00 times the shear strength of the control specimens with the higher density fabric performing slightly better than the lower density fabric. The U-wrapped specimens with the higher density fabric (U90C5 and U90S5) had an average shear strength 1.47 times that of the control specimen while the lower density fabric specimens (U90C3 and U90S3) had a 1.35 times improvement. It should be noted that no significant increase was demonstrated when the FRP strips were placed continuously as opposed to discretely at a centre-to-centre spacing of 500 mm. In this study as in others, the U-wrapped specimens failed by debonding of the FRP fabric whereas the fully wrapped beams failed either in bending or by rupture of the FRP sheets.

1.3.2 T-Beams Reinforced in Shear Using Externally-Bonded FRP

Belarbi et al. (2011) reported on the results of the Ph.D. thesis research conducted by Murphy (2010) in which eight reinforced concrete T-beams strengthened in shear with FRP were tested. The beams had an overall depth of 940 mm, a flange thickness of 178 mm and a web width of 457 mm. The flexural reinforcement was provided by 12-No. 11 bars (35.8 mm diameter) in two layers of six. The shear reinforcement consisted of No. 3 closed stirrups (9.5 mm diameter) spaced at either 203 mm or 305 mm with a yield strength of 276 MPa. This low yield strength was selected to mimic the reinforcement of the Troy, New York bridge constructed in 1932. The T-beams were designed to fail in shear before the flexural resistance could be exceeded. The concrete compressive strength at time of testing of the T-beams was between 18.3 MPa and 28.9 MPa. The CFRP sheets used to strengthen the beams in shear had a thickness of 0.165 mm, an ultimate strength of 3791 MPa and an elastic modulus of 228 GPa.

Murphy (2010) tested numerous parameters including orientation of the FRP strips with respect to the beam longitudinal axis, the effect of pre-cracking, different FRP mechanical anchorages, negative moment conditions, corrosion damage and fatigue loading conditions. For the purposes of this paper and for the sake of comparison with the experimental program, only those T-beams with 90° FRP orientation (S90) and no anchorage (NA) or horizontal strip anchorage (HA) will be discussed. The beams in question are therefore: RC-8-Control, RC-12-Control, RC-8-S90-NA, RC-12-S90-NA and RC-12-S90-HA-PC. Note that the last T-beam listed showed the presence of pre-existing cracks (PC) before testing. The two control specimens had no CFRP applied whereas the other three specimens used a U-wrapping strengthening scheme with 254 mm wide strips at a spacing of 381 mm. Specimen RC-12-S90-HA-PC had a CFRP anchorage system applied to the top of the web immediately below the T-beam flange. This consisted of a continuous bi-directional (+45°/-45°) CFRP strip with a width of 178 mm.

In order to account for the different concrete compressive strengths, the data was normalized with respect to the applicable control specimen for each of the CFRP strengthened beams. Specimens RC-8-S90-NA and RC-12-S90-NA showed normalized shear gains of 22 % and 26 % respectively. Specimen RC-12-S90-HA-PC with the additional horizontal anchorage strip performed significantly better with a normalized shear gain of 53 %. It was also noted by Murphy (2010) that the pre-existing cracks in specimen RC-12-S90-HA-PC did not seem to adversely impact the performance of the CFRP shear strengthening.

The control specimens tested failed in a diagonal tension failure mode after yielding of the steel stirrups crossing the critical shear crack. All the other specimens of interest listed above failed in diagonal tension after debonding of the CFRP reinforcement crossing the critical shear crack. The horizontal CFRP strip anchorage system delayed the debonding slightly but could not prevent it completely. Thus, rupture of the CFRP strips was not achieved.

1.3.3 I-Girders Reinforced in Shear Using Externally-Bonded FRP

The literature is sparse regarding precast prestressed concrete I-girders strengthened in shear with FRP strips. Three papers which address the topic of these non-rectangular sections whose results can be compared with those obtained from this experimental program are discussed below.

1.3.3.1 Kang and Ary (2012)

Kang and Ary (2012) investigated the effects of carbon fibre reinforced polymer strip spacing on the shear behaviour of relatively small prestressed concrete I-beams. The girders tested had a total depth of 508 mm with a 102 mm web thickness and 254 mm clear web height. U-wrapped CFRP was applied to two test beams. Specimens IB-05 and IB-10 had strips placed at 127 mm and 254 mm respectively. The control specimen had no CFRP applied. The addition of the CFRP strips resulted in an increase in shear capacity of 1.5 % in the case of specimen IB-10 and 37.85 % for IB-05. Both specimens experience fracture as the CFRP failure type. The authors note that special attention should be paid to CFRP bonding at inside corners. With regard to the marginal increase in shear capacity of specimen IB-10, the authors indicate that CFRP spacings of greater than half the effective shear depth are ineffective in the strengthening of I-beams in shear.

1.3.3.2 Belarbi et al. (2011)

Belarbi et al. (2011) reported on the Ph.D. research of Murphy (2010) who ran an extensive experimental program in which 16 girders with varying cross-sections, CFRP fibre orientation and anchorage systems were tested. Four of these experience diagonal tension failures in the web. These girders had a total depth of 1194 mm with a 203 mm thick deck slab. The web had a thickness of 152 mm with a clear height of 508 mm. Three of the girders used vertically oriented FRP strips and had three different FRP anchorage systems. The fourth was a control specimen. The cross-section corresponds to the Missouri Department of Transportation Type 3 girder and all four specimens discussed had a stirrup spacing of 457 mm. The control girder T3-18-Control, had a shear capacity of 1121 kN. The girders strengthened with CFRP used 305 mm wide strips at a spacing of 305 mm. Girder T3-18-S90-NA was reinforced with only vertical FRP strips and failed at a load of 961 kN. The CFRP strips applied to girder T3-18-S90-HS were anchored with the addition of horizontal strips at the top and bottom of the web. This girder failed at a load of 983 kN. Girder T3-18-S90-SDMA used a special anchorage detail wherein the CFRP strips were clamped around CFRP plates and bolted through the web. The girder experience diagonal tension failure at a load of 1045 kN.

1.3.3.3 Kim et al. (2012)

Kim et al. (2012) conducted an experimental study to determine the feasibility of using anchored CFRP shear strengthening on large bridge girders. Among the specimens tested were four AASHTO type IV I-girders. The girders had a total depth of 1372 mm and no deck slab. The web thickness was 203 mm and the clear web height was 584 mm. These girders were externally strengthened in flexure to ensure shear failure using four post-tensioned DYWIDAG bars stressed to 34 MPa. Three vertical clamps were also used to prevent horizontal shear failure and to prevent failure in an untested region of the beam where there was a wide stirrup spacing. Three different CFRP details were tested and compared with the shear capacity of the control girder I-1 which was found to be 1819 kN. Girder I-2, reinforced with vertical CFRP extending to the top of the web and anchored with CFRP anchors at the top and bottom of the web, failed at a shear of 1855 kN. Girder I-3 was fully wrapped with vertical and horizontal strips covering the entire web and had over 150 CFRP anchors. It had a shear capacity of 2504 kN. Girder I-4 used vertical CFRP strips extending to the top of the beam as well as horizontal strips at the top, bottom and mid-height of the girder. This beam utilized close to 100 CFRP anchors and failed at a shear of 2504 kN. The authors concluded that vertical CFRP shear strengthening delays cracking significantly but does not add much shear capacity. In order to achieve a significant increase in shear capacity, vertical and horizontal strips such as those used in girders I-3 and I-4 are required. This construction detail was found to increase the ultimate load by about 38 %. They also noted that CFRP makes the failure of the beam occur in a more brittle manner.

1.4 Previous Analytical Studies & Design Guidelines

Numerous design guidelines have been published attempting to provide the best method for quantifying the shear resistance increase provided by FRP strips. What follows is a description of some of these guidelines which are representative of the approaches to externally bonded FRP shear reinforcement within the engineering community.

In modern design codes, shear resistance of a beam is calculated by summing the contributions of the concrete (due to aggregate interlock and dowel action of the longitudinal reinforcement) and the steel shear reinforcement (i.e. stirrups and inclined bars). If present, the contribution of inclined prestressing steel tendons or bars is accounted for through a separate term. Most researchers follow this framework by endeavoring to determine the contribution of the FRP to shear resistance and then adding it to the concrete and steel terms to determine the total shear resistance of the concrete member. The FRP reinforcement is often treated analogously to internal steel reinforcement by assuming that the FRP only carries normal stresses in the principal fibre direction.

Most guidelines centre around finding the effective FRP strain (ε_{FRPe}) which is the strain experienced by the FRP sheets at failure of the beam. This strain is typically lower than the FRP rupture strain and is highly dependent on whether the FRP experiences debonding or fracture as its failure mode. Once this strain is computed, it can be multiplied by the FRP elastic modulus (E_{FRP}) to determine the effective FRP stress (f_{FRPe}). Multiplying by the FRP cross sectional area (A_{FRP}) then determines the force carried by the FRP at shear failure of the specimen. Equation 1-1 gives the shear contribution of the FRP according to the ACI 440.2R-08 (2008) design guide. This is typical of the guidelines discussed below, though some give the equation in different formats. Notice that the shear contribution of the FRP is directly analogous to the shear contribution of internal shear reinforcement but with yield stress replaced by effective stress. In Equation 1-1, α is the angle of the FRP strips with respect to the long axis of the member, d_{FRP} is the effective depth of the FRP shear reinforcement and s_{FRP} is the spacing of the FRP strips.

$$V_{FRP} = \frac{A_{FRP} f_{FRPe} (\sin \alpha + \cos \alpha) d_{FRP}}{s_{FRP}} \tag{1-1}$$

1.4.1 Triantafillou (1998)

Triantafillou (1998) attempted to determine the contribution of FRP to the total shear capacity of reinforced concrete beams using data obtained from an experimental study. He noted based on the literature that the FRP strain at failure of a specimen was lower than the FRP tensile fracture strain (ε_{FRPu}). An experimental program was conducted involving the testing of eleven 1000 mm long beams concrete beams. Using the results obtained, combined with others from the literature, a best-fit analysis was used to correlate the effective FRP strain (ε_{FRPe}) with the FRP axial rigidity ($\rho_{FRP}E_{FRP}$). In order to perform this analysis, the FRP contribution to shear resistance was taken to be the difference between the shear resistance of the FRP strengthened specimens and the average shear resistance of the control specimens without FRP. Using that FRP shear contribution value and Equation 1-1, the relationship between ε_{FRPe} and $\rho_{FRP}E_{FRP}$ was determined. It was shown that ε_{FRPe} decreases as $\rho_{FRP}E_{FRP}$ increases. The implication being that as the FRP laminates become thicker and/or stiffer, the strain in the FRP at failure of the specimen is decreased as the debonding failure mechanism takes over from tensile fracture of the FRP. It was found that both debonding and tensile fracture failures followed the same trendline and so a single relationship was found between ε_{FRPe} and FRP axial rigidity (Equations 1-2 and 1-3). The term ρ_{FRP} is the FRP shear reinforcement ratio and is defined in Equation 1-4.

$0\ GPa \leq \rho_{FRP}E_{FRP} \leq 1\ GPa$:

$$\varepsilon_{FRPe} = 0.0104(\rho_{FRP}E_{FRP})^2 - 0.0205(\rho_{FRP}E_{FRP}) + 0.0119 \tag{1-2}$$

$\rho_{FRP}E_{FRP} > 1\ GPa$:

$$\varepsilon_{FRPe} = -0.00065(\rho_{FRP}E_{FRP}) + 0.0024 \tag{1-3}$$

$$\rho_{FRP} = \frac{2t_{FRP}}{b_w}\frac{w_{FRP}}{s_{FRP}} \tag{1-4}$$

1.4.2 Khalifa et al. (1998)

Khalifa et al. (1998) expanded on the conclusions of Triantafillou (1998) and Maeda et al. (1997) to arrive at design equations which were ultimately incorporated into the ACI 440.2R-08 (2008) and CSA S6-14 (2014) design codes. As originally noted by Triantafillou (1998), a discussion of FRP contribution to shear resistance requires an analysis of the two primary failure modes of the FRP sheets, FRP rupture and FRP debonding. Failure due to FRP rupture occurs because of stress concentrations at corners and debonded areas which results in an FRP stress at beam failure which is lower than the ultimate tensile strength of the FRP. Debonding failure can occur as the concrete bodies on either side of the crack move apart vertically. The FRP sheets spanning this crack must develop tensile stresses which are transferred to the concrete through interfacial bond stresses. FRP bond failure occurs if this interfacial bond is compromised before tensile rupture of the FRP sheet occurs. The major contribution of Khalifa et al. (1998) was twofold. Firstly, the FRP effective strain model proposed by Triantafillou (1998) was expanded and simplified based on additional experimental data. Secondly, a bond failure mechanism model was developed based on the contributions of Maeda et al. (1997) and Horiguchi and Saeki (1997). The design equations are summarized at the end of this section.

The FRP fracture mechanism model proposed by Triantafillou (1998) and called the effective strain model was modified by Khalifa et al. (1998) by incorporating additional data and simplifying the ε_{FRPe} versus $\rho_{\mathrm{FRP}}\mathrm{E}_{\mathrm{FRP}}$ relationship. The ratio of effective strain to ultimate strain of the FRP ($R = \varepsilon_{FRPe}/\varepsilon_{FRPu}$) was introduced in order to eliminate the effect of different FRP types. The proposed design procedure centres around finding this R ratio which in subsequent design codes is divided up into its constituent parts in order to simplify design and make it more intuitive for the designer. A limit of 0.50 for R was suggested (Equation 1-5), limiting the FRP strain to between 4,000 $\mu\varepsilon$ and 5,000 $\mu\varepsilon$ and ensuring that cracks in the concrete were not so large as to eliminate the aggregate interlock mechanism. The same procedure as used by Triantafillou (1998) was again used to determine the relationship between ε_{FRPe} and $\rho_{\mathrm{FRP}}\mathrm{E}_{\mathrm{FRP}}$ expressed through the R ratio. The equation was further simplified by realizing that the data used never exceeds a $\rho_{\mathrm{FRP}}\mathrm{E}_{\mathrm{FRP}}$ of 1.1 GPa. The resulting Equation 1-6 incorporates neither the concrete strength nor the bonded surface configuration and is thus applicable only to an FRP rupture failure mechanism.

The authors also proposed a bond-based design approach which incorporates results from Maeda et al. (1997), regarding the bond mechanism between FRP and concrete and Horiguchi and Saeki (1997), regarding the effect of concrete strength on bond strength. Only the portion of FRP extending past a shear crack by the effective bond length will be able to be engaged. Thus, an effective FRP width (w_{FRPe}) is suggested assuming a 45° crack angle as illustrated in Figure 1.5. Only the FRP strips within this width are able to carry shear, thus the R equation includes the term w_{FRPe}/d_{FRP} to account for the effective FRP strips. These considerations result in Equation 1-7 for the R ratio assuming bond-based failure of the FRP. The reduction factor, or effective strain to ultimate strain ratio is taken as the least value given by the three equations related to aggregate interlock, FRP fracture and FRP debonding. From that ratio, the effective FRP strain and stress can be determined and the FRP shear contribution calculated. The proposed procedure tends to give conservative estimates when compared to experimental results.

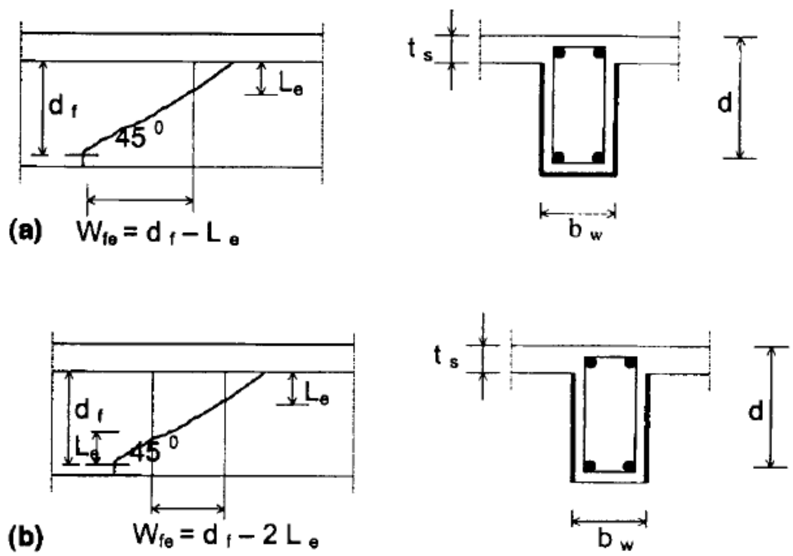

Figure 1.5: Effective FRP width for (a) U-wrapped and (b) Side bonded wrapping schemes (Khalifa et al., 1998)

$R = 0.50$ *Aggregate Interlock (1-5)*

$0\ GPa \leq \rho_{FRP}E_{FRP} \leq 1.1\ GPa$:

$$R = 0.5622(\rho_{FRP}E_{FRP})^2 - 1.2188(\rho_{FRP}E_{FRP}) + 0.778 \qquad \textit{FRP Rupture} \quad (1\text{-}6)$$

$$R = \frac{0.0042(f_c')^{2/3} w_{FRPe}}{(E_{FRP}t_{FRP})^{0.58}\varepsilon_{FRPu}d_{FRP}} \qquad \textit{FRP Debonding} \quad (1\text{-}7)$$

1.4.3 ACI 440.2R-08 (2008) & CSA S6-14 (2014)

Both the Guide for the Design and Construction of Externally Bonded FRP Systems for Strengthening Concrete Structures (ACI 440.2R-08, 2008) and the Canadian Highway Bridge Design Code (CSA S6-14, 2014) use the bond-based design approach proposed by Khalifa et al. (1998). The ACI code recommends the exact model with only a slight change to the strength reduction factor. The CSA code incorporates the angle of inclination of the principal diagonal compressive stresses (θ) into its equation which is adapted into Equation 1-8 below. In the studies discussed above, the authors neglect this angle and use 45° as the assumed shear crack angle. Equation 1-8 excludes the material resistance factor from the code for the sake of easier comparison with the other design equations presented in this section. In both the ACI and CSA design codes, the ratio of effective FRP strain to ultimate FRP strain denoted by R in the work of Khalifa et al. (1998) is called the bond-reduction coefficient (κ_v). This coefficient incorporates the active bond length (L_e) as well as two modification factors accounting for concrete strength (k_1) and type of wrapping scheme used (k_2). This procedure, described in more detail in Section 4.1 of this paper may seem quite different from that proposed by Khalifa et al. (1998) but the difference is only in the form of the equations. The final values for κ_v are identical to those for the R ratio described in Equation 1-7.

$$V_{FRP} = \frac{A_{FRP} f_{FRPe} \sin\alpha(\cot\theta + \cot\alpha) d_{FRP}}{s_{FRP}} \qquad (1\text{-}8)$$

In both design codes, fully-wrapped sections are assumed to experience FRP fracture. Rather than use equations previously proposed in the literature for determining the effective FRP strain, ε_{FRPe} is limited to the lesser of 0.004 mm/mm and $0.75\varepsilon_{FRPu}$. These limits are based on the work of Priestley et al. (1996) and also account for the aggregate interlock mechanism.

1.4.4 Triantafillou and Antonopoulos (2000)

The developments made by Khalifa et al. (1998) to the work of Triantafillou (1998) prompted a response by Triantafillou and Antonopoulos (2000) who modified the effective strain model to differentiate between FRP fracture and FRP debonding failures. The authors used a best-fit analysis of experimental data to determine separate effective strain versus axial rigidity expressions for two failure modes, namely FRP fracture and FRP debonding as shown in Equations 1-9 and 1-10 respectively. They noted that FRP debonding is not likely to dominate in the cases of fully wrapped FRP and so only the equation for FRP fracture is used. For U-shaped or side bonded FRP, the minimum of the two values is taken. It should be noted that as the data used to calibrate the expressions came from mainly CFRP strengthened specimens, the equations are focused on that type of fibre reinforced polymer. The data was also normalized for the concrete tensile stress by finding the relationship between ε_{FRPe} and $\rho_{FRP}E_{FRP}/(f_c')^{2/3}$ and ultimately including an $(f_c')^{2/3}$ term in the expressions for effective strain.

$$\varepsilon_{FRPe} = 0.17 \cdot \varepsilon_{FRPu}\left(\frac{{f_c'}^{2/3}}{E_{FRP}\rho_{FRP}}\right)^{0.30} \qquad \textit{FRP Rupture} \quad (1\text{-}9)$$

$$\varepsilon_{FRPe} = 0.65\left(\frac{{f_c'}^{2/3}}{E_{FRP}\rho_{FRP}}\right)^{0.56} \times 10^{-3} \qquad \textit{FRP Debonding} \quad (1\text{-}10)$$

$$Note\text{: } f_c' \text{ is in } MPa \text{ and } E_{FRP} \text{ is in } GPa.$$

Triantafillou and Antonopoulos (2000) used the Eurocode format throughout their paper and as such deal with a characteristic value for the effective FRP strain (ε_{FRPke}) which the authors limit to a maximum value (ε_{max}) of 0.005 mm/mm. This characteristic value is found by multiplying the effective FRP strain (ε_{FRPe}) found from the two best-fit equations (Equation 1-9 and 1-10) by a reduction factor (α) which the authors set to be 0.8. The characteristic value for effective FRP strain is then divided by the material partial safety factor in the equation for determining FRP contribution to shear capacity. It is noted that when the maximum value is divided by the material partial safety factor, the FRP strain is then limited to approximately 0.004 mm/mm which is generally accepted to be the upper limit at which the aggregate interlock mechanism can be activated in the concrete. The partial safety factor for CFRP (Υ_{FRP}) is taken as 1.20 for FRP fracture, 1.30 for FRP debonding and 1.30 if $\varepsilon_{FRPke} = \varepsilon_{max}$ (aggregate interlock mechanism dominates). More detail for the Eurocode format procedure is given below in the paragraph on the *fib* Bulletin 14 (2001).

Triantafillou and Antonopoulos (2000) plotted the FRP contribution determined from their model versus $\rho_{FRP}E_{FRP}$ for certain concrete and FRP material properties. The results show that there is a limiting value of $\rho_{FRP}E_{FRP}$, $(\rho_{FRP}E_{FRP})_{lim}$ below which design is governed by the aggregate interlock mechanism and FRP failure by fracture or debonding does not occur. In this region, the FRP contribution to shear capacity is directly proportional to $\rho_{FRP}E_{FRP}$. The authors also note that when failure is governed by FRP debonding, $\rho_{FRP}E_{FRP}$ plays a secondary role to concrete strength with respect to shear capacity. If FRP fracture governs, the opposite is true and $\rho_{FRP}E_{FRP}$ plays the primary role in contributing to shear capacity. The authors therefore go on to propose that $\rho_{FRP}E_{FRP}$ should not exceed $(\rho_{FRP}E_{FRP})_{lim}$ given in Equation 1-11 unless debonding can be prevented through mechanical anchorage or full wrapping. At values above $((\rho_{FRP}E_{FRP})_{lim}$ for situations in which U-wrapping or side wrapping is used, the gain in shear capacity by adding additional FRP or using stiffer FRP fabric is small.

$$(\rho_{FRP}E_{FRP})_{lim} = \left(\frac{0.65\alpha \times 10^{-3}}{\varepsilon_{max}}\right)^{1/0.56} f_c'^{\,2/3} = 0.018 \cdot f_c'^{\,2/3} \qquad (1\text{-}11)$$

1.4.5 *fib* Bulletin 14 (2001)

The *fib* Bulletin 14 (2001) uses the best-fit expressions given by Triantafillou and Antonopoulos (2000) for the determination of the effective FRP strain (ε_{FRPe}). These expression result from an evaluation of the published experimental results reported up to early 1999. It expresses the FRP contribution to shear capacity in the Eurocode format, the equation of which is reproduced in Equation 1-12 where $\varepsilon_{FRPd,e}$ is the design value of effective FRP strain. The design value is determined from the characteristic effective FRP strain by dividing by the partial safety factor (Υ_{FRP}) which is similar to that given by Triantafillou and Antonopoulos (2000) but differentiates between prefabricated and hand-layup methods of FRP application. The bulletin also recommends limiting the effective strain to around 0.006 in order to maintain the integrity of the concrete aggregate interlock mechanism. Additional conservativeness is provided by an FRP effective strain reduction factor and a partial safety factor.

$$V_{FRP} = 0.9\varepsilon_{FRPd,e}\rho_{FRP}E_{FRP}b_w d(\cot\theta + \cot\alpha)\sin\alpha \qquad (1\text{-}12)$$

1.4.6 Deniaud and Cheng (2004)

Deniaud and Cheng (2004) developed a simplified shear design method based on the strip method and shear friction approach for the design of reinforced concrete beams strengthened in shear with external FRP reinforcement. This model builds upon the approach originally developed by Deniaud and Cheng (2001) which combined the strip method devised by Alexander and Cheng (1998) and the shear friction approach by R. E. Loov (1998). The specific changes are discussed in further detail below, but the main improvement by Deniaud and Cheng (2004) was to eliminate the need for iteration to find the critical shear crack path. The shear friction approach takes as its assumption that slippage occurs along a web shear crack. In contrast, the modified compression field theory as proposed by Vecchio and Collins (1986) assumes a continuous uniform concrete strut across the shear span. FRP sheets can only develop stresses across a shear crack and thus the shear friction approach was deemed by the authors to be more appropriate for the development of an FRP shear design method.

The strip method is used to determine the shear contribution of FRP sheets. The FRP sheet is divided into discrete strips which are evaluated individually to determine the bond strength of each strip and its corresponding maximum allowable strain. Firstly, a crack angle is assumed (usually 45°) and the bonded length (L_x) of each strip above and below the crack is determined. From this bonded length and the effective bond length (L_e) of the FRP, the mean bond strength (τ_x) of each strip can be calculated using the interface shear stress curve. The maximum allowable strain (ε_x) for each strip is then found based upon a free-body diagram (FBD) of a unit FRP strip as well as the anchorage details at the top and bottom of the strip. An example of this is discussed in further detail by Deniaud and Cheng (2003). Figure 1.6 presents the FBD of an FRP strip bonded to a T-beam. The horizontal FRP strip portion in the diagram is where the strip is bonded to the underside of the T-beam top flange. Equation 1-13 expresses the maximum allowable strain as determined from force and moment equilibrium of the FBD in Figure 1.6.

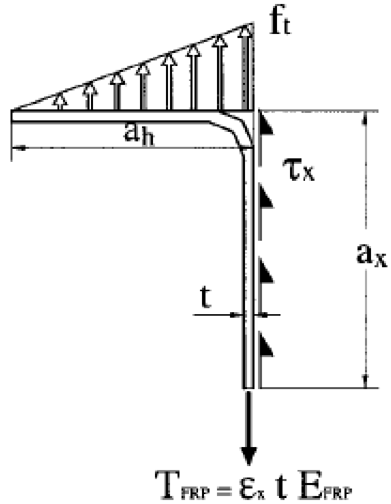

Figure 1.6: Free-body diagram of an FRP strip bonded to a T-beam (Deniaud & Cheng, 2003)

$$\varepsilon_x = \frac{0.5a_h f_t + a_x \tau_x}{t_{FRP} E_{FRP}} \leq \varepsilon_{FRPu} \qquad (1\text{-}13)$$

The smallest ε_x will be present in the strip with the shortest bonded length. This strain is applied to all the strips assuming a uniform strain distribution. The FRP shear load can then be determined. The strips are then assumed to peel off in order of increasing bonded length and the load carried by the debonded strips is redistributed to the remaining strips. The procedure is repeated until the load carried by the remaining strips reaches a maximum which is recorded. Additionally, the maximum FRP strain (ε_{max}) and the remaining bonded width over the initial width ratio (R_L) is recorded.

The interface shear stress curve used by Deniaud and Cheng (2004) was initially developed by Alexander and Cheng (1998) and uses the effective bond length as developed by Maeda et al. (1997). The effective bond length (L_e) corresponds to the load above which no further increase in load can be sustained by the FRP-concrete bond and is given by Equation 1-14 below. In Equations 1-15 and 1-16 representing the interface shear stress curve, τ is the average concrete bond strength over the joint length (L_{FRP}). The factor 0.23 in the interface shear stress curve accounts for the concrete bond shear stress resistance and was determined from a best-fit regression analysis.

$$L_{eff} = exp(6.134 - 0.58\, ln(t_{FRP} E_{FRP})) \qquad (1\text{-}14)$$

$$Note\!: E_{FRP}\ is\ in\ GPa.$$

$$\frac{\tau}{\sqrt{f_c'}} = 0.23 \cdot \left(2 - \frac{L_{FRP}}{L_{eff}}\right)\ \ when\ L_{FRP} < L_{eff} \qquad (1\text{-}15)$$

$$\frac{\tau}{\sqrt{f_c'}} = 0.23 \cdot \left(\frac{L_{eff}}{L_{FRP}}\right)\ \ when\ L_{FRP} \geq L_{eff} \qquad (1\text{-}16)$$

Deniaud and Cheng (2004) also showed that the concrete crack angle (θ) affects the number of strips crossing the crack and therefore the load carried by the FRP sheets. It does not however affect the maximum allowable strain if the same number of strips is assumed. The authors also showed that for the purposes of calculating the maximum FRP strain and R_L ratio, the strip width chosen has little bearing on the final results if a reasonable width is chosen.

The authors then performed a parametric study using the above procedure to arrive at compact equations for ε_{max} and R_L. The five parameters identified to be significant were concrete strength (${f_c}'$), height of FRP sheets (d_{FRP}), stiffness per unit width of the FRP sheets ($t_{FRP}E_{FRP}$), angle of inclination of principal fibres (α) and a factor accounting for the anchorage of the FRP sheets (k_a). Figure 1.7 shows the k_a factor for various anchorage end conditions. The resulting equations for ε_{max} and $R_L$are shown below in Equations 1-17 and 1-18 respectively where k_e is an integer describing the number of debonded ends of the FRP strip.

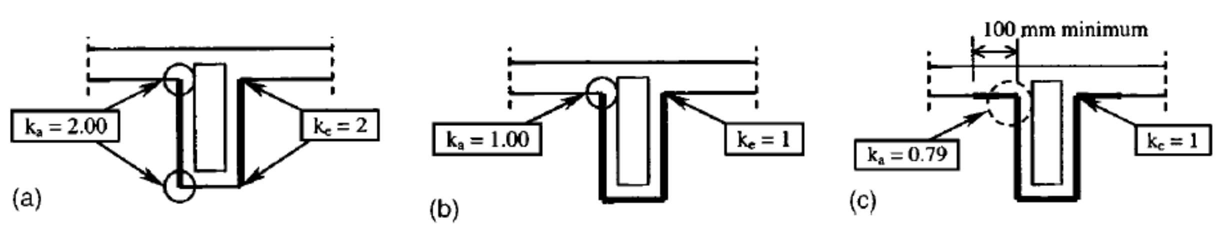

Figure 1.7: k_a factor for various FRP anchorages and end conditions (a) Side-bonded, (b) U-wrapped and (c) U-wrapped with FRP extended underneath top flange (Deniaud & Cheng, 2004)

$$\varepsilon_{max} = \frac{3\sqrt{f_c'} \cdot d_{FRP}^{0.16}}{(t_{FRP} \cdot E_{FRP})^{0.67}(k_a \cdot sin\,\alpha)^{0.1}}\ \% \qquad (1\text{-}17)$$

$$R_L = 1 - 1.2\,exp\left(-\left(\frac{d_{FRP}}{k_e L_{eff}\,sin\,\alpha}\right)^{0.4}\right) \qquad (1\text{-}18)$$

The shear friction approach was used by Loov (1998) to review the CSA A23.3-94 (1994) simplified method of shear design. The equation for shear strength along a plane crossing n FRP spaces and $n-1$ stirrups is in a discrete format and requires the evaluation of multiple shear planes in order to find the weakest shear strength of the beam. The author takes that equation and differentiate with respect to n to arrive at the continuous shear friction design equation presented below in Equation 1-19. This avoids needing to iterate to determine the critical shear plane. The experimentally determined factor, k was developed by Loov and Peng (1998) and is expressed in Equation 1-20. The tension force in the stirrups and the FRP strips are represented by the variables T_v and T_{FRP} respectively and are defined by Equations 1-21 and 1-22 assuming that they are placed at 90° to the longitudinal axis of the beam. In the equations below, d_s is the height of the steel stirrups, s is the spacing of the steel stirrups, A_v is the area of the steel stirrups and f_y is the yield strength of the steel stirrups.

$$V_r = k\sqrt{\frac{f_c' b_w h (T_v + T_{FRP}) d_s}{s}} - T_v \qquad (1\text{-}19)$$

$$k = 2.1(f_c')^{-0.4} \qquad (1\text{-}20)$$

$$T_v = A_v f_y \qquad (1\text{-}21)$$

$$T_{FRP} = d_{FRP}(t_{FRP} E_{FRP})\varepsilon_{max} R_L \left(\frac{w_{FRP}}{s_{FRP}}\right)^2 \frac{s}{d_s}\ \ with\ \varepsilon_{max} \le \varepsilon_{FRPu} \qquad (1\text{-}22)$$

The simplified shear design method as proposed by Deniaud and Cheng (2004) has been shown to conservatively predict experimental test results. Additionally, the method has the advantage of requiring no iteration and is adaptable to other FRP anchorage details.

1.4.7 Perera and Ruiz (2012)

An interesting paper by Perera and Ruiz (2012) approaches the challenge of developing design equations for FRP shear reinforcement in an unconventional way. The authors take the FRP shear design equations proposed by the Federation for Structural Concrete, the American Concrete Institute, the Concrete Society in the UK and the Italian National Research Council and modify them with coefficients. The concrete and steel contributions to shear resistance are also modified with similar coefficients for a total of seven variables. These variables are solved for using genetic algorithms in a multi-objective framework to determine the Pareto-optimal solutions for each design guide with the criteria of producing a conservative estimate of the shear resistance when compared to the experimental results. Using the determined coefficients, the new shear design equations developed for the four design codes showed an average absolute error with respect to the experimental results of approximately 25 % using conservative equations. Perera and Ruiz (2012) conclude that these equations are simple and more accurate than the design equations provided in the current shear design guidelines.

1.5 Bond Behaviour and Anchorage

1.5.1 Ultimate Bond Strength of FRP-Concrete Interfaces

The interface between FRP and concrete is critical to the performance of FRP strengthened concrete members. Many bond strength models have been proposed in the literature and verified using single or double shear test specimens. These bond strength models have been proposed based on both theoretical and empirical evidence and generally take into account some or all of the following parameters: concrete compressive strength, FRP stiffness, effective bond length and concrete to FRP width ratio. The bond strength models discussed here are based on the fracture energy (G_f) and theoretical bond strength (P_u) of simple shear joints as expressed in Equation 1-23.

$$P_u = w_{FRP}\sqrt{2G_f E_{FRP} t_{FRP}} \qquad (1\text{-}23)$$

Chen and Teng (2001) state that for FRP-concrete bonding, the typical slip value at maximum bond stress is 0.02 mm and the maximum slip at failure of the joint is an order of magnitude larger at 0.2 mm. Because of the large difference, the authors proposed a linearly decreasing bond stress-slip model. Using nonlinear fracture mechanics and data acquired from the literature, the authors arrived at the proposed model for ultimate bond strength presented in Equations 1-24 to 1-27. Nonlinear fracture mechanics involves determining the fracture energy of the FRP-concrete bond, which is taken as the area under the bond stress-slip curve. Chen and Teng (2001) noted that if the FRP had a width smaller than that of the concrete on which it was bonded, a nonuniform stress distribution developed across the width of the concrete. This in turn may result in a higher adhesive shear stress. The β_p coefficient was used to account for this effect (Equation 1-25). The proposed model was shown to be an excellent predictor for both FRP-concrete and FRP-steel ultimate bond strength with an average error of 4 % (Yao et al., 2005).

$$P_u = 0.427\beta_P\beta_L\sqrt{f_C'}w_{FRP}L_e \tag{1-24}$$

$$\beta_P = \sqrt{\frac{2-w_{FRP}/b_c}{1+w_{FRP}/b_c}} \tag{1-25}$$

$$\beta_L = \begin{Bmatrix} 1 \\ sin\left(\frac{\pi L_{FRP}}{2L_e}\right) \end{Bmatrix} \begin{matrix} if\ L_{FRP} \geq L_e \\ if\ L_{FRP} < L_e \end{matrix} \tag{1-26}$$

$$L_e = \sqrt{\frac{E_{FRP}t_{FRP}}{\sqrt{f_C'}}} \tag{1-27}$$

Wu et al. (2009) attempted to provide a model for practical FRP-concrete bond design based on the FRP-concrete joint fracture energy. The authors modified the theoretical bond strength equation with the inclusion of the compressive concrete strength. Using a parametric statistical analysis, the authors arrived at a model which accounts for the FRP bonded length as a ratio of the effective bond length. These expressions are shown in Equations 1-28 to 1-30 below. The model takes into account the ratio of the width of the FRP sheet to the width of the concrete member through the k_b factor (similar to β_p from Chen and Teng (2001)). The proposed model is similar to that of Chen and Teng (2001) in composition. It was developed based on a database of 311 tests and was shown to give closer agreement with these experimental results than other models.

$$P_u = \begin{cases} 0.585 k_b w_{FRP} {f_c'}^{0.1} (E_{FRP} t_{FRP})^{0.54} & if\ L > L_e \\ 0.585 k_b w_{FRP} {f_c'}^{0.1} (E_{FRP} t_{FRP})^{0.54} \left(\frac{L_{FRP}}{L_e}\right)^{1.2} & if\ L \leq L_e \end{cases} \tag{1-28}$$

$$k_b = \sqrt{\frac{2.25 - \left(\frac{w_{FRP}}{b_c}\right)}{1.25 + \left(\frac{w_{FRP}}{b_c}\right)}} \tag{1-29}$$

$$L_e = \frac{0.395 (E_{FRP} t_{FRP})^{0.54}}{{f_c'}^{0.09}} \tag{1-30}$$

Kamel et al. (2006) noticed in their study on the behaviour of CFRP sheets bonded to concrete that the strain distribution was not uniform across the FRP width. The strain was found to be on average 58 % higher at the edge of the sheet as compared to the centre of the sheet. This difference was found to be greater near a concrete crack and increased as the load increased. The authors were unable to derive a stress distribution across the FRP width from the strain distribution due to difficulties involving the shear lag effect and uneven debonding across the sheet. Narrow FRP strips experience a more uniform stress distribution across their width and can thus reach higher maximum loads per unit width than wider strips. This width effect requires further investigation in order to be properly included in bond strength models.

1.5.2 Modelling the FRP-Concrete Bond

In order to model FRP strengthened concrete structures in finite element software, modelling bond behaviour is essential. To be capable of replicating bond behaviour at all load stages, these models must be more sophisticated than simpler ultimate bond strength models. There are many models in the literature which attempt to quantify the strength and behaviour of the FRP-concrete interface. In general, these models tend to fall into one of two categories. The first approach involves modelling the concrete elements immediately adjacent to the adhesive layer and assuming that debonding is governed by the cracking and failure of these interfacial concrete elements. The second approach maintains that debonding can be simulated using a layer of interface elements between the concrete and the FRP. These interface elements are governed by the specified bond-slip model and debonding occurs upon failure of these elements. The simplest of these assumes a “perfect” bond with no slip between FRP and concrete. This model is unconservative in many cases due to the fact that FRP debonding is not taken into account, leading to higher stiffness and ultimate load carrying capacity.

One approach for simulating the FRP-concrete interface is to assume that debonding is controlled by the thin (2 – 5 mm) layer of concrete immediately under the epoxy resin used to bond the FRP sheet to the concrete. Lu et al. (2005b) used the fixed angle crack model and treated the concrete in compression as an elastoplastic material and the cracked concrete using the smeared crack approach. The authors demonstrated that their finite element model is in good agreement with test results and can accurately predict ultimate load, effective bond length and strain distributions in the FRP. Pham et al. (2006) took this approach further by combining the smeared crack model with discrete cracks in order to allow for displacement discontinuity across a crack and use both mode I and mode II crack prediction criteria. The authors also found their model to be in good agreement with experimental results. One disadvantage of the approach of using cracked concrete elements to predict FRP debonding is that small concrete elements are required which increases both computational intensity and modelling difficulty.

Sun et al. (2017b) attempted to develop a bilinear bond-slip model using digital image correlation as well as a computational model that can be used to determine the load-slip relationship of the FRP strip. A bilinear model with ascending and descending branches was chosen over the more accurate exponential curve because it is easier to implement in finite element software. In order to define the curve, the three critical parameters are the final slip (s_f), maximum bond stress (τ_m) and corresponding slip (s_0). A typical bilinear bond stress-slip curve is illustrated in Figure 1.8. Based on the results of eighteen test specimens, the authors arrived at their bilinear bond stress-slip relationship as described by Equations 1-31 to 1-35. A finite element model was then constructed in the ANSYS software and used to evaluate the proposed bond stress-slip relationship. Various strips widths, axial stiffnesses and bond lengths were evaluated in the single shear test simulation. It was found that the proposed model performed well in predicting bond stress-slip response when compared to experimental results.

The digital image correlation technique used by Sun et al. (2017b) helped to eliminate some of the past difficulties in determining a reliable bond stress-slip model. As described by Ueda and Dai (2005), the difficulties are in placing many strain gauges in a small interface area and the small bending stiffness exhibited by FRP sheets causing a large scatter in strain data due to local deformations. Another solution to the problem of obtaining accurate strain readings to determine bond stress-slip relationships is to base the model on the predictions of a finite element model which has been calibrated to closely match experimental results. This strategy was employed by Lu et al. (2005a) among others.

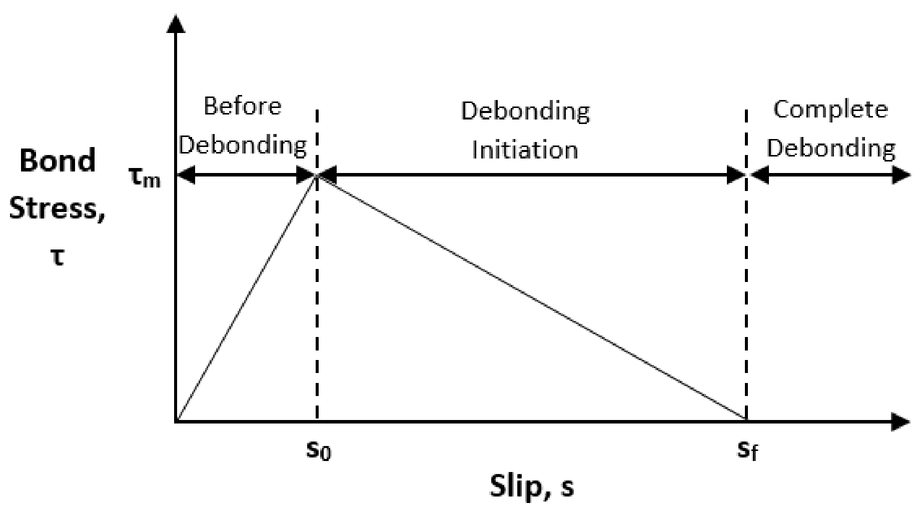

Figure 1.8: Typical bilinear bond stress-slip model

$$\tau_m = 1.35 + 0.25\beta_w f_t + 0.62 f_t \qquad (1\text{-}31)$$

$$s_0 = 0.016 - 0.0046\beta_w f_t + 0.11\beta_w \qquad (1\text{-}32)$$

$$s_f = -0.06 + (0.88 - 0.23\beta_w^2) f_t^{-0.5} \beta_w^{0.5} \qquad (1\text{-}33)$$

$$\beta_w = \sqrt{\frac{1.9 - w_{FRP}/b_c}{0.9 + w_{FRP}/b_c}} \qquad (1\text{-}34)$$

$$f_t = 0.62\sqrt{f_c'} \qquad (1\text{-}35)$$

In a separate paper, Sun et al. (2017a) used their previously developed bond model to produce closed-form solutions for the load-displacement response of FRP strips externally bonded to concrete members in a single shear test. They derived two sets of equations: from their proposed bond stress-slip model and also from numerical finite element predictions.

For the solution derived from the bond stress-model the interfacial fracture energy (G_f) was determined by taking the area under the bond stress-slip curve. Then, using the theoretical bond stress formula (Equation 1-23) and assuming that before debonding initiation the displacement (Δ) of the FRP strip is equal to the interfacial slip (s), the load-displacement response can be described by Equation 1-36. The typical load-displacement responses of FRP strips with adequate bond length and inadequate bond length are shown in Figure 1.9. The figure describes the four stages that FRP strips experience when loaded. The elastic stage, softening stage, plateau stage and unloading stage are present in cases with adequate bond length whereas inadequate bond length produces a response which is much less ductile and excludes the plateau stage.

Using the bond stress-slip model previously discussed, finite element simulations were conducted and load-displacement curves were parametrically determined for FRP strips debonding from a concrete substrate. Additionally, an equation for determining effective bond length was also proposed. For brevity the equations are not reproduced here but rest assured, they are quite extensive. Sun et al. (2017a) found their closed-form solutions to be in close agreement with experimental and numerical results.

$$P = \begin{Bmatrix} w_{FRP}\sqrt{E_{FRP}t_{FRP}\tau\Delta} \\ w_{FRP}\sqrt{E_{FRP}t_{FRP}(\Delta\tau_m + \tau\Delta - s_0\tau)} \end{Bmatrix} \begin{matrix} \Delta \leq s_0 \\ s_0 < \Delta \leq s_f \end{matrix} \qquad (1\text{-}36)$$

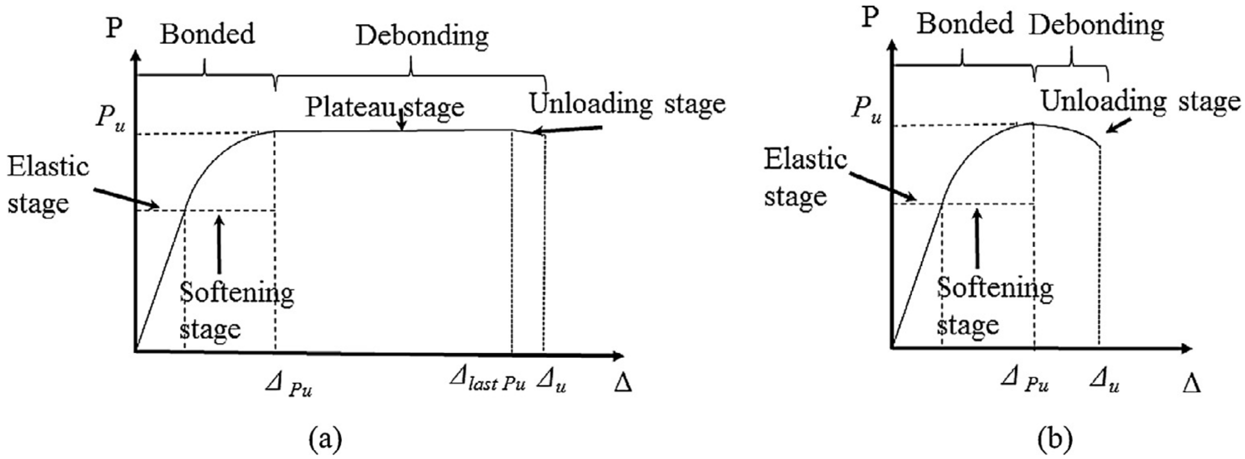

Figure 1.9: Typical load-displacement responses of FRP strips with (a) adequate bond length and (b) inadequate bond length (Sun et al., 2017a)

Yuan et al. (2004) give an excellent overview of the debonding process assuming a bilinear bond stress model. Figure 1.10 shows the shear stress distribution stages as well as the propagation of softening and debonding. Note that in this figure, τ_f denotes the maximum bond stress which is the same as τ_m as used above. At small loads (Fig. 1.10a), the entire length of the FRP-concrete interface is in the elastic stress state (state I). Once the shear stress at the loaded end of the FRP strip reaches τ_f (Fig. 1.10b), part of the strip enters the softening stress state (state II). Interfacial softening occurs due to micro-cracking of the concrete substrate. As the load continues to increase (Fig. 1.10c), part of the strip is in the elastic state and part is in the softening state.

The softening zone (zone a) increases until debonding (as initiated by macro-cracking or fracture of the concrete substrate) occurs at $a = a_d$ (Fig. 1.10d). The load at this stage is at its maximum. Debonding propagates quickly (Fig. 1.10e) and the maximum bond stress location moves towards the unloaded end of the FRP strip. The FRP strip at this point is in three states simultaneously depending on location along its length: elastic state (state I), softening state (state II) or debonded state (state III, bond stress is zero). The debonded zone (zone d) continues to increase until $L_{FRP} - d = a_u$ at which point the softening front has reached the unloaded end of the member (Fig. 1.10f) and none of the FRP is experiencing elastic bond stress. During the final stage (Fig. 1.10g), the softening zone (zone a) remains constant and the interfacial shear stress at the unloaded end decreases linearly with the load.

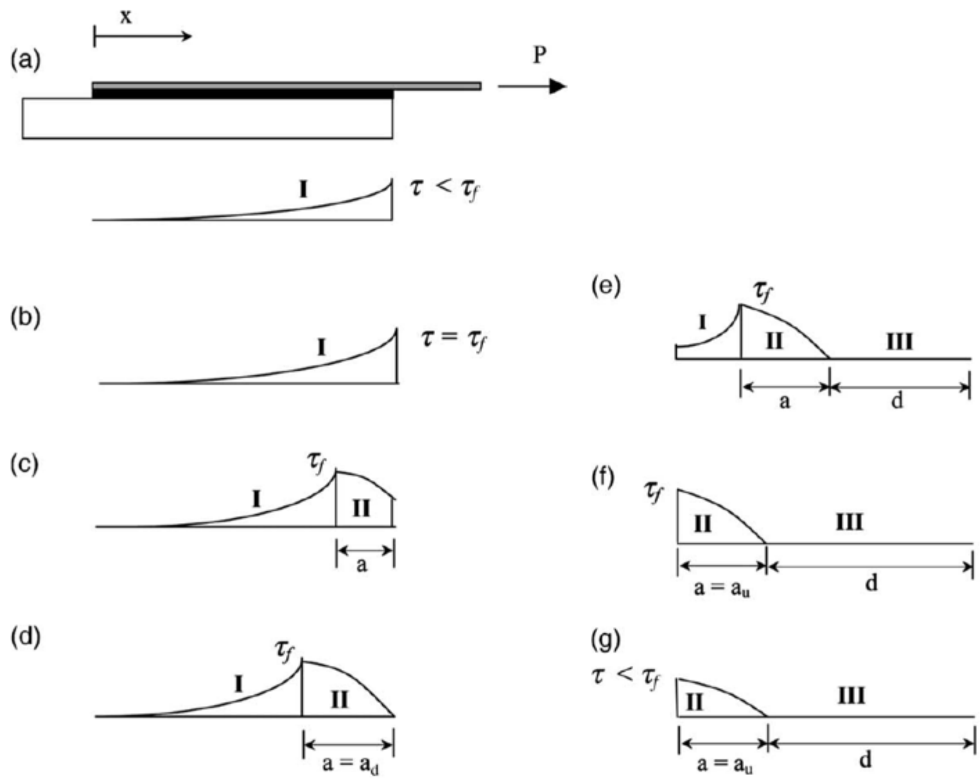

Figure 1.10: Interfacial shear stress distribution for large bond length (Yuan et al., 2004) (a) Elastic stress, (b) Initiation of softening at x = L, (c) Propagation of softening zone, (d) Initiation of debonding at x = L, (e) Propagation of debonding, (f) Peak shear at x = 0, (g) Linear unloading

1.5.3 Peeling and Mixed-Mode Loading of FRP Strips

One of the difficulties inherent in designing FRP shear strengthening for I-girders is the treatment of the re-entrant corners at the top and bottom of the web. The FRP in these areas is subject to mixed-mode I/II loading, i.e. normal tensile stress combined with shear stress parallel to the FRP strips. This has been shown by Yao et al. (2005) among others to negatively affect the bond strength and can lead to debonding at re-entrant corners leading to a redistribution of stresses and subsequent debonding of the entire strip and failure of the specimen.

In order to better understand the effects of mixed-mode I/II loading on FRP strips, Ghorbani et al. (2017) conducted an experiment program in which 31 concrete prism specimens were tested in single-lap shear tests. The goal of the study, as illustrated in Figure 1.11, was to investigate the effect of loading angles induced in flexural FRP reinforcement upon the appearance of flexural and flexural/shear cracks. The specimens were 330 mm long and had a square cross-section with 150 mm sides. The FRP used had an elastic modulus of 230 GPa and a tensile strength of 3900 MPa. Both positive and negative loading angles with respect to the plane of the FRP strip were tested introducing both tensile and compressive normal stresses (mode I) respectively as well as the shear stress (mode II) which is commonly associated with FRP shear and flexural strengthening.

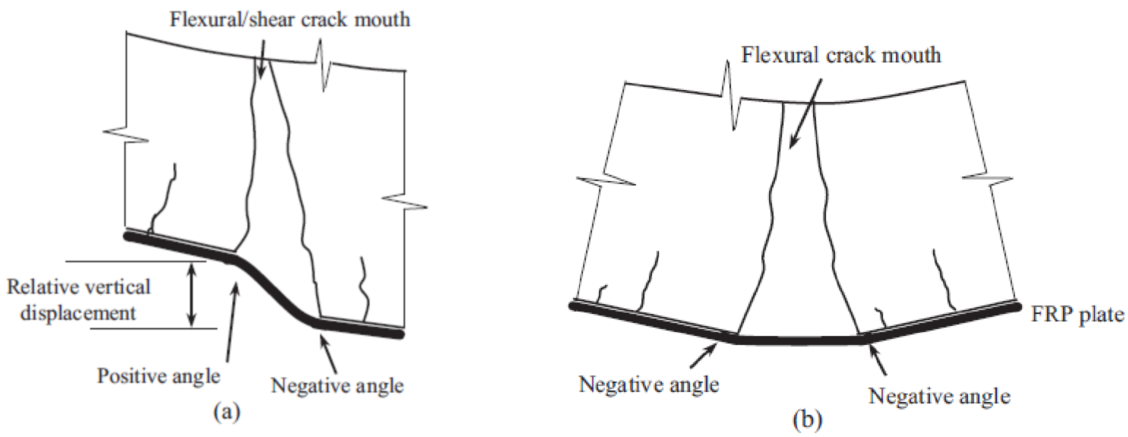

Figure 1.11: Loading angles induced in FRP at location of (a) Flexural/shear crack and (b) Pure flexural crack (Ghorbani et al., 2017)

The results of the tests show that negative loading angle increases the bond strength. This is explained by the authors as being due to the additional confinement of the concrete in the bonded area and the additional aggregate interlock in the debonded area. Both effects are provided by the compressive stresses induced due to the negative loading angle. Confinement increases the energy required to initiate a crack thereby increasing the load required to initiate FRP debonding. Once debonding has started, the compressive stress normal to the interface plane increases the friction and ability of the aggregates to interlock and therefore increases the bond strength. It was also noted that increasing the bond length served to ensure that both mechanisms remained active by increasing the area remaining bonded after initial debonding initiates and ensuring that there is enough bond strength to transfer the interfacial shear stresses. For loading angles decreasing from -2.3° to -6.0°, the bond strengths were found to increase by between 7.2 % and 27.9 % for the 100 mm bonded length and by between 14.7 % and 37.3 % for the 150 mm bonded length.

Positive loading angles have the opposite effect on the bond strength. Debonding was found to occur at lower loads due to the reduction in interface resistance caused by the induced tensile stresses. After debonding has initiated, the separation of concrete and FRP caused by the tensile normal stresses reduced the residual ability of the interface to transfer shear stresses. Ghorbani et al. (2017) noted that for shorter bonded lengths, the reduction in bond strength is more severe due to insufficient anchorage length along the un-debonded portion of the bonded length. For loading angles increasing from +2.4° to +4.7°, the bond strength was found to decrease by between 21.9 % and 41.2 % for 100 mm bonded length and by between 12.3 % and 16.3 % for 150 mm bonded length.

Based on their experimental results, Ghorbani et al. (2017) proposed a model for the prediction of bond strength under mixed-mode I/II loading in which an existing mode II (pure shear) model is modified with a β_α factor to account for the effect of loading angle on bond strength. This factor was determined based on a linear regression analysis of the experimental data. The proposed model of Ghorbani et al. (2017) is reproduced in Equations 1-37 and 1-38. In these equations, α is the loading angle in degrees, L_{FRP} is the FRP bond length and P_{II} is the mode II bond strength. Also, the units used are MPa and mm. Combined with the model of Chen and Teng (2001), the average error of the proposed model when compared to the experimentally measured results was 0.64 % for the 100 mm bonded length and 1.33 % for the 150 mm bonded length, showing good agreement with experimental results.

It should be noted that the authors chose small loading angles for their tests in order to simulate the effects of vertical movement at flexural and shear cracks on FRP flexural reinforcement (i.e. along the longitudinal axis of the girder). The results of the authors cannot be immediately applied to the re-entrant corners of typical I-girders which have much larger angles in the order of 45°. For positive loading angles which reduce the bond strength, it is likely that the observed decrease in strength would be more pronounced. More research is needed on this topic and how the decrease in bond strength can be reduced through anchorage systems.

$$P_{II,\alpha} = \beta_\alpha P_{II} \quad (1\text{-}37)$$

$$\beta_\alpha = \left(\frac{0.08L_{FRP}-61}{1000}\right)\alpha + \left(\frac{855+1.1L_{FRp}}{1000}\right) \quad (1\text{-}38)$$

1.5.4 FRP Shear Strengthening Anchorage Systems

Murphy (2010) tested four FRP anchorage systems on T-beams and prestressed concrete I-girders. The simplest system tested was horizontal strip anchorage (HS). The three systems of mechanical anchorage of the CFRP strips tested were the continuous pre-cured CFRP plate anchorage (CMA), discontinuous pre-cured CFRP plate anchorage (DMA) and discontinuous pre-cured CFRP plate anchorage with sandwiched ends (SDMA). These anchorage systems were tested on both T-beams and I-girders in shear. Figure 1.12 shows the various I-girder anchorage schemes which were tested. The T-beam dimensions and reinforcement details are described in Section 1.3.2. The I-girders were of varying cross-section with web heights of between 508 mm and 635 mm and various deck configurations cast separately onto the top flange of the girders. The steel shear reinforcement consisted of No. 3 (71 mm^2) double legged steel stirrups with a specified yield strength of 414 MPa. The stirrup spacing was either 305 mm or 457 mm. The longitudinal reinforcement was made up of 15.24 mm diameter prestressing tendons stressed to 40 % of ultimate for cross-section Types I and II and 60 % of ultimate for cross-section Types III and IV. The concrete compressive strength of the girders varied between 61.3 MPa and 73.5 MPa with deck slab concrete compressive strengths of between 36.1 MPa and 77.8 MPa. The I-girders were strengthened with U-wrapped CFRP strips with a width of 305 mm and a spacing of 457 mm.

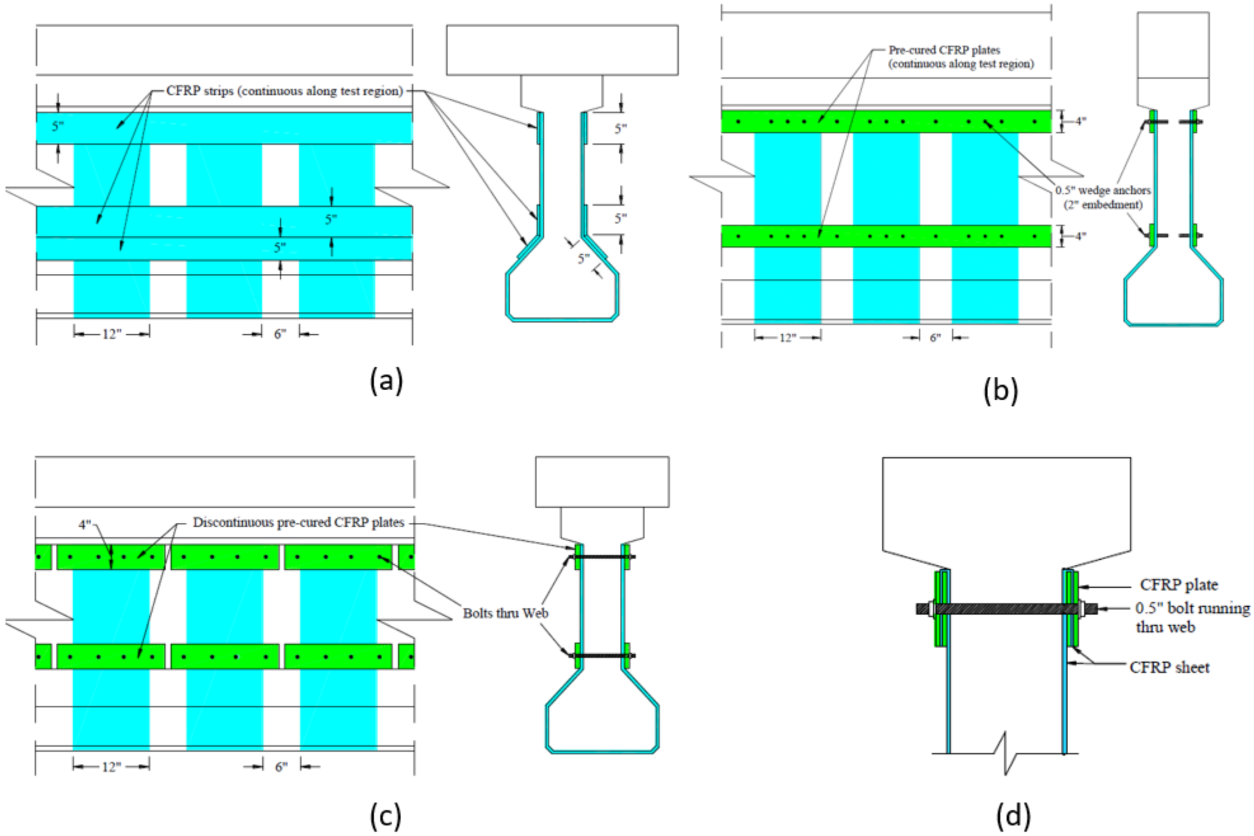

Figure 1.12: Anchorage systems (a) Horizontal strip (HS), (b) Continuous plate (CMA), (c) Discontinuous plate (DMA) and (d) Sandwiched discontinuous plate (SDMA) (Murphy, 2010)

The results of the I-girders tests were inconclusive in determining shear resistance increase provided by CFRP shear strengthening. At most, a shear resistance increase of approximately 5 % (58 kN) was observed between the control specimen and CFRP reinforced specimen with sandwiched discontinuous plate anchorage. In the analysis of the failure modes of the various I-girders and CFRP anchorage systems, interesting conclusions can be drawn about the effects of CFRP shear reinforcement on the behaviour of the girders.

The main failure mode noticed in the Type I and II girder cross-sections was the propagation of shear cracks into the top flange which ran horizontally along the longitudinal compression reinforcement. The lack of confinement and insufficient amount of compression reinforcement caused the bars to buckle and ultimately lead to this failure mode. This type of failure is not prevented by the addition of CFRP reinforcement regardless of anchorage system. Debonding of the CFRP strips was present in most of the failed specimens. The debonding often took place in the concrete substrate which in these thin webbed sections can significantly decrease the ability of the web to withstand the shear forces. This can lead to web crushing as the ultimate failure mode of the girders as it did in two specimens without anchorage systems. Mechanical anchorage failure was observed in the specimen reinforced with continuous pre-cured CFRP plate anchorage due to buckling of the CFRP plate in the compression zone of the girder. Additionally, the wedge anchors used to secure the plates had insufficient embedment and thus were observed to pull out of the member. Rupture of the CFRP fibres occurred to a limited degree in one specimen strengthened with discontinuous pre-cured CFRP plate anchorages. Rupture of the fibres results in a sudden redistribution of stresses akin which can significantly reduce the ultimate strength of the member.

The SDMA system was found to perform the best of all anchorage techniques by preventing slippage of the FRP strips. The DMA system provided a lesser increase but has the benefit of being more practical and easy to install. CMA and HS anchorage systems were found to be relatively ineffective in preventing FRP strip debonding.

The CSA S6-14 (2014) – Canadian Highway Bridge Design Code specifies that the external FRP shear reinforcement be anchored in the compression zone of the beam or column in accordance with Figure 1.13. The figure shows example anchorages for vertical FRP strips. The anchorage can be provided by the section being fully wrapped or by anchorage near the compression flange of T-beams. This compression zone anchorage can be provided by horizontal strips or embedment in the flange itself. The code does not provide guidance for the anchorage of FRP shear strips applied to I-girders.

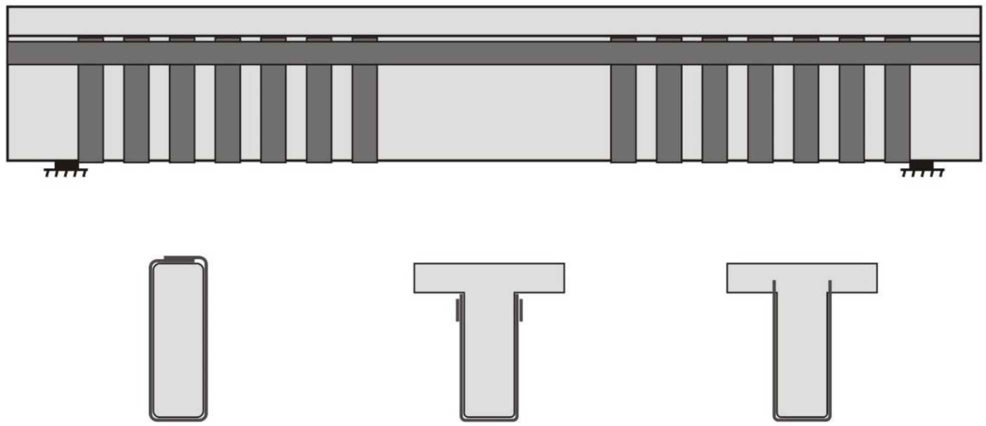

Figure 1.13: Anchorage of externally bonded FRP as adapted from the CSA S6-14 (2014)

1.5.5 Surface Preparation

Proper adhesion is necessary to transfer stress between the externally-bonded FRP and the concrete substrate. Thus, the bond effectiveness is critical to the performance of the FRP system. This bond strength is influenced by the material properties of the fibres, epoxy matrix and concrete. If the bond strength is insufficient, delamination of the FRP can occur before reaching the required strength. To aid in adhesion, surface preparation of the concrete substrate through wire brushing, bush-hammering, sandblasting or grinding is necessary to ensure that the substrate is clean, sound and properly roughened. Iovinella et al. (2013) found that between grinding, brushing, bush-hammering and sandblasting, sandblasting and bush-hammering were the most effective surface preparation techniques as measured by single-shear tests. Bush-hammering and sandblasting were found to increase the bond strength by more than 30 % and 50 % respectively when compared to the control specimens which had no surface preparation. In the same paper, the authors proposed a coefficient that can be used to incorporate surface roughness into the prediction equations used in codes and guidelines. Another finding was that while single-shear bond strength correlates well to surface preparation, pull-off tests do not and should therefore not be used to quantify bond strength.

Experimental studies by Mostofinejad and Mahmoudabadi (2010), Liu (2014), and Tudjono et al. (2017) among others have shown that surface preparation in the form of grooves ground into the concrete substrate can significantly improve bond strength and prevent FRP delamination. It was found that the orientation of the grooves (Figure 1.14) had no significant effect on the bond strength with all orientations producing failure in the concrete substrate in both tension and shear tests (Tudjono et al., 2017).

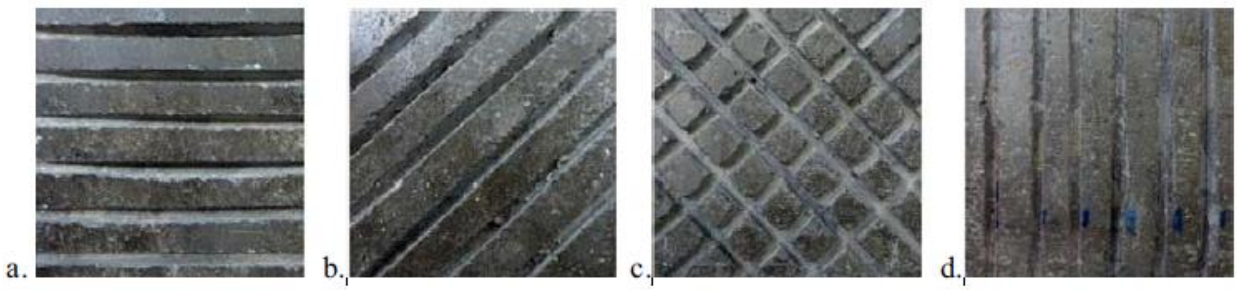

Figure 1.14: Concrete grooved surface preparation, (a) Perpendicular, (b) Diagonal, (c) Crosses and (d) Parallel (Tudjono et al., 2017)

1.6 Research Objectives

The objectives of this research program are:

(1) To study the effects of CFRP shear strengthening on the shear performance and failure modes of pretensioned concrete I-girders.

(2) To study the effects of CFRP shear strengthening on the width of inclined shear cracks.

(3) To investigate the influence of CFRP horizontal anchorage strips and curved epoxy putty transitions at web re-entrant corners in preventing debonding of FRP strips.

(4) To experimentally determine the components of shear resistance (stirrups, concrete and CFRP) and compare them to analytically determined values.

(5) To compare the predictions made using the 2014 Canadian Highway Bridge Design Code to the experimental results.

(6) To study the restraint on the web provided by the stiff top and bottom flanges and predict this effect using non-linear finite element analysis.

2 Experimental Program

2.1 Description of the Specimens

The experimental program was carried out in the Jamieson Structures Laboratory at McGill University. It consisted of two full-scale prestressed concrete I-girders of which each side was treated as a separate specimen, for a total of four specimens. The two girders are identical in cross-section with 150 mm web thickness and 600 mm web heights and have the same amount of steel shear reinforcement. They have a total length of 7.30 m. Each side of the girder was strengthened in shear with FRP in a different configuration and tested separately.

2.1.1 Steel Reinforcement Details

Figure 2.1 shows the elevation view and cross-sections at the midspan and support regions of the two precast pretensioned I-girders as well as the reinforcement details. Each girder was 7.30 m long with two loading points each located 250 mm from the centre of the girder. The shear span, as measured from the centre of the loading plate to the centre of the bearing plate is 3.00 m. The total depth of the girder is 1125 mm with a 150 mm web thickness and 600 mm web clear height. The top flange was cast at the same time as the rest of the girder and simulates the presence of a deck slab. It is 150 mm thick and 800 mm wide. The top and bottom flange haunches extend out from the web at a 45° angle.

The steel shear reinforcement is composed of single-legged 10M Grade 400 stirrups at a spacing of 400 mm. The reinforcement ratio is thus 0.0017 which is typical of older bridge girders and meets the minimum amount of shear reinforcement as specified in Section 8.9.1.3 of CSA S6-14 (2014) as shown in Equation 2-1. Assuming a concrete compressive strength of 42 MPa and steel yield stress of 400 MPa, the 400 mm stirrup spacing requires $A_{v,min}$ = 58 mm^2. Using single-legged 10M (A_v = 100 mm^2) stirrups provides 1.7 times the minimum amount of transverse reinforcement steel required.

$$A_{v,min} = 0.15 f_{cr} \frac{b_v s}{f_y} = 0.15 \times 0.4\sqrt{f_c'} \frac{b_v s}{f_y} \qquad (2\text{-}1)$$

According to Section 8.14.6 of the CSA S6-14 (2014), the stirrup spacing when under significant shear load should not exceed the lesser of $0.33d_v$ or 300 mm. With an effective prestressing depth of 1060 mm, the maximum stirrup spacing is 300 mm (Equation 2-2). The chosen 400 mm stirrup spacing thus exceeds the maximum stirrup spacing by 33 %.

$$Min\begin{Bmatrix} 0.33d_v = 0.33 \times 0.9 \times 1060 = 315\ mm \\ 300\ mm \end{Bmatrix} = 300\ mm \tag{2-2}$$

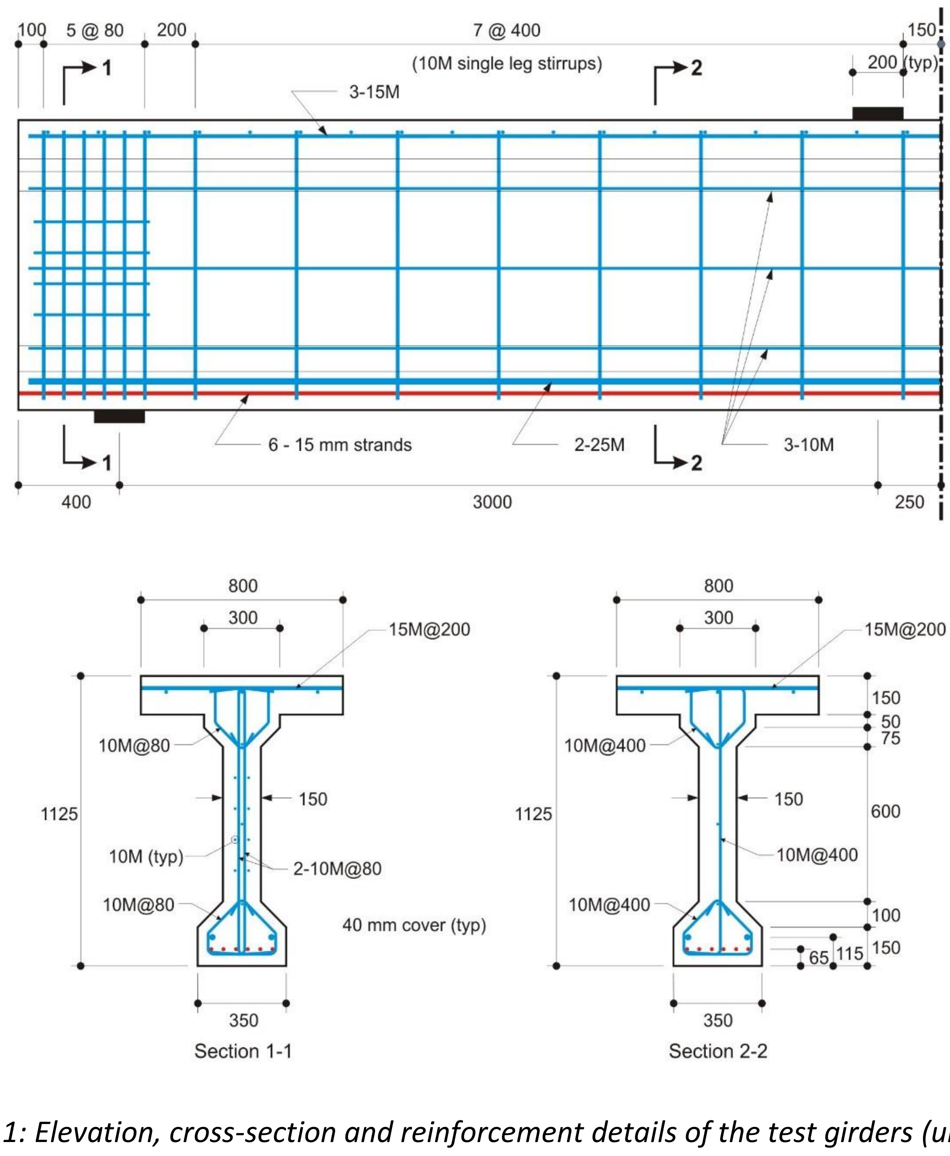

Figure 2.1: Elevation, cross-section and reinforcement details of the test girders (units: mm)

The prestressing steel is made up of 6 – 15.24 mm diameter strands with a minimum specified tensile strength of 1860 MPa. The strands are located in a single layer at a distance of 65 mm from the bottom of the flange of the girder and at an on-centre spacing of 50 mm from each other. The resulting effective depth to the prestressing steel (d_v) is thus 1060 mm. The strands were straight and not harped or inclined with respect to the vertical axis of the girder. The strands were pretensioned prior to the concrete being placed to a stress equal to 70 % of the minimum specified ultimate stress given by the manufacturer. The prestress transfer was accomplished by flame cutting after 6 days of moist curing when concrete cylinder tests indicated that the concrete had reached a strength of at least 30 MPa.

The conventional longitudinal reinforcement is made up of 2-25M bars with a combined area of 1000 mm^2. These bars were placed at a distance of 115 mm from the bottom face of the bottom flange giving an effective depth to the tension reinforcement of 1025 mm including the contribution of both the prestressing steel and conventional longitudinal reinforcement. The addition of the 25M reinforcing bars was done to increase the flexural strength of the beams such that shear failure as opposed to flexural failure would occur. Three 10M longitudinal reinforcing bars were placed at the top, bottom and at mid-height of the web. These reinforcing bars were continuous along the length of the girders with no splices. They were placed in order to provide an anchor point for the top and bottom flange reinforcing bar cages and stirrups.

Figure 2.2 shows the steel reinforcement placed in the formwork before casting of the concrete as well as the prestressing bed and stirrup strain gauge placement. Additional horizontal and vertical steel reinforcement was placed in the girder end regions (Figure 2.3) in order to control concrete cracking due to prestressing.

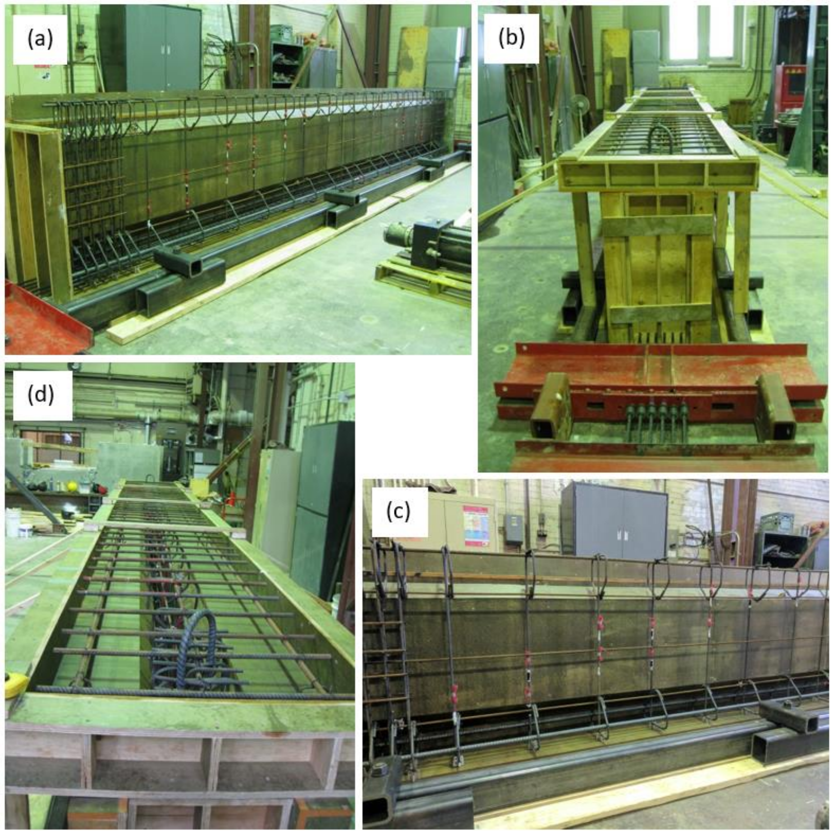

Figure 2.2: Girder reinforcing steel and formwork, clockwise from top left: (a) Side view of reinforcing bars and formwork, (b) End view and stressing bed, (c) Stirrup strain gauges and (d) Top view of slab reinforcement

Figure 2.3: Additional reinforcement in end region to control concrete cracking due to prestressing

2.1.2 FRP Reinforcement Details

Girder 1, as shown in Figure 2.4 contains specimens S1 and S2. Specimen S1 has no FRP reinforcement and acts as the control specimen. Specimen S2 is the most heavily reinforced with vertical FRP at a spacing of 150 mm and three horizontal anchorage strips bonded to the web and flange haunches (one at top of web and two at bottom of web). These anchorage strips placed in an effort to improve the anchorage of the vertical FRP strips at the re-entrant corners which were identified as the most likely place for debonding to occur. These re-entrant corners were also built up with epoxy putty to achieve a curved transition and again help with preventing debonding.

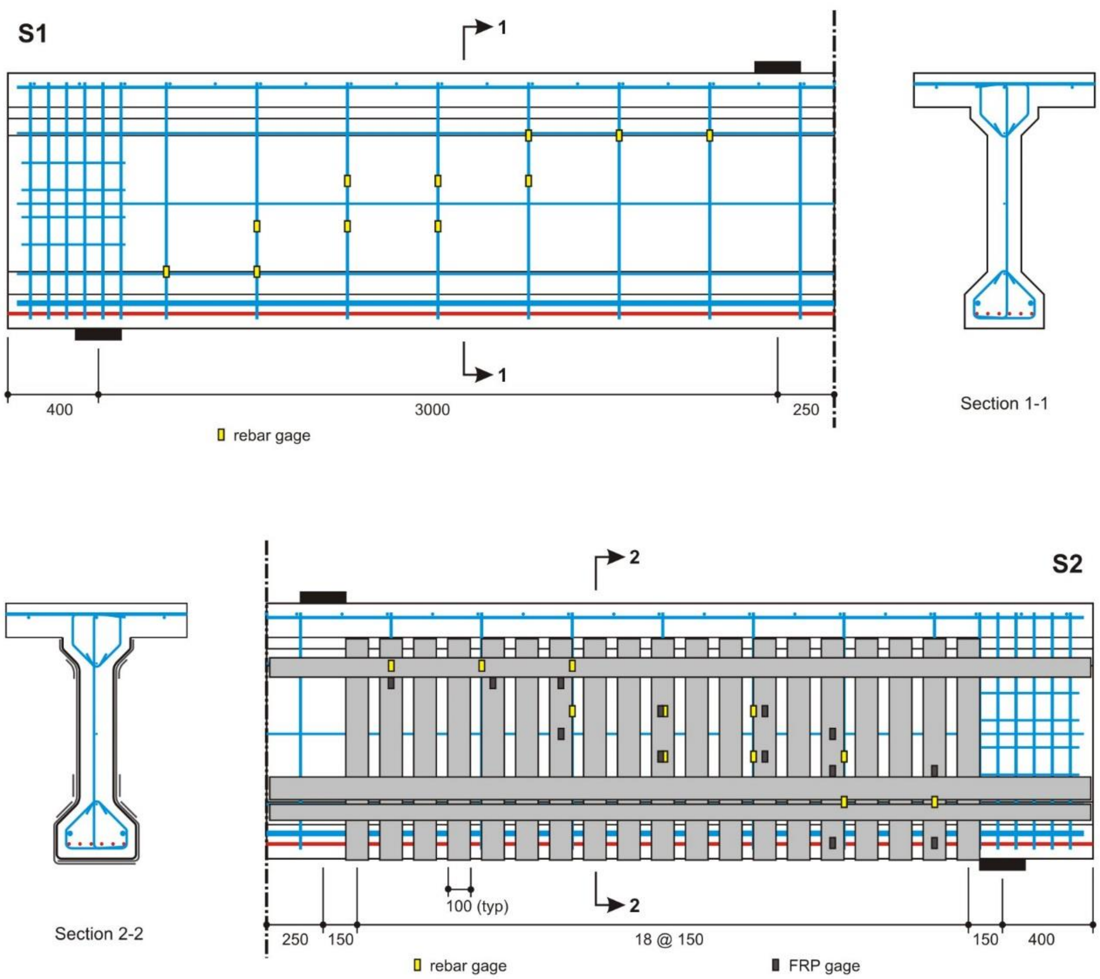

Figure 2.4: Details of specimens S1 and S2 (girder 1) (units: mm)

Girder 2, as shown in Figure 2.5 contains specimens S3 and S4. Both specimens are reinforced with vertical FRP strips at a spacing of 200 mm. Specimen S3 has no horizontal anchorage strips or curved epoxy putty transition at the re-entrant corners. Specimen S4 has the same horizontal anchorage as specimen S2 with one at the top of the web and two at the bottom as well as the curved putty transition at the re-entrant corners.

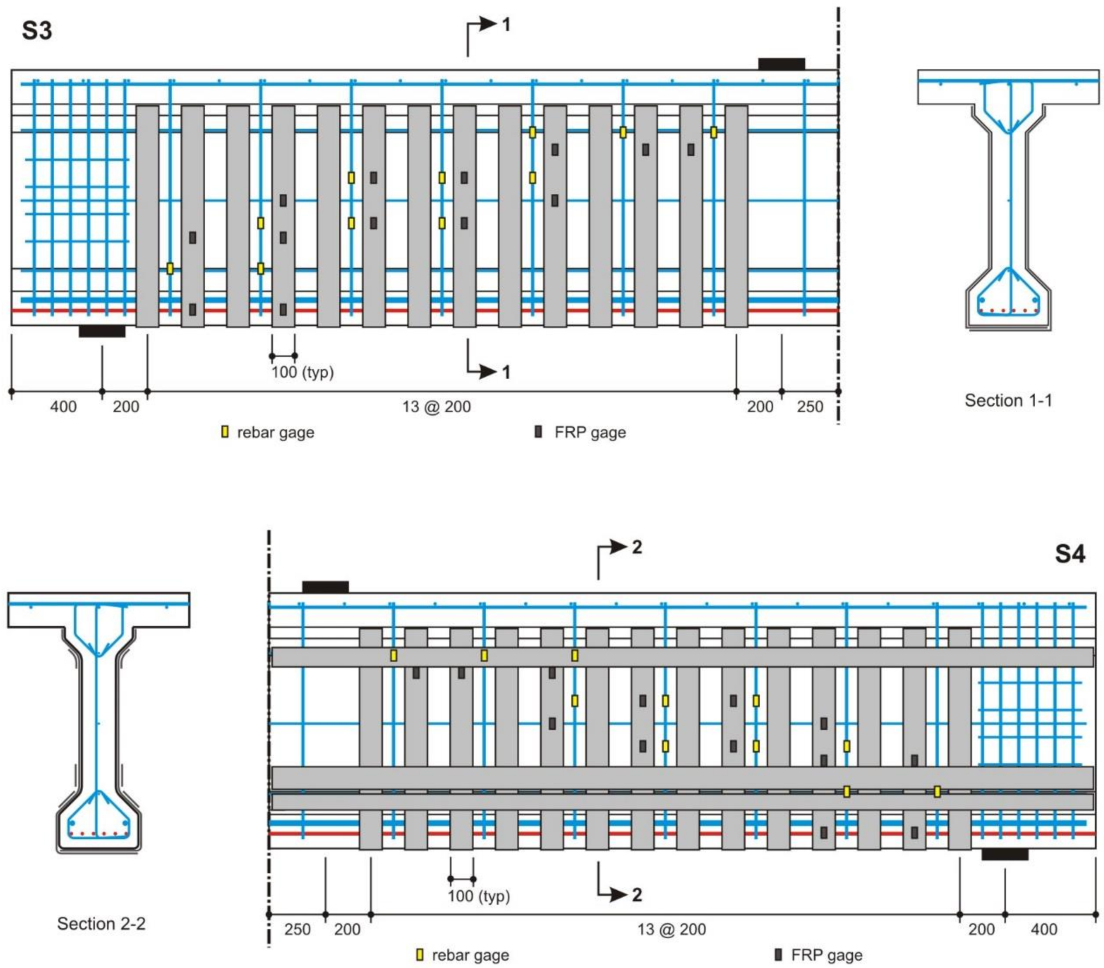

Figure 2.5: Details of specimens S3 and S4 (girder 2) (units: mm)

2.2 Construction

2.2.1 Pretensioning, Casting and Strand Release

Figure 2.6 shows the different sections of the prestressing bed as well as the hydraulic pretensioning operation. The stressing bed consisted of a self-reacting steel frame between the stressing end and dead (fixed) end and can be seen beside the girder in Figure 2.2a and 2.2b. Rectangular HSSs were used for the pretensioning frame and were bolted down through the laboratory strong floor in order to prevent buckling. The ends of the stressing bed consisted of built-up structural steel channels with appropriately spaced holes through which the strands could pass.

The six strands were anchored at the dead end using wedge anchorages provided by the manufacturer (Fig. 2.6a). The hollow hydraulic cylinder was then used to pretension the strands starting with the outermost strands and working inward (Fig. 2.6c). The hydraulic pressure was monitored to ensure that the correct force was applied to each strand. The strands were tensioned to a stress level corresponding to $0.7f_{pu} = 0.7 \times 1860 = 1302\ MPa\ 0.7f_{pu}$. In order to minimize prestressing losses due to anchorage set, the strands were first stressed to the desired level and then retracted to allow the anchor wedge to set. Once all strands were tensioned and anchors set, the operation was repeated a second time at which point the anchorage set was taken up using steel shims (Fig. 2.6b).

The concrete was ordered from a ready-mix plant and delivered to the Jamieson Structures laboratory at McGill University. The concrete was placed into a hopper attached to the overhead gantry crane for better control of the casting process. Concrete vibrators were used to consolidate the concrete with special care taken to ensure the internal strain gauges were not damaged. The girder surface was trowelled flat and the concrete allowed to moist cure covered in wet burlap and plastic sheeting for three days at which point the side formwork was removed (Figure 2.7).

(a) Dead end anchorage

(b) Steel shims used for second stressing of strands

(c) Stressing with hydraulic jack

Figure 2.6: Prestressing operation

(a) Girder during moist curing

(b) Girder and stressing bed after form removal

Figure 2.7: Concrete curing

After about five days, the concrete had reached a compressive stress of about 30 MPa and the prestress transfer was carried out. The prestressing release was carried out by flame cutting with an oxyacetylene torch (Figure 2.8a). The strands were released starting with the innermost strands and working outwards. The torch operator was sure to preheat the strands before cutting. The girder end after flame cutting can be seen in Figure 2.8b.

(a) Flame cutting of strands at dead end anchorage

(b) Girder end view after prestressing strand release

Figure 2.8: Prestressing strand release

2.2.2 FRP Application

The FRP strips were applied using the dry-layup technique as specified by the manufacturer, MAPEI Inc. Figure 2.9 shows the steps taken to prepare the concrete surface for the FRP application. The concrete was first bush-hammered using a rotary hammer power tool with a specialized bush-hammer bit. The purpose of this is to roughen the concrete substrate to ensure good adhesion with the FRP. The concrete surface was then brushed and vacuum in order to remove any loose debris. On the day of FRP application, the first step taken was to prime the surface using MapeWrap Primer 1 SP. The primer is a low viscosity epoxy resin which serves to consolidate and prime the surface. It is applied with normal paint rollers.

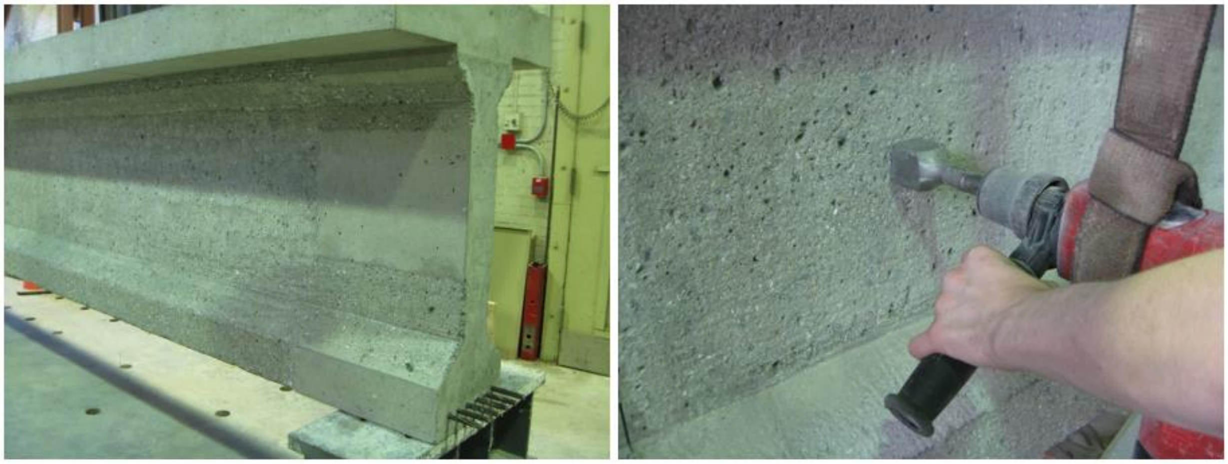

(a) Bush hammering of concrete surface

(b) Epoxy primer application

Figure 2.9: Preparation of concrete surface before FRP application

Figure 2.10 shows the steps taken in the application of the FRP shear strengthening fabric. The next step was to level the concrete surface through the application of MapeWrap 11 levelling putty (Fig. 2.10a). The putty is a two-component thixotropic epoxy paste which is applied with notched trowels and then smoothed with wide putty knives. Care is taken to ensure that the putty was worked into all the small pockets formed through bush-hammering. Specimens S2 and S4 received a curved transition using the levelling putty applied with a custom tool cut to a curved radius (Fig. 2.10b). This transition was formed at the re-entrant corners between the web and the two flange in order to improve the bond of the vertical FRP strips.

Figure 2.10c shows the dry-layup technique specified by the manufacturer. MapeWrap 31 epoxy resin is rolled in a thick layer onto the levelling putty at the surface of the girder where the FRP strips will be located. The vertical FRP strips are then placed onto this layer and are held in place by the gelatinous resin. A second layer of resin is then applied to the outer surface of the FRP strips in order to impregnate the fabric. A special grooved roller is then used to force the epoxy to completely saturate the fabric and remove air pockets. The horizontal FRP strips are then applied in the same manner. Figure 2.10d shows specimen S2 after the vertical and horizontal strips have been applied.

(a) Epoxy levelling putty application

(b) Forming curved transition at re-entrant corner

(c) Wet-layup of vertical FRP strips

(d) Vertical and horizontal FRP strips bonded to Specimen S2

Figure 2.10: Application of FRP strips

2.3 Test Setup and Instrumentation

2.3.1 Test Setup

Figures 2.11 and 2.12 show the test setup used in the experimental program. The 7.30 m long girders were loaded at two points located 250 mm on either side of midspan. The loads were applied using threaded rods passing through the strong floor and being tensioned by hydraulic jacks reacting against the strong floor as illustrated in Figure 2.13. The supports are located 400 mm from the end of the girders and are made up of rockers and rollers. All loading and bearing plates are 200 mm in length, giving a shear span of 3.00 m measured centre-to-centre of the loading and bearing plates. Wooden blocks placed under the girder (Fig. 2.12) serve to catch the girder and limit displacement if a brittle shear failure were to occur.

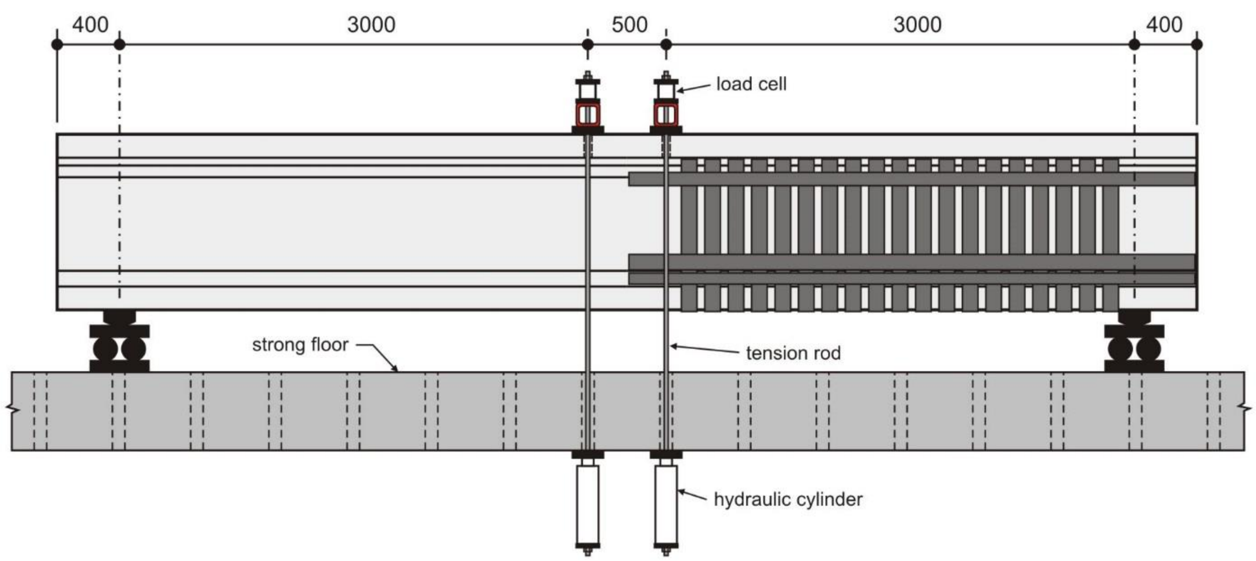

Figure 2.11: Girder test setup schematic (units: mm)

Figure 2.12: Girder test setup

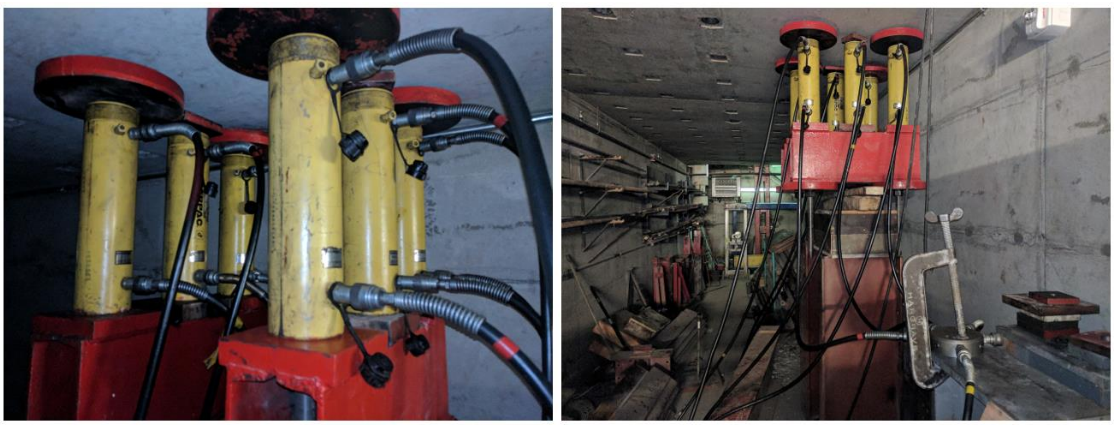

Figure 2.13: Hydraulic loading jacks underneath laboratory strong floor

2.3.2 Instrumentation

Figure 2.14 shows some of the instrumentation used in this experimental program. In order to eliminate support settlement in the analysis, linear variable differential transformers (LVDT's) were placed at each support to measure vertical displacement (Fig. 2.14a). The applied shear was measured using load cells under each of the four loading points (Fig. 2.14b). The displacement at midspan was measured using a string potentiometer under each loading point (Fig. 2.14c). Additionally, the longitudinal displacement of the tension face of the girders was measured using an LVDT (Fig. 2.14c near top of image) in order to determine flexural strains.

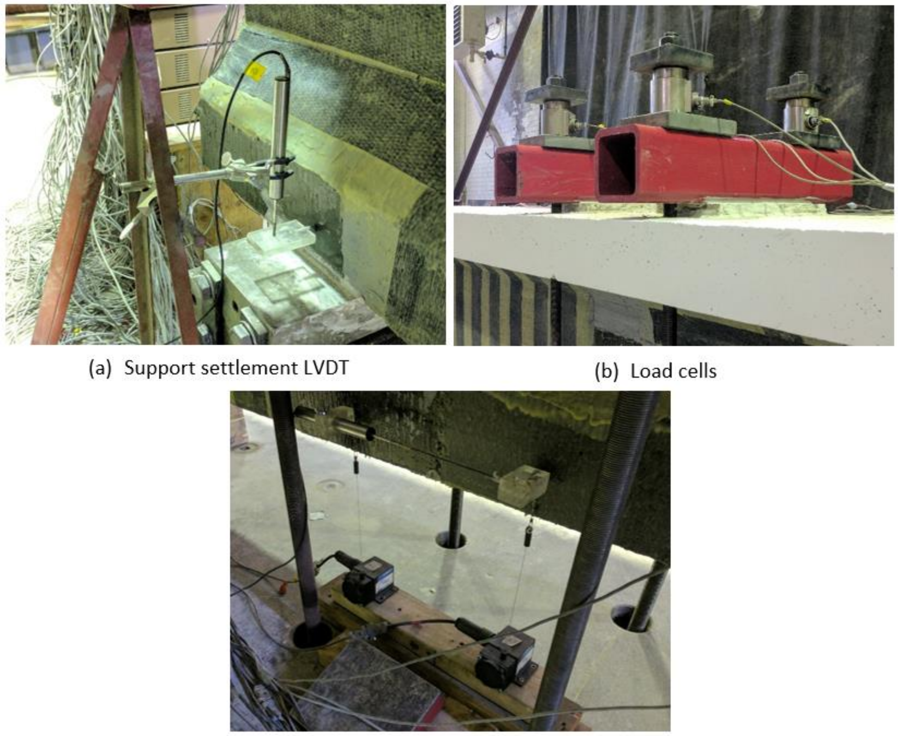

(a) Support settlement LVDT

(b) Load cells

(c) String potentiometers and midspan tension flange LVDT

Figure 2.14: Instrumentation for measuring support settlement, applied shear, midspan deflection and longitudinal displacement at tension face of the girders

Figures 2.4 and 2.5 (Section 2.1.2) show the stirrup and FRP strain gauge placement. To measure strain in the stirrups and FRP, each specimen was instrumented with eleven stirrup strain gauges and thirteen FRP strain gauges. Their locations were chosen to monitor strains as close as possible to the predicted critical shear crack. These strains were used to determine corresponding stresses and ultimately the various components of shear resistance. An additional strain gauge was also placed on each longitudinal 25M reinforcing bars in order to monitor yielding of the flexural reinforcement.

LVDT rosettes were also attached to the side of the web on each specimen. The rosettes consisted of nine LVDTs for each specimen. Details of the LVDT rosette placement with respect to the stirrup strain gauges are shown in Figure 2.15. The LVDT rosettes were placed in order to monitor the concrete strains as close as possible to the centre of the shear span while avoiding drilling into the FRP strips adhered to the surface of the web. Figure 2.16 shows photos of the LVDT rosettes in place on specimen S4.

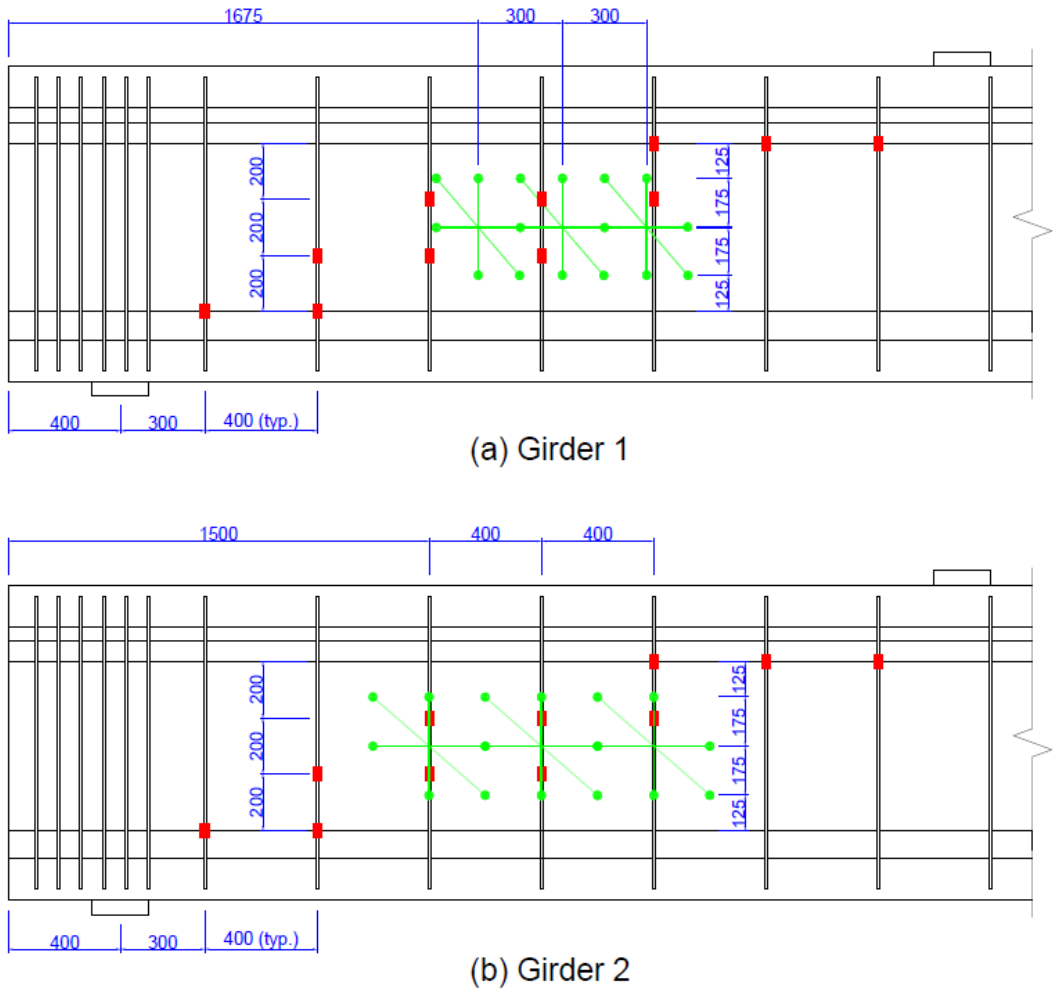

Figure 2.15: Instrumentation showing LVDT rosette locations with respect to stirrup strain gauges for (a) Girder 1 (specimens S1 and S2) and (b) Girder 2 (specimens S3 and S4) (units: mm)

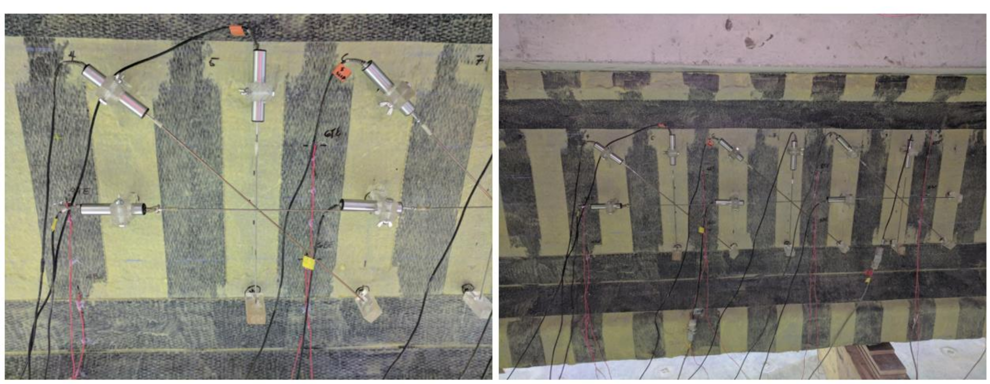

(a) LVDT rosette

(b) LVDT rosette configuration

Figure 2.16: LVDT rosette details for specimen S4

2.4 Material Properties

2.4.1 Concrete

The girders were cast using two batches of ready-mix concrete. Batch 1 was used for girder 1 (specimens S1 and S2) and batch 2 was used for girder 2 (specimens S3 and S4). The concrete was moist cured for three days in the formwork while covered by wet burlap and plastic sheeting to retain moisture. After three days, the burlap and plastic was removed and the girders allowed to cure at room temperature conditions until prestress release was carried out. The mix proportions as provided by the ready-mix plant are given in Table 2.1.

Table 2.1: Concrete mix proportions

Component	Quantity per m^3
Type GU blended cement (granulated slag and silica fume)	360 kg
Concrete sand	763 kg
10-20 mm limestone aggregate	640 kg
5-14 mm limestone aggregate	427 kg
Water	143 L
Air	6.5 %
Air entraining agent (ml/100 kg)	14.72 ml/100 kg
Retarding agent	174.00 ml/100 kg
High-range water-reducing admixture	0.23 L

Prior to placing the concrete, the slump and air content were measured. Batch 1 had a slump of 215 mm and an air content of 8 %. Batch 2 had a slump of 200 mm and an air content of 8.5 %.

Compression and split-cylinder tests were carried out on cylinders which were 100 mm in diameter and 300 mm in length in accordance with the CSA A23.2-12C-14 (2014) standard. Four-point bending tests were carried out with rectangular beams measuring 100 mm square and 300 mm in length in accordance with the CSA A23.2-8C-14 (2014) standard.

The concrete material tests were performed to determine the average concrete compressive strength ($f_c{}'$), the splitting tensile strength (f_{sp}) and the modulus of rupture (f_r) of the concrete in accordance with CSA A23.2-9C-14 (2014), CSA A23.2-13C-14 (2014) and CSA A23.2-8C-14 (2014) respectively. The concrete material properties thus determined are presented in Table 2.2. The table also contains the concrete compressive strengths at prestress transfer (5 days after casting for girder 1 and 6 days for girder 2). A typical compressive stress-strain relationship for the two concrete batches is shown in Figure 2.17.

Table 2.2: Concrete material properties

	Age at Testing	f_c' (MPa) (STDEV)	ε_c' (STDEV)	f_{sp} (MPa) (STDEV)	f_r (MPa) (STDEV)
Girder 1	5 days	28.5 (1.949)	0.00211 (0.001)	-	-
	70 days	40.7 (1.208)	0.00178 (0.000)	3.97 (0.374)	5.95 (0.301)
Girder 2	6 days	34.7 (0.632)	0.00178 (0.000)	-	-
	80 days	44.2 (2.159)	0.00174 (0.000)	4.11 (0.335)	6.25 (0.381)

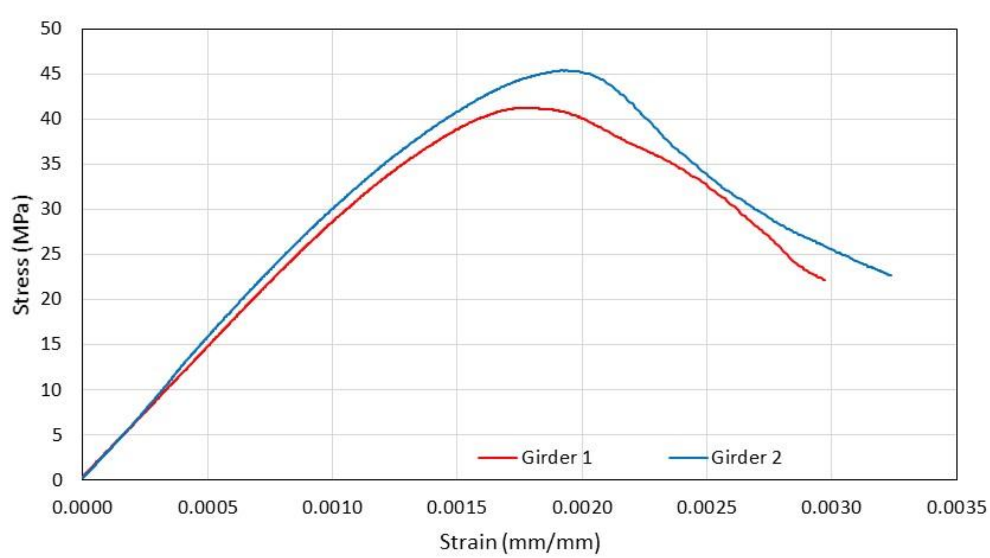

Figure 2.17: Typical concrete compressive stress-strain relationships for girders 1 and 2

2.4.2 Reinforcing Steel

All the deformed reinforcing bars used in this experimental program were weldable grade reinforcement in compliance with the CSA G30.18-09 (2009). Tension tests were carried out on three samples of each bar size and type in accordance with ASTM A615/A615M-16 (2016). The tension tests were used to determine the yield strength (f_y), ultimate strength (f_u), strain at onset of strain hardening (ε_{sh}) and strain at failure (ε_u). A summary of the reinforcing bar material properties resulting from the tensile tests can be found in Table 2.3. The 10M bars used for the stirrups and the longitudinal bars used in the web show different values because they came from different batches. The longitudinal bars were ordered in longer lengths to avoid having to splice shorter lengths together. A typical tensile stress-strain curve for each size and type of reinforcing bar can be found in Figure 2.18.

Table 2.3: Reinforcing bar material properties

	f_y MPa) (STDEV)	f_u (MPa) (STDEV)	ε_y (STDEV)	ε_{sh} (STDEV)	ε_u (STDEV)
10M Stirrups	431.1 (3.34)	543.7 (9.70)	0.00216 (0.001)	0.0193 (0.001)	0.199 (0.012)
10M Long. Bars	464.4 (12.80)	562.6 (9.15)	0.00232 (0.000)	0.0300 (0.001)	0.160 (0.009)
15M	471.9 (7.51)	590.4 (7.12)	0.00236 (0.000)	0.0236 (0.001)	0.144 (0.019)
25M	449.9 (1.33)	622.7 (0.71)	0.00225 (0.000)	0.0127 (0.001)	0.169 (0.006)

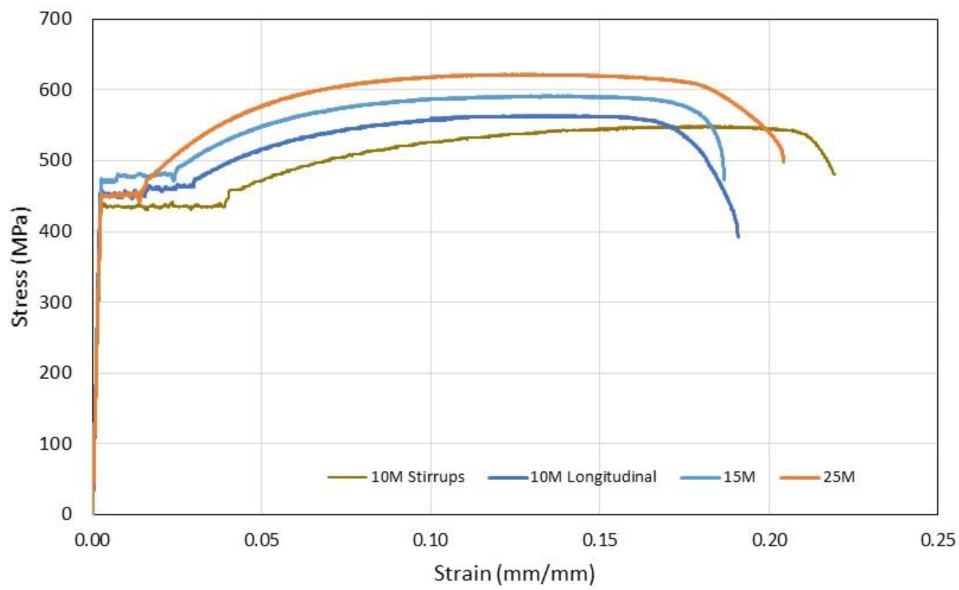

Figure 2.18: Typical tensile stress-strain curves for the reinforcing bars

2.4.3 Prestressing Steel

The prestressing steel used in this experimental program was low-relaxation 7-wire strand with a diameter of 15.24 mm, an area of 140 mm^2 and a minimum specified ultimate strength of 1860 MPa. The strand met the requirements of the ASTM A416/A416M-12 (2012) standard. The ultimate strength was 1949 MPa and the modulus of elasticity was 200.5 GPa. These values as well as the stress-strain curve given in Figure 2.19 were taken directly from the manufacturers data sheet for this particular batch of prestressing steel and were experimentally determined.

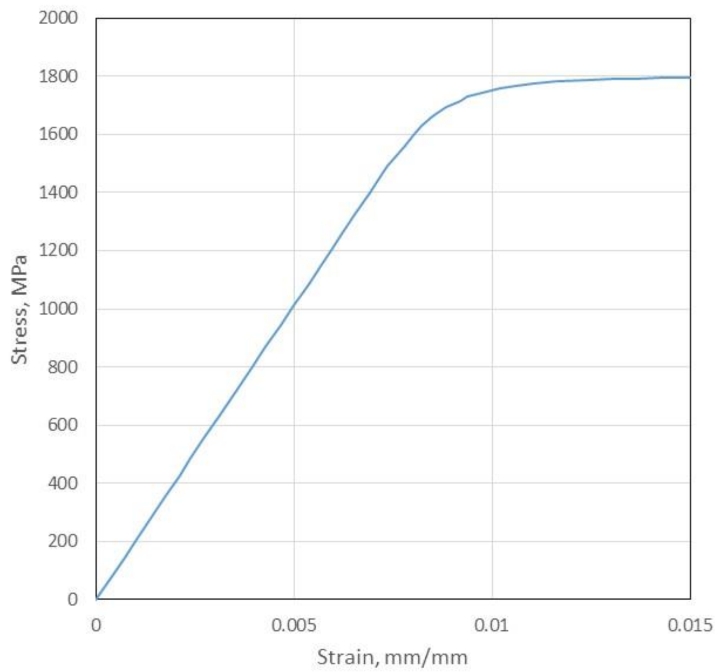

Figure 2.19: Tensile stress-strain curve for the 15.24 mm diameter low-relaxation prestressing steel

2.4.4 Carbon Fibre-Reinforced Polymer Strips

The FRP used in this experimental program were obtained from MAPEI Inc. The fabric made up of woven fibres is called MapeWrap C Uni-Ax 600 with a density of 600 gm/m^2. The fabric comes in a roll with a width of 100 mm and a thickness of 1.01 mm as per the manufacturer's specifications. The composite material (denoted with subscript "FRP") is made up of a woven unidirectional carbon-fibre fabric (denoted with subscript "f") and two-part epoxy resin matrix (denoted with subscript "m"). The properties of the individual components and of the composite as a whole are shown in Table 2.4 and were provided by the manufacturer.

Table 2.4: Fibres, epoxy matrix and FRP composite material properties

Symbol	Definition	Property
E_f	Tensile modulus of carbon fibre	252,000 MPa
f_f	Tensile strength of carbon fibre	4900 MPa
t_f	Thickness of carbon fibre	0.331 mm
v_f	Volumetric ratio of carbon fibre	0.33
E_m	Tensile modulus of epoxy matrix	2000 MPa
f_m	Tensile strength of epoxy matrix	30 MPa
E_{FRP}	Tensile modulus of composite	81,897 MPa
t_{FRP}	Thickness of composite	1.01 mm
f_{FRPu}	Tensile strength of composite	1448 MPa
ε_{FRPu}	Ultimate strain of composite	0.0177

3 Experimental Results

3.1 Specimen Behaviour

3.1.1 Girder 1

Girder 1, containing the control specimen, S1 and the most heavily reinforced specimen, S2 with vertical FRP strips at 150 mm and three horizontal strips was the first to be tested. The concrete compressive strength was 40.7 MPa. The testing took place in three segments. Specimen S1 was tested first and brought close to failure. Specimen S1 was then reinforced with external shear clamps and specimen S2 was brought to failure. These shear clamps consisted of rectangular HSSs on the top and bottom of the girder. The clamping was provided by pretensioned threaded rods passing through the steel sections and holes drilled in the girder top flange. The clamping configuration for specimen S1 is shown in Figure 3.1. Following the failure of specimen S2, the clamps were then repositioned to specimen S2 and specimen S1 was brought to failure.

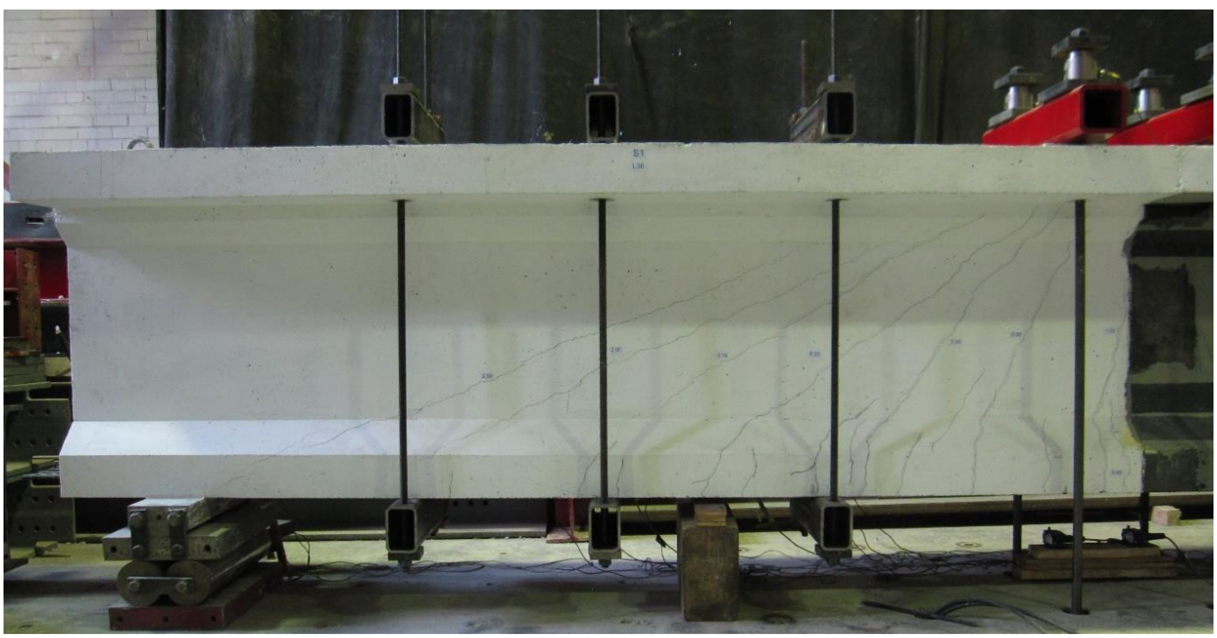

Figure 3.1: External shear clamps on specimen S1

3.1.1.1 Specimen S1

Loading of girder 1 initially took place in load stages of approximately 50 kN with time allowed between load stages for photos and record keeping. The first hairline flexural cracks began to appear at load stage L7 at an applied shear of 350 kN. The first clear shear crack appeared soon after at load stage L8 at an applied shear of 400 kN. The initial shear crack width was 0.15 mm and coincided with cracking noises coming from the FRP applied to specimen S2, indicating stress uptake. From this point onward loading took place in smaller increments of approximately 10 – 15 kN. At a shear of 458 kN, the maximum inclined crack width was 0.5 mm, indicating yielding of the stirrups. New shear and flexural cracks began to appear, and the existing ones continued to widen until an applied shear of 532 kN was reached at load stage L17. As shown in Figure 3.2, significant diagonal shear cracks with a maximum width of 2.50 mm had appeared at this stage and the loading was stopped in order to strengthen specimen S1 with external shear clamps. This was done in order proceed with the testing of specimen S2 without fear of catastrophic failure of specimen S1.

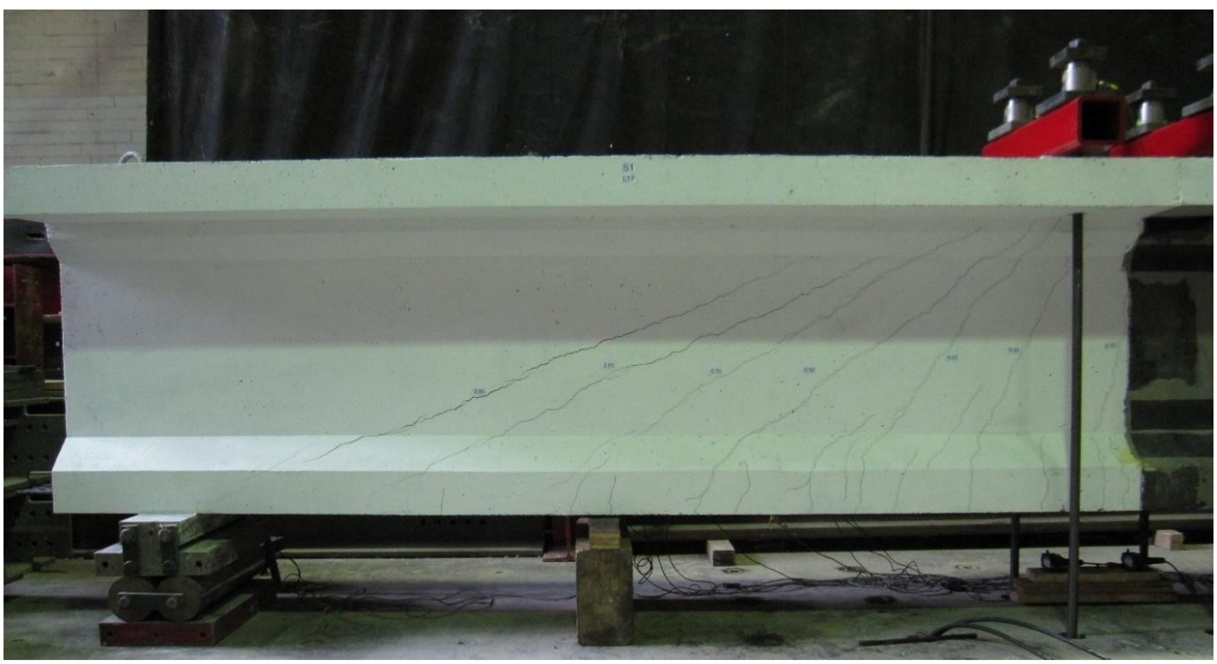

Figure 3.2: Specimen S1 at a shear of 532 kN and maximum shear crack width of 2.50 mm

After testing specimen S2 to failure, the clamps were removed from specimen S1 and placed on specimen S2 to allow further testing of the control specimen starting at load stage L38. The specimen was first loaded to near the load achieved from previous testing. Figure 3.3 shows the failure of specimen S1 occurring after load stage L49. The maximum applied shear achieved was 660 kN at load stage L46. The diagonal shear cracks present in the web had widened to 14.0 mm prior to failure. Failure of the specimen occurred when the shear cracks progressed through the top and bottom flanges. The transverse steel stirrups ruptured at failure. Figure 3.3 also shows the bending of the top and bottom flanges in the region of significant inclined cracks. This illustrates the web restraint provided by the flanges of I-girders.

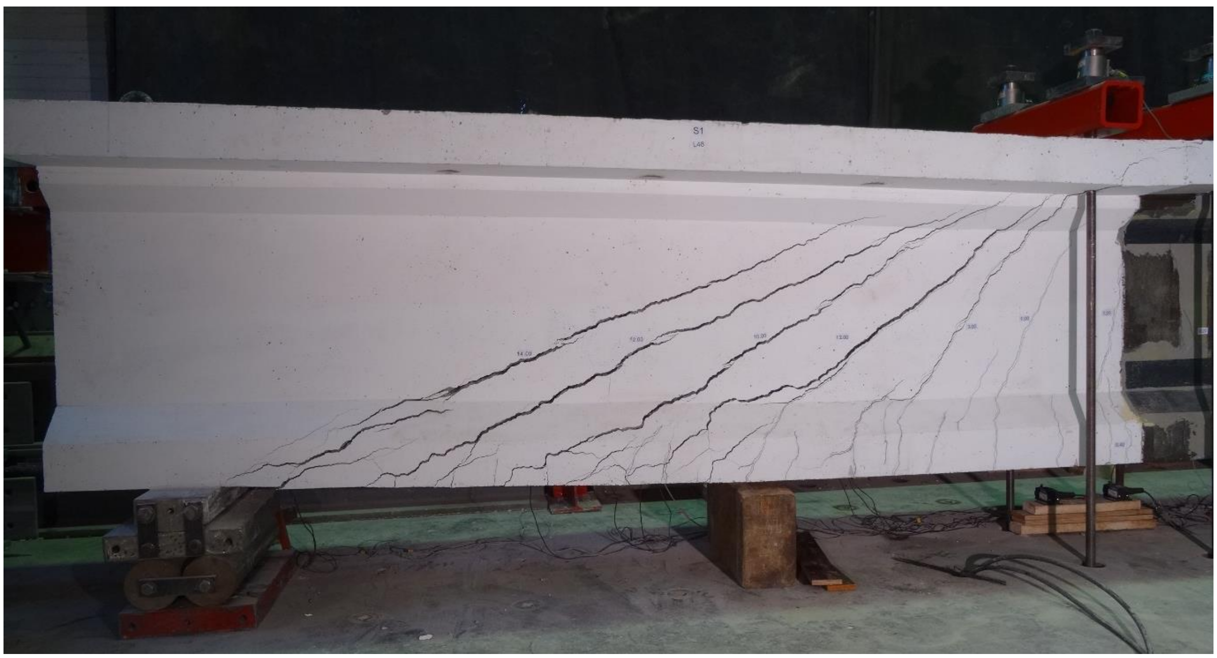

Figure 3.3: Failure of specimen S1

3.1.1.2 Specimen S2

Cracks began to appear on specimen S2 during the initial testing of specimen S1 when the specimen was unclamped. Diagonal shear cracks appeared at an applied shear of around 450 kN which was 15 kN higher than the control specimen S1. These cracks were well controlled by the FRP and remained consistently at a width of 0.10 mm throughout the initial loading of specimen S1. During this same period, specimen S1 showed a maximum shear crack width of 2.5 mm.

As stated above, specimen S2 was tested after the initial testing of specimen S1 and prior to the final test of the control specimen in which it was brought to failure. During the entire testing of specimen S2, specimen S1 was reinforced using external shear clamps. The loading was started at load stage L19 and progressed in 50 kN increments until an applied shear of 550 kN at load stage L30 which coincided with the load reached during the initial testing of specimen S1. Loading then progressed at smaller increments.

At load stage L32 and an applied shear of 625 kN, the shear cracks had reached a maximum width of 0.20 mm and it was noticed that FRP strips 5, 6 and 10 had begun to delaminate near the bottom of the web above the horizontal strips. It was noticed at the following load stage L33 that eight of the nineteen FRP strips had begun to delaminate at the crack locations at a shear of 645 kN. This was in addition to the delamination occurring at the bottom of the web. The delamination was observed by the hollow sound produced by tapping the FRP strips in addition to a discolouration of the epoxy surrounding and adhered to the FRP strips.

The maximum applied shear of 660 kN occurred at load stage L34. The girder at this load stage can be seen in Figure 3.4. The excellent crack control exhibited by the FRP strips is illustrated by the fact that the crack widths at this stage had only reached 0.35 mm despite strips four through twelve exhibiting varying degrees of delamination. Full delamination began to occur between load stages L34 and L35 and the applied shear dropped to 600 kN. The diagonal shear cracks jumped up in width at this point to 2.5 mm. The load was then increased until a brittle shear failure caused by debonding of FRP strips one through seventeen occurred. Specimen S2 at this stage is shown in Figure 3.5. The figure also shows the bending of the top and bottom flanges of the I-girder indicating that they provided vertical restraint that enhanced the shear strength of the web.

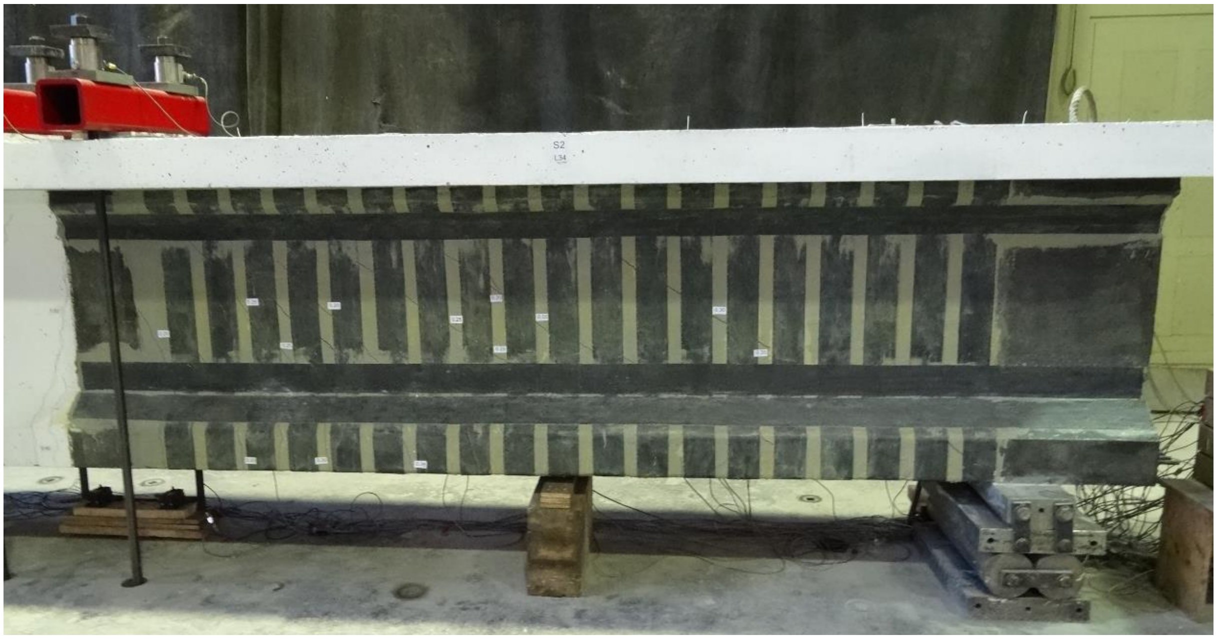

Figure 3.4: Specimen S2 at a shear of 660 kN and maximum crack width of 0.35 mm

Figure 3.5: Failure of specimen S2

3.1.2 Girder 2

The vertical FRP strips applied to girder 2 were spaced at 200 mm on both shear spans. Specimen S3 had no horizontal anchorage strips whereas specimen S4 had three anchorage strips at the top and bottom of the web as well as on the inclined portion of the bottom flange, identical to specimen S2. The internal reinforcement was identical to girder 1 and the concrete compressive strength was 44.2 MPa. The girder was tested in three segments. Specimen S3 was brought to failure first and then clamped. The clamping configuration for specimen S3 is shown in Figure 3.6. Specimen S4 was then tested and due to the concerns of achieving flexural failure, the shear span was reduced by repositioning the supports and the specimen was then loaded to achieve a shear failure. The new shear span was reduced from to 2.7 m.

e


Figure 3.6: External shear clamps on specimen S3

3.1.2.1 Specimen S3

The loading took place in load stages in which a shear of 50 kN was applied incrementally. Initial midspan flexural cracking occurred at load stage L8 at an applied shear of 365 kN. The first shear crack on specimen S3 occurred at an applied shear of 447 kN at load stage L10. The diagonal crack was 0.05 mm in width while the vertical flexural crack had reached a width of 0.10 mm. The FRP began to make audible cracking noises while loading was stopped between load stages L13 and L14 at around 543 kN. At this point there were multiple diagonal shear cracks, the largest of which had reached a width of 0.25 mm. Delamination near the bottom of FRP strip six began at 595 kN. At an applied shear of 656 kN, the shear cracks were well controlled compared to the control specimen S1. They had reached a maximum width of 0.50 mm which was about 0.15 mm larger than those exhibited in specimen S2. Specimen S3 at this stage can be seen in Figure 3.7.

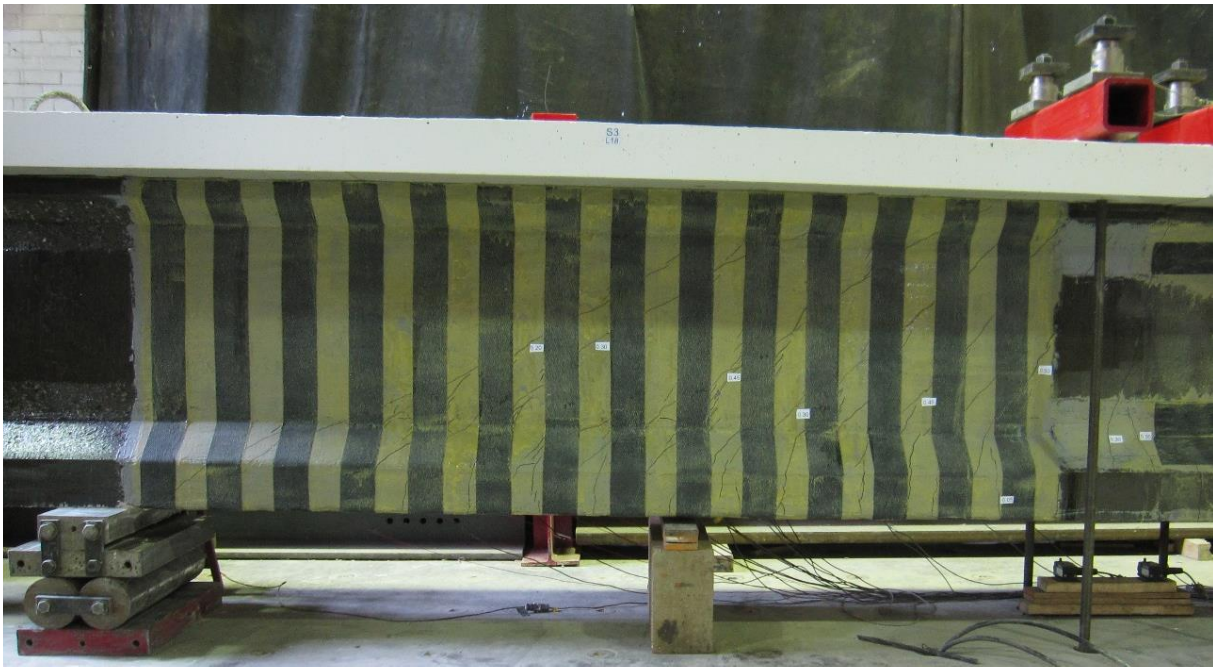

Figure 3.7: Specimen S3 at a shear of 656 kN and a maximum crack width of 0.50 mm

Prior to failure, delamination of strips six and nine through twelve had begun. This was less warning than had been provided by specimen S2 which had shown more delamination as indicated by epoxy discolouration and hand taping. Failure of specimen S3 occurred after reaching a maximum applied shear of 665 kN as shown in Figure 3.8. It was a brittle shear failure caused by delamination and loss of anchorage of the FRP shear strips. The loss of anchorage was noticed to occur mainly in the region of the re-entrant corners which did not have horizontal anchorage strips. The major shear crack occurred in the web and crossed the top and bottom flanges. Severe damage was done to the web and flanges in the area surrounding the primary shear crack and many of the 10M stirrups were ruptured at failure.

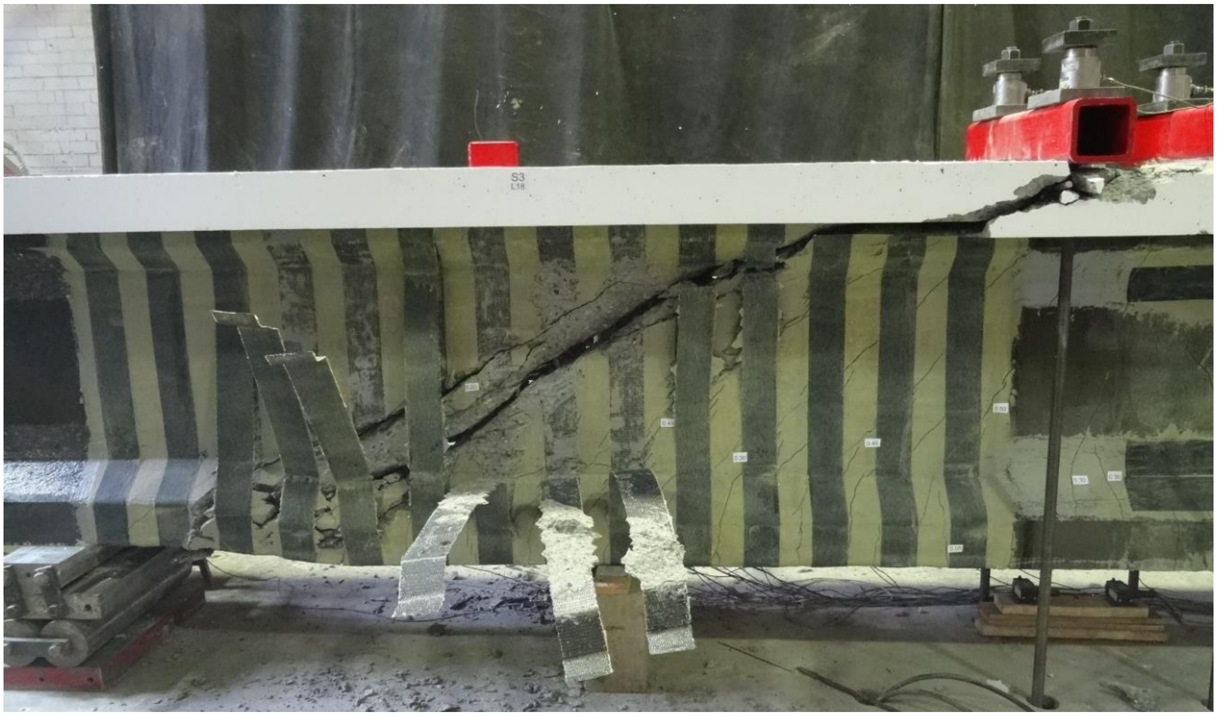

Figure 3.8: Failure of specimen S3

3.1.2.2 Specimen S4

Before testing began, specimen S3 was repaired using concrete compacted into the severe shear cracks that passed through both the web and flanges. Pretensioned shear clamps and steel plates at both the top and bottom flanges were used to increase the capacity of specimen S3 and ensure that specimen S4 could be tested.

The testing of specimen S4 began similarly to the other specimens but was quickly brought up to an applied shear of 560 kN by the load stage L21 which was the first of the test. Both the shear and flexural cracks had reached a maximum width of 0.30 mm at this stage. The first signs of delamination in FRP strips seven through fourteen began to show at an applied shear of 652 kN with crack width of 0.60 mm in shear and 1.00 mm in flexure. The delamination was visible near the mid-height of the web. The maximum load achieved with this shear span was 687 kN at load stage L27. At this stage the flexural cracks were significant. It was decided that the specimen could fail in flexure and the testing was stopped.

In order to ensure shear failure rather than flexural failure, the shear span of the girder was reduced from 3.0 m to 2.7 m on both ends of the girder. Specimen S4 was then brought up to the maximum applied shear seen previously of 687 kN. Specimen S4 at this applied shear can be seen in Figure 3.9. The crack widths were the same as with the shorter shear span at 2.0 mm in flexure and 0.70 mm in shear. Significant cracking noises, indicating FRP delamination were audible at an applied shear of 722 kN. Figure 3.10 shows the shear failure which occurred after debonding of the FRP strips near the middle of the shear span. The extremely brittle shear failure occurred after a peak applied shear of 742 kN was reached. As can be seen by the creasing of the anchorage strips in the figure, the horizontal CFRP strips helped to improve the anchorage of the vertical shear strips at the re-entrant corners.

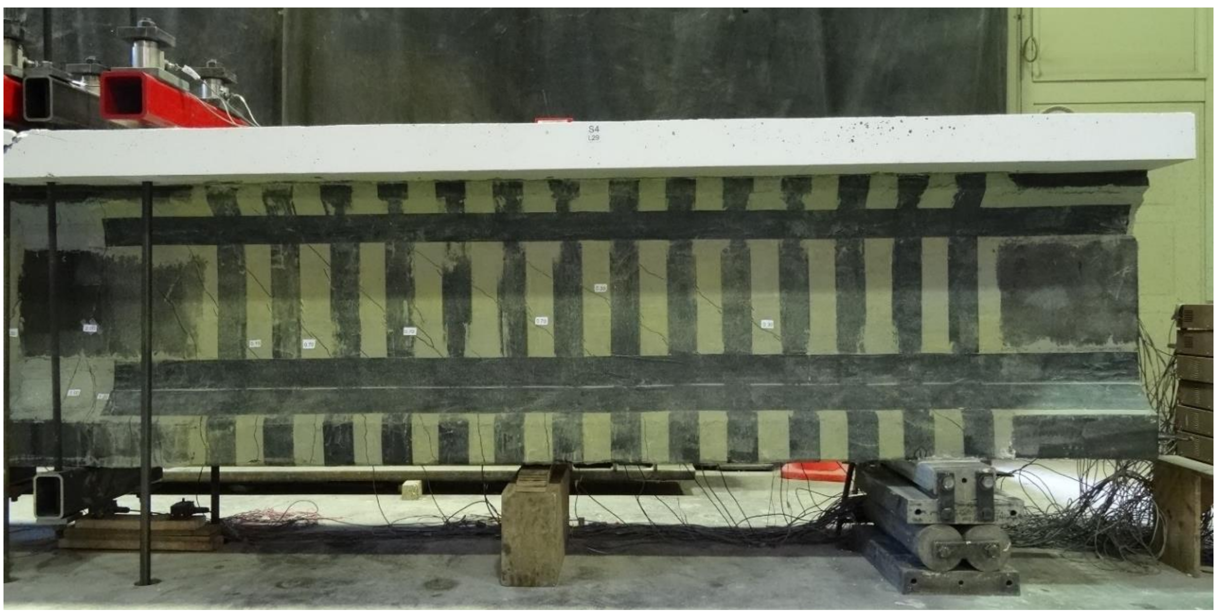

Figure 3.9: Specimen S4 at a shear of 687 kN and a maximum shear crack width of 0.70 mm

Figure 3.10: Failure of specimen S4

3.2 Shear vs. Maximum Shear Crack Width

Figures 3.11 and 3.12 show the responses of the specimens in terms of the applied shear vs. the measured maximum shear crack width. To keep the scale of the figures readable, specimen S1 is not shown to failure and the graphs are truncated at a crack width of 6.0 mm in Figure 3.11 and 1.0 mm in Figure 3.12. The figures show the significant decrease in shear crack width that comes with the application of FRP shear strips.

Specimen S1 reached a relatively high failure load but experienced severe web cracking with shear cracks reaching a maximum width of 14 mm prior to shear failure at an applied shear of 660 kN. The graph for specimen S1 becomes horizontal and very large shear cracks begin to form in the web at an applied shear of approximately 458 kN. At this point the web was considered to be failing in shear and any additional load increase was due to the flexural stiffness of the top and bottom flanges. Complete failure of the control specimen did not occur until the critical inclined crack penetrated the stiff top and bottom flanges of the I-girder. Figures 3.11 and 3.12 show the beneficial effects of CFRP shear strips in controlling shear cracking when compared to unstrengthened I-girders. The specimens with CFRP shear strips, namely S2, S3 and S4 failed by debonding of the CFRP strips, resulting in extremely brittle shear failures.

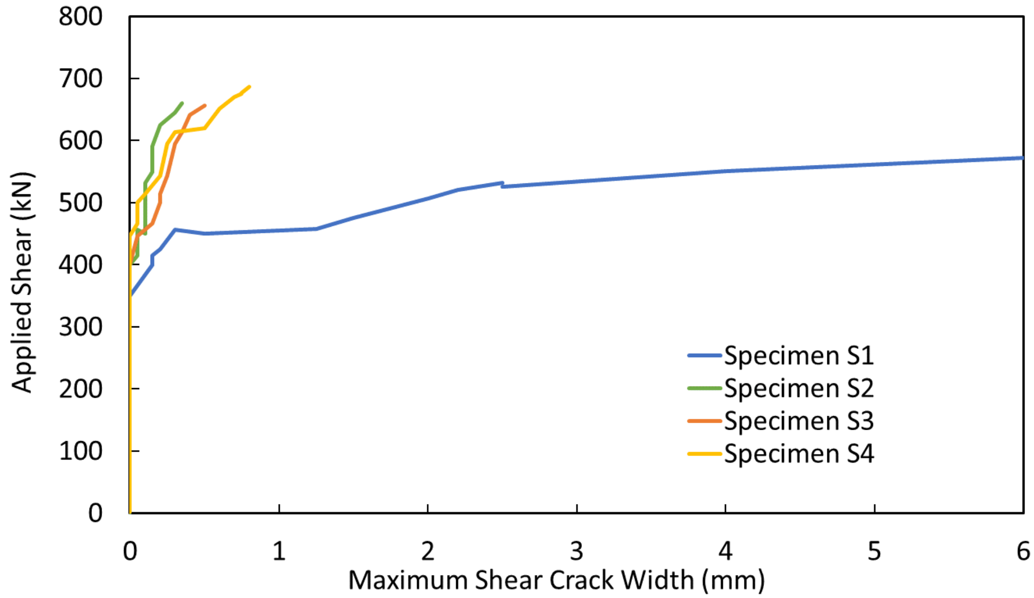

Figure 3.11: Shear vs. maximum shear crack width showing vastly increased crack widths in specimen S1

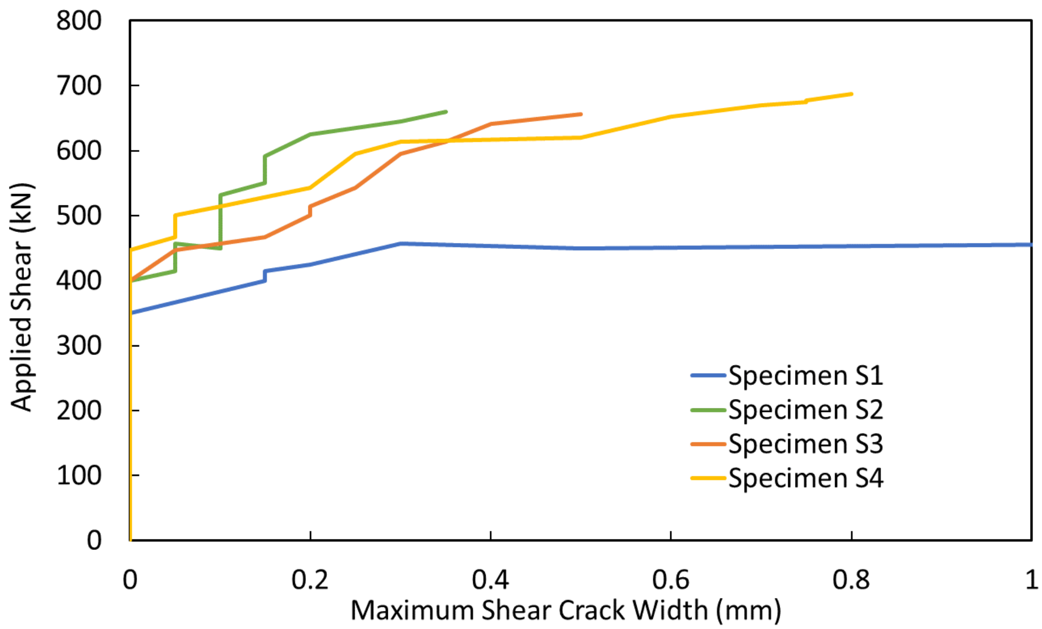

Figure 3.12: Shear vs. maximum shear crack width showing greater detail for specimens S2, S3 and S4

3.3 Shear-Deflection Response

Figure 3.13 shows the responses of the four specimens in terms of the shear versus deflection graph. The deflection was taken as the average of the deflections at the two load locations while the shear was determined from the load cell readings. The increased strength and stiffness of specimen S4 near failure was due to the reduction in shear span required to achieve shear failure. It is clear that the specimens with FRP shear strips (S2, S3 and S4) did not show a significant increase in shear resistance compared to the control specimen S1. However, the CFRP vertical strips significantly enhanced the performance of the webs, with specimen S1 experiencing general yielding of the stirrups starting at a load of 458 kN.

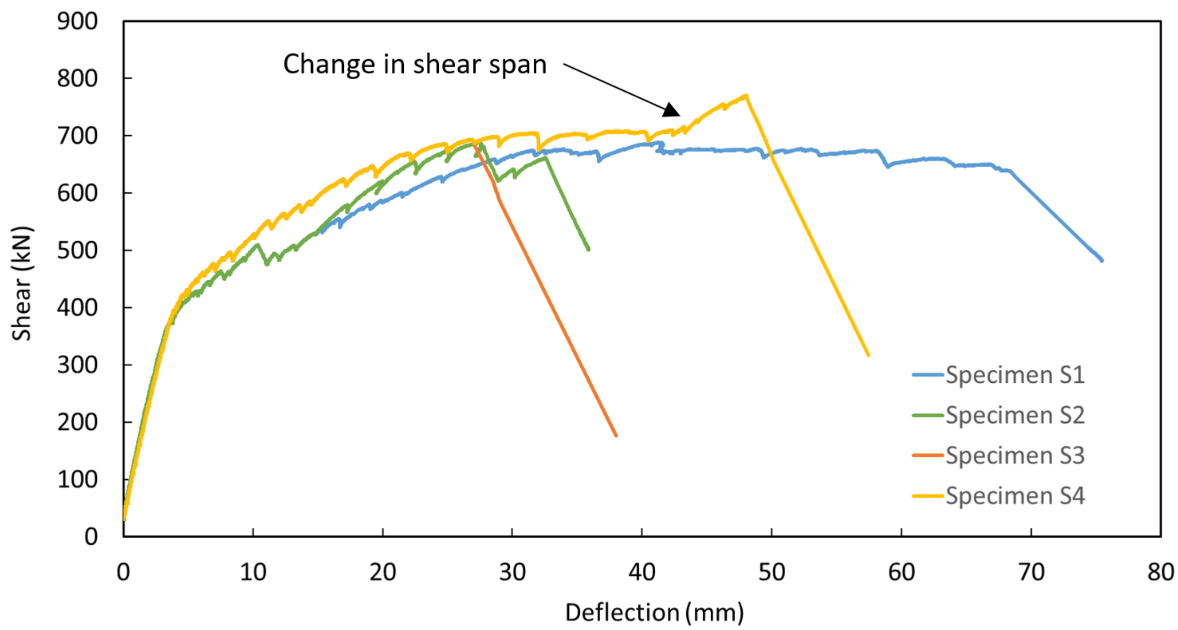

Figure 3.13: Comparison of load vs. deflection response of the four test specimens

3.4 Components of Shear Resistance

In order to quantify the additional shear resistance provided by the FRP, the results from the strain measurements on the steel stirrups and FRP strips were employed to estimate the components of shear resistance at each load level. The stirrups and FRP strips crossed by the major inclined shear crack were first determined from photos of the specimens taken after the test. These photos were used to produce drawings of the major shear crack patterns as shown in

Figure 3.14. From the crack patterns, free-body diagrams of the specimens separated along the critical shear crack could be constructed as shown in Figure 3.15. The locations of the external FRP strips and the locations of the stirrups were used to determine which internal steel stirrups and which CFRP strips were crossed by the crack.

The strain measurements taken closest to the major inclined shear crack were then used to determine the stresses and hence the forces carried by the stirrups and FRP strips at each load level. The shear components carried by the stirrup (V_s) and the vertical FRP strips (V_{FRP}) were determined by summing these forces for the stirrups and strips crossed by the critical crack. The shear component carried by the concrete (V_c) was then taken as the total shear (V_{test}) minus the shear components carried by the stirrups and FRP strips. This approach was also taken by Belarbi et al. (2011) in their assessment of pretensioned I-girders strengthened in shear using FRP strips. The results of the shear component calculation can be seen in Figure 3.16.

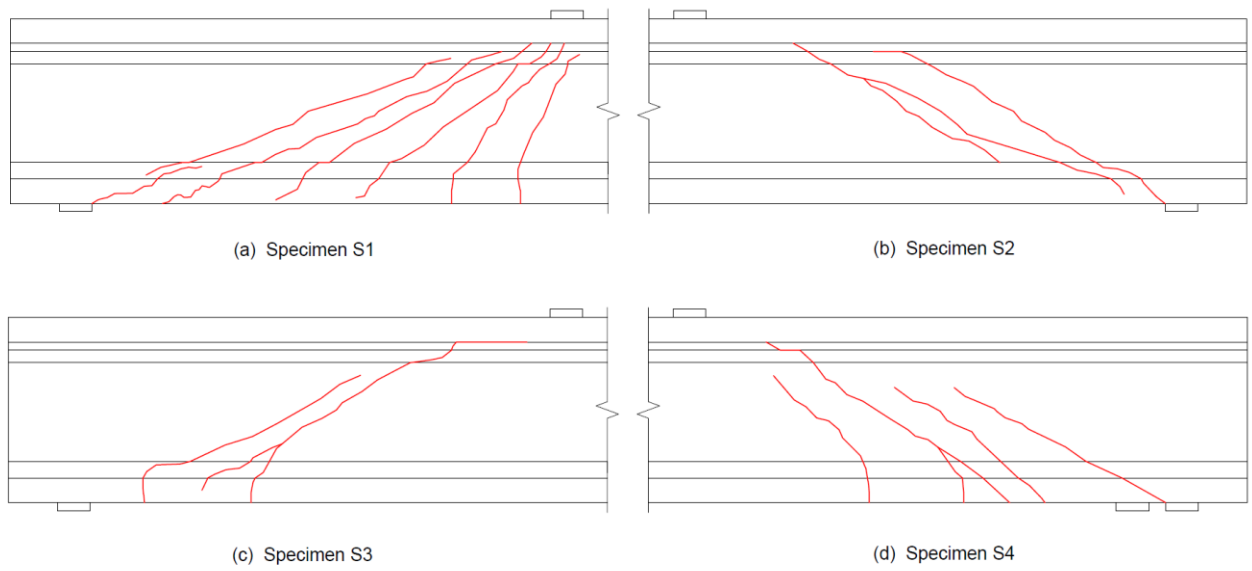

Figure 3.14: Major shear crack patterns

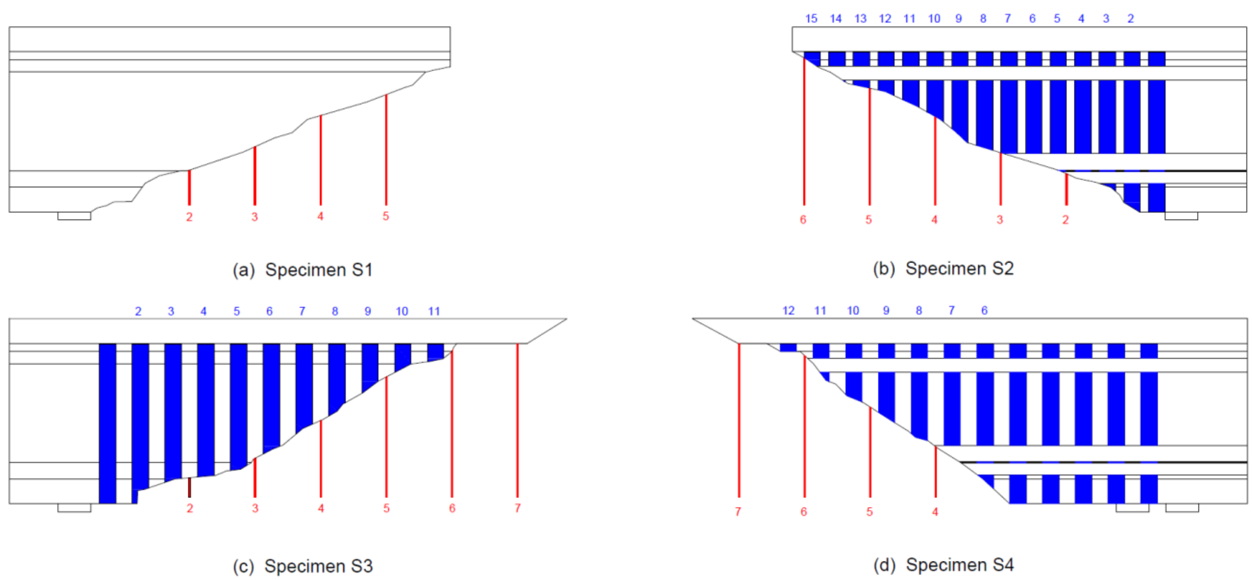

Figure 3.15: Free-body diagrams for shear component analysis

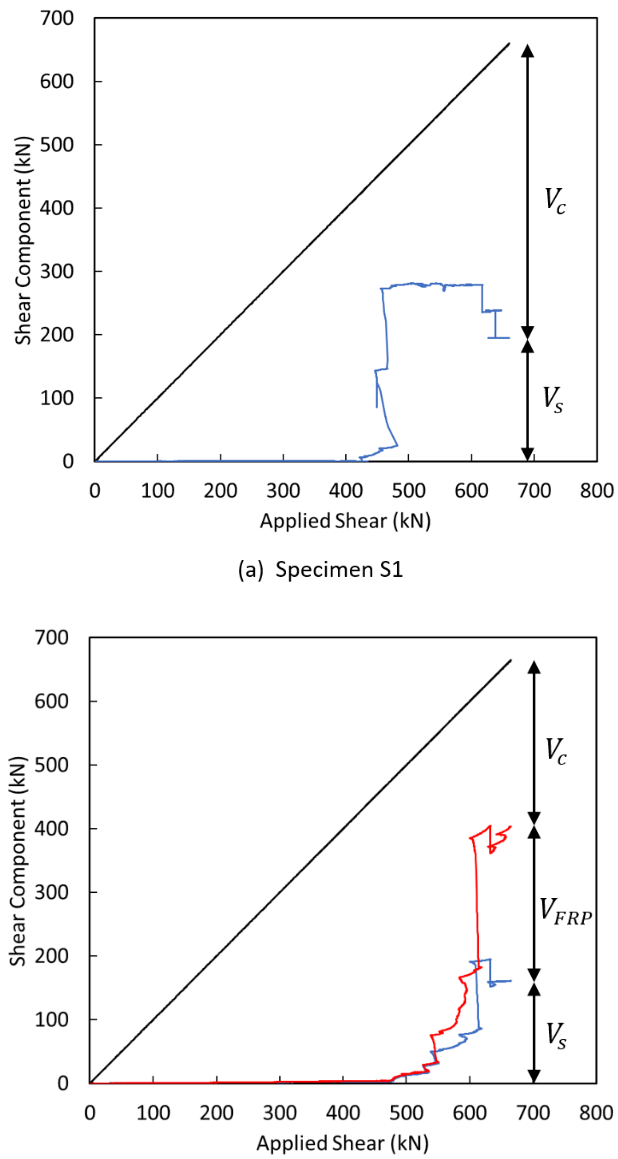

(a) Specimen S1
(b) Specimen S2
(c) Specimen S3
(d) Specimen S4

Figure 3.16: Components of shear resistance

3.5 FRP Pull-Off Test Results

Pull-off strength tests were performed on samples of the FRP strips which had been applied to unstressed regions of the girders at the same time that the CFRP strips were applied. The additional FRP required for these tests was applied to the end-regions and between the two loading points. Five tests per specimen were conducted for a total of 15 tests. Testing was performed using the Elcometer 106/6 concrete coatings tester shown in Figures 3.17 and 3.18 and was in compliance with the ASTM D7522/D7522M-15 (2015) standard test method.

Figure 3.17: Elcometer 106/6 adhesion tester for coatings on concrete (courtesy of Elcometer Inc.)

Figure 3.18: Elcometer 106/6 in use on specimen S2

The tests were conducted after load testing of the specimens had already occurred. This adhesion tester works via a ratchetting wrench which must be rotated at approximately 30 sec/turn in order to achieve the 1 MPa/min requirement of the ASTM standard. The dollies or pucks used were 50 mm in diameter and were adhered to the FRP surface using epoxy. The surface of the FRP was first roughened with a medium-grit sandpaper and then a 50 mm diameter wet-cut hole saw was used to score the FRP and concrete to a depth of approximately 10 mm. A steel ring was provided with the adhesion tester to place between the tester feet and FRP in order to ensure that all three feet of the tester were firmly placed. The test was then conducted and the results read off of the MPa scale printed on the tester body.

All the tests were evaluated based on their observed failure mode as illustrated in Figure 3.19. Observations of the dollies after pull-off testing indicated failure modes F and G exclusively. Three of the tests showed failure mode F and had an between 50 - 80 % failure in the concrete substrate. An example of a tested dolly and scored hole are shown in Figure 3.20. The results of the pull-off adhesion tests are presented in Table 3.1.

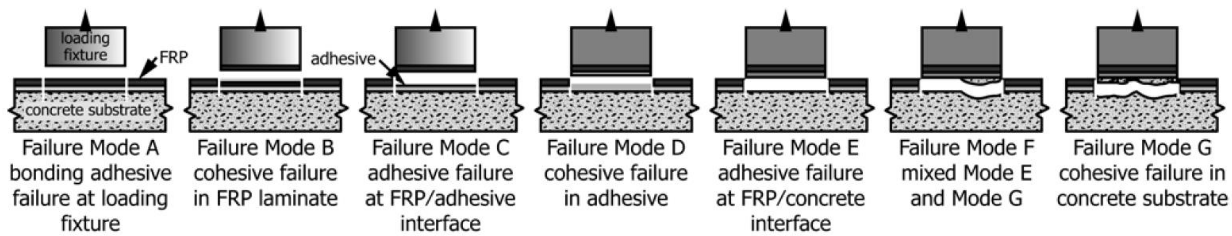

Figure 3.19: Possible pull-off test failure modes (ASTM D7522/D7522M-15, 2015)

Figure 3.20: Dollies with bonded concrete and tested section of FRP-concrete bond showing failure in concrete substrate

Table 3.1: Pull-off bond test results

Specimen	Average Pull-Off Strength (MPa)	Standard Deviation (MPa)	Coefficient of Variation (%)
S2	2.138	0.314	14.7
S3	1.400	0.324	23.1
S4	1.210	0.263	21.7

The evaluation of pull-off test result depends highly on the application and engineering requirements. Typically, a pull-off strength of between 1.0 and 1.5 MPa is required. Specimen S2 had a greater pull-off strength of 2.14 MPa, while specimens S3 and S4 exhibit resistances within the range of acceptable pull-off strengths. The results show that girder 2 had on average lower pull-off strength than girder 1. This result is contrary to the measured concrete compressive strengths which was lower for girder 1 (40.7 MPa) than girder 2 (44.2 MPa). This reduction in pull-off strength could be due to the surface preparation technique used. Bush-hammering could possibly induce micro-cracks in the concrete substrate which could possible reduce the pull-off strength. Surface preparation techniques deserve additional research consideration as does the analysis of different testing techniques which could possible correlate better with the bond strength of FRP-concrete interfaces in shear.

4 Analyses and Comparisons

4.1 Shear Resistance Predicted Using 2014 Canadian Highway Bridge Design Code

The nominal shear resistance was determined using the general method of the Canadian Highway Bridge Design Code (CSA S6-14, 2014). This design approach has its basis in the Modified Compression Field Theory (Bentz & Collins, 2006; Collins et al., 1996). The critical shear section was located at a distance equal to the effective shear depth (d_v) from the inner face of the support. This effective shear depth was taken as 90 % of the effective depth (d) of the tension reinforcement.

4.1.1 Sectional Shear Design

In determining the nominal shear resistance, an iterative approach was required since the value of the applied shear appears in the expression for the longitudinal strain, ε_x. For these predictions the nominal resistances have been used (material resistance factors taken as 1.0). The steps are as follows:

(1) Assume a value for nominal shear resistance (V_n)

(2) Evaluate the expression for the longitudinal strain (ε_x)

$$\varepsilon_x = \frac{M_n/d_v + V_n - A_{ps}f_{po}}{2(E_sA_S + E_pA_p)}$$

where M_n is the moment at the critical shear section corresponding to V_n, A_s is the area of reinforcing steel, A_{ps} is the area of prestressing steel, E_s is the steel elastic modulus, E_p is the prestressing steel elastic modulus and f_{po} is the stress in the prestressing steel when the stress in the surrounding concrete is zero.

(3) Calculate the factor which accounts for the shear resistance of the cracked concrete (β) for the member which contains at least the minimum transverse reinforcement required by Clause 8.9.1.3

$$\beta = \frac{0.4}{1 + 1500\varepsilon_x}$$

(4) Calculate the angle of principal compression (θ)

$$\theta = 29 + 7000\varepsilon_x$$

(5) Calculate the nominal shear resistance provided by the diagonally cracked concrete (V_c)

$$V_c = \beta\sqrt{f_c{}'}b_v d_v$$

where $f_c{}'$ is the concrete compressive strength, b_v is the effective web width (150 mm for these girders) and d_v is taken as the greater of 0.72 times the member height and 0.9 times the effective depth of the tension reinforcement.

(6) Calculate the nominal shear resistance provided by the vertical steel stirrups (V_s)

$$V_s = \frac{f_y A_v d_v \cot\theta}{s}$$

where s is the stirrup spacing

(7) Calculate the nominal shear resistance

$$V_n = V_c + V_s + V_{FRP}$$

where V_c is the concrete contribution, V_s is the steel contribution and V_{FRP} is the FRP contribution to shear resistance.

(8) Compare this value of V_n with the value assumed in step (1) and revise the assumed value until the solution converges

4.1.2 FRP Shear Contribution

The nominal shear resistance provided by the FRP strips was determined using the method given in Clause 16.11.3.2 of the Canadian Highway Bridge Design Code (CSA S6-14, 2014). This design approach is based on the developments in ACI 440.2R-08 (2008). A description of the relevant variables is given below.

ϕ_{FRP} = Resistance factor for the FRP composite = 0.75 x 0.80 = 0.60 for hand-layup of externally bonded CFRP. Note that to obtain the nominal resistance, this factor was taken as 1.0.

E_{FRP} = Modulus of elasticity of the FRP composite (MPa)

E_{FRPe} = Effective strain in the FRP (mm/mm)

A_{FRP} = Area of cross-section of the FRP composite including both sides of the girder (mm^2)

d_{FRP} = Effective shear depth of the FRP composite (mm). Note that for these calculations, this was taken as 600 mm which is the clear height of the web.

θ = Angle of inclination of the principal diagonal compressive stress to the longitudinal axis of the member (degrees)

s_{FRP} = Spacing of externally-bonded FRP sheets (mm)

t_{FRP} = Thickness of FRP sheets (mm)

f_{FRPu} = Ultimate stress in the FRP (MPa)

The procedure for determining the shear contribution of the FRP sheets is as follows:

(1) Determine the concrete strength factor (k_1)

$$k_1 = \left(\frac{f_c'}{27}\right)^{2/3}$$

(2) Determine the effective anchorage length of the FRP sheets (L_e)

$$L_e = \frac{23300}{(t_{FRP}E_{FRP})^{0.58}}$$

(3) Determine the FRP bond configuration factor (k_2)

$$k_2 = \frac{d_{FRP} - L_e}{d_{FRP}}$$

(4) Determine the ultimate strain in the FRP (ε_{FRPu})

$$\varepsilon_{FRPu} = \frac{f_{FRPu}}{E_{FRP}}$$

(5) Determine the bond-reduction coefficient (κ_v)

$$\kappa_v = \frac{k_1 k_2 L_e}{11900\varepsilon_{FRPu}} \leq 0.75$$

(6) Determine the effective strain in the FRP (ε_{FRPe})

$$\varepsilon_{FRPe} = \kappa_v \varepsilon_{FRPu} \leq 0.004$$

For fully wrapped sections, $\varepsilon_{FRPe} = 0.004 \leq 0.75\varepsilon_{FRPu}$

(7) Calculate the cross-sectional area of the FRP sheets including both sides of the girder (A_{FRP})

$$A_{FRP} = 2w_{FRP}t_{FRP}$$

(8) Calculate the nominal shear contribution of the FRP composite (V_{FRP})

$$V_{FRP} = \frac{\Phi_{\mathrm{FRP}}E_{FRP}\varepsilon_{FRPe}A_{FRP}d_{FRP}(\cot\theta + cot\alpha)\sin\alpha}{s_{FRP}}$$

4.1.3 Comparison of Predictions with Experimental Results

4.1.3.1 Rectangular Beams

Figure 4.1 compares the experimentally determined shear strengths of the control specimen and specimens U90S5-a, U90S5-b and W90S5 tested by Alzate et al. (2013) and discussed in further detail in Section 1.3.1. The shear strength predictions as determined using the CSA S6-14 (2014) – Canadian Highway Bridge Design Code are presented in the figure. For beams with U-wrapped FRP, the predicted effective strain limit (ε_{FRPe}) was less than 0.004 while for the fully wrapped beams it was taken as 0.004. This higher strain accounts for the improved anchorage of the fully wrapped beam and results in a higher predicted shear strength. The predicted values are reasonable estimates of the beam shear strengths.

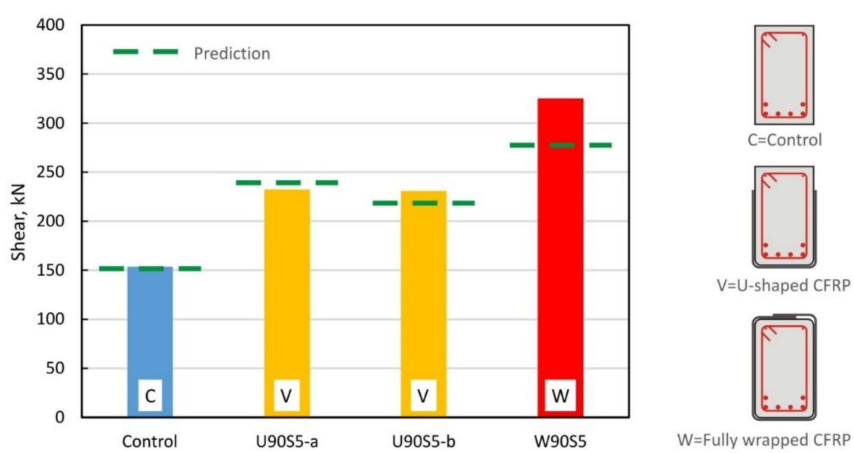

Figure 4.1: Rectangular beam experimental and predicted shear strengths as adapted from Alzate et al. (2013)

4.1.3.2 T-Beams

Figure 4.2 compares the experimentally determined shear strengths of the T-beams described in Section 1.3.2 as tested by Murphy (2010) and reported by Belarbi et al. (2011). The figure shows the beneficial effects of the horizontal anchorage with beam RC-12-S90-HA-PC having an increased shear strength when compared to the beams with no CFRP anchorage. Figure 4.2 also shows the shear strength predictions for the beams as per the CSA S6-14 (2014) code. These predictions are within 13 % of the experimentally determined shear strengths.

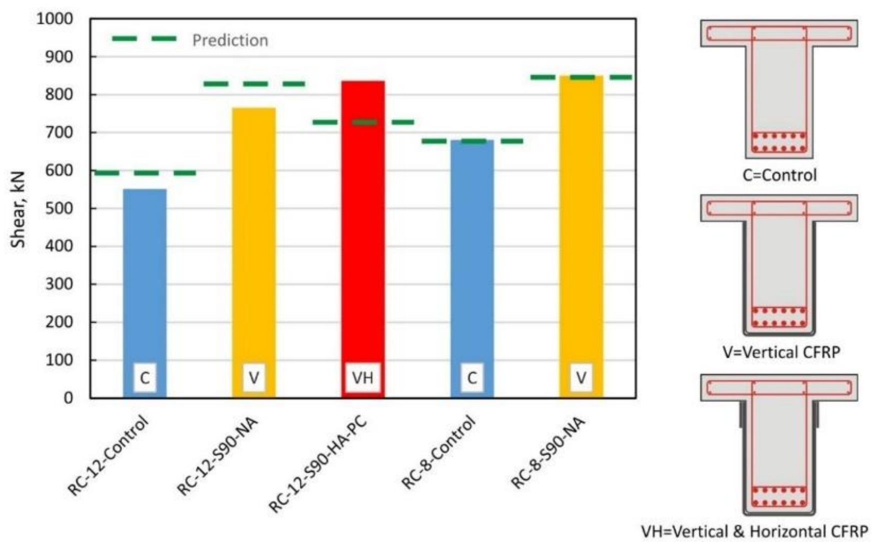

Figure 4.2: T-beam experimental and predicted shear strengths as adapted from Murphy (2010)

4.1.3.3 I-Girders

The I-girders described in Section 1.3.3, as tested and reported on by Kang and Ary (2012), Belarbi et al. (2011) and Kim et al. (2012) are illustrated in Figure 4.3 along with the results from this experimental program. The shear strengths reported in the figure are the ultimate shear strengths for the control specimens and FRP strengthened specimens. The results clearly show that the FRP shear strips did not result in a dependable increase in the ultimate shear strength of the full-scale I-girders. In some cases the strips can actually lead to a loss in strength.

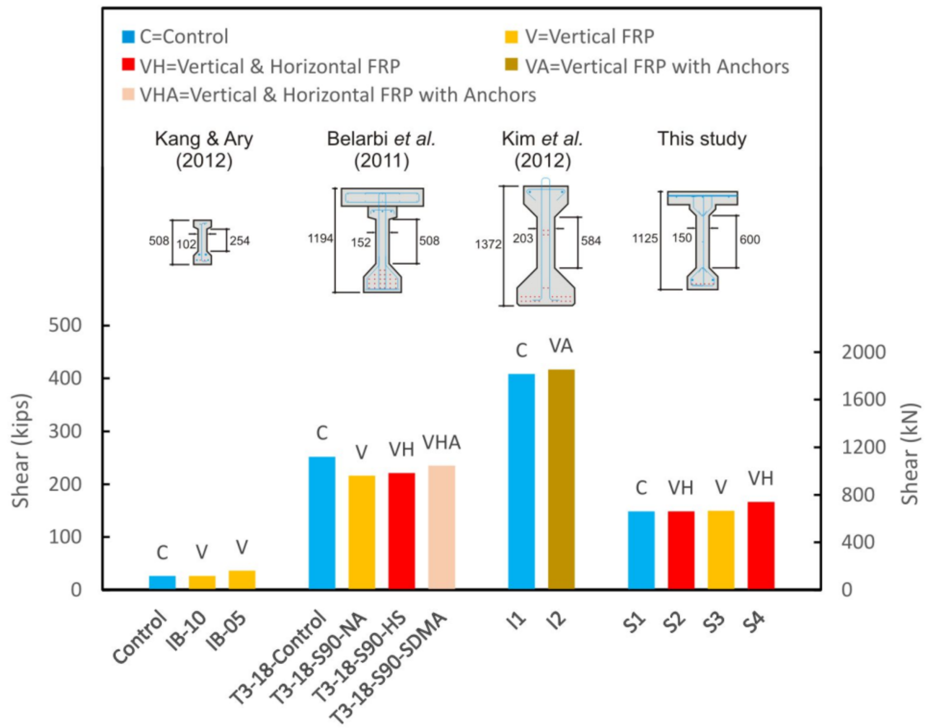

Figure 4.3: I-girder experimental shear strengths as adapted from Kang and Ary (2012), Belarbi et al. (2011) and Kim et al. (2012) compared with the test results from this study

Figure 4.4 compares the shear strength of the four I-girders described and tested as part of this experimental program. Whereas Figure 4.3 contains the shear strengths as obtained by the applied shear at failure of the specimens, Figure 4.4 shows a smaller failure shear of 458 kN for the control girder, specimen S1. At this shear, extremely large diagonal cracks had formed in the web resulting in general yielding of the web. The failure shears of the FRP strengthened girders resulted in increases of between 44 and 62 % in shear strength compared with the shear causing general yielding of the web in specimen S1. Specimen S2, with the more closely spaced FRP strips had the best crack control but lower shear strength than specimen S4 which was identical except for having a larger FRP strip spacing. Specimen S3 without the curved re-entrant corner transitions and horizontal anchorage strips behaved better than expected and was almost identical to specimen S4. Figure 4.4 also shows the shear strength predictions as determined using the provisions of the CSA S6-14 (2014) code. These provisions are shown to provide conservative predictions.

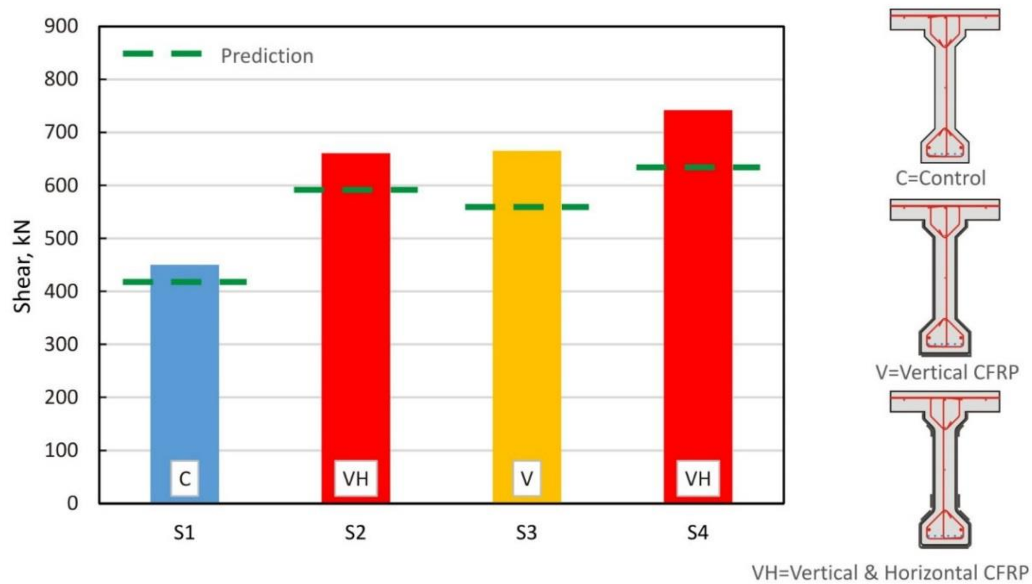

Figure 4.4: I-girder experimental and predicted shear strengths from this study

4.2 Shear Response Predicted Using Non-Linear Finite Element Analysis

An analysis of the test specimens was carried out using the 2D non-linear finite element software VecTor2. The program is based on the Modified Compression Field Theory (Vecchio & Collins, 1986) and uses a smeared rotating crack model. The analysis was carried out to investigate the web restraint provided by the presence of reinforced concrete flanges. The sectional design approach as discussed above is not capable of accounting for this effect. The 2-D non-linear finite element analysis accounted for effects such as tension stiffening and compression softening as well as using more detailed material properties.

4.2.1 Finite Element Model

FormWorks is the preprocessor software used to generate input files for the finite element analysis software VecTor2. The analysis models used for the experimental predictions were the default models as suggested by FormWorks and explained in the VecTor2 & FormWorks User's Manual (Wong et al., 2013).

The ductile steel reinforcement stress-strain response consisted of three parts, an initial linear-elastic portion, a yield plateau and a non-linear strain-hardening phase. The prestressing steel was modelled using a Ramsberg-Osgood formulation and had a stress-strain response consisting of a linear-elastic branch which transitioned to a second linear strain-hardening branch. The concrete was modelled using a parabola for the pre-peak compression response and the modified Park-Kent post-peak compression response which takes into account concrete confinement. All material property inputs were taken directly from the material property tests conducted as part of this experimental program.

Figure 4.5 shows an isometric view of the finite element model mesh for specimen S1 in which the different colours represent the different material types used in the model. One half of the girder was modelled with horizontal restraints applied at the midspan region. The longitudinal reinforcing and prestressing steel were modelled using discrete truss elements and assuming a perfect bond with the concrete. The rest of the steel reinforcement, including the 15M longitudinal bars in the slab, 10M longitudinal bars in the web, end-region reinforcement, perpendicular 15M bars in the slab and 10M stirrups were all modelled as smeared reinforcement. This meant that the reinforcement ratio for the different girder regions and in three directions (longitudinal, transverse and perpendicular) had to be determined. Also, the width of each portion of the girder (web, flanges, slab, etc.) had to be accounted for with a different material type. In total, 25 materials were used to represent the I-girder specimens as can be seen in Figure 4.6 in which each material is represented in a different colour.

Discrete truss elements were used to represent the externally bonded FRP and were bonded to the concrete surface using contact and link elements. These contact and link elements are different types of bond or interface elements. Using a bond stress-slip curve and knowing the surface area of contact between the FRP and concrete, they can represent the imperfect bond between the FRP and the concrete. The way these elements work is by connecting the concrete element nodes to the adjacent FRP element nodes via a bond element which allows for relative displacement, or slip, to take place. Using the constitutive relationship, bond stresses can be determined and the force transferred determined by multiplying by the bonded area. Two different bond elements were investigated. Both types as well as various bond stress-slip relationships and methods for determining the bonded surface area were used in the model and compared with the experimental results. Ultimately, it was decided that an in-depth calibration of this finite element model was beyond the scope of the research program. For the predictions described in this thesis, the externally bonded FRP was accounted for as a smeared reinforcement similarly to the steel stirrups. Ten material types containing smeared FRP were created for each portion of the girders and are coloured black in Figure 4.6.

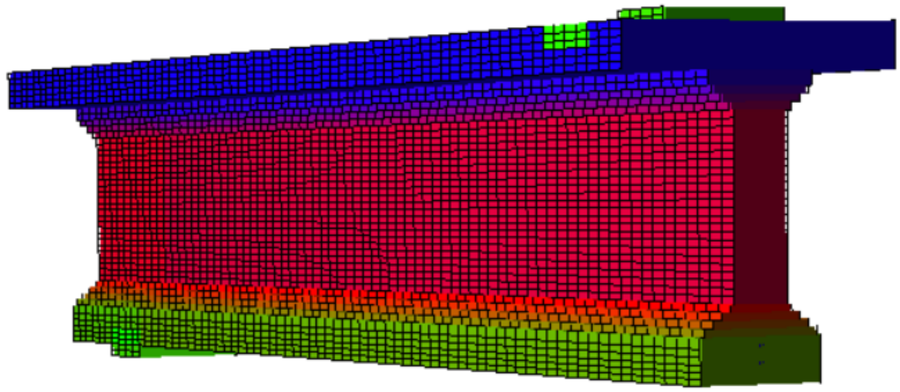

Figure 4.5: Isometric view of specimen S1 finite element mesh

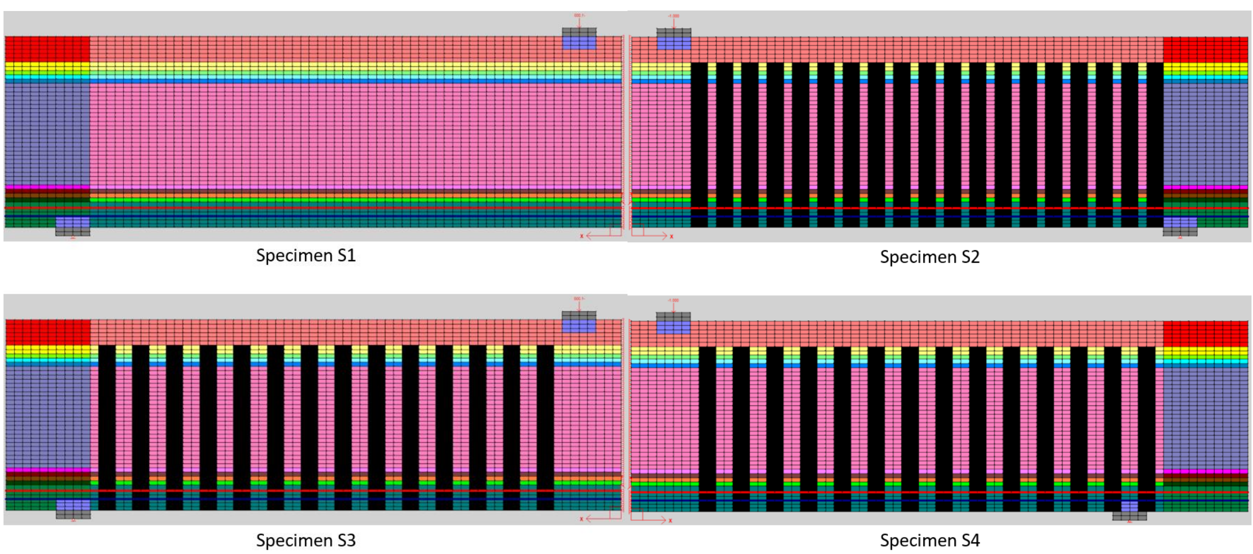

Figure 4.6: FormWorks finite element input mesh

4.2.2 Comparison with Experimental Results

For specimen S1, the finite element model produced a predicted shear capacity of 677 kN which was within 3 % of the actual shear capacity of 660 kN. This analysis accounts for the beneficial restraint of the web provided by the girder flanges. Figure 4.7 shows the deformed shape and crack pattern of specimen S1 at a shear of 660 kN. The deformation is magnified by a power of five and the red lines indicate crack directions with their thickness being proportional to predicted crack width. Both the actual girder and the analysis prediction show the bending of the top and bottom flanges in the region of significant diagonal tension.

Due to the fact that in the finite element model the FRP was assumed to be perfectly bonded to the concrete, and the fact that debonding of the FRP was observed in the testing of the specimens, it is unrealistic to predict a shear capacity for specimens S2, S3 and S4 based on the finite element model results without limiting the strain in the CFRP strips. The effective strain calculated in accordance with the CSA S6-14 code was used to limit the strain in the CFRP. This effective strain was 0.00342 and hence the maximum stress that could develop in the CFRP is $0.00342 \times 81897\ MPa = 280\ MPa$.

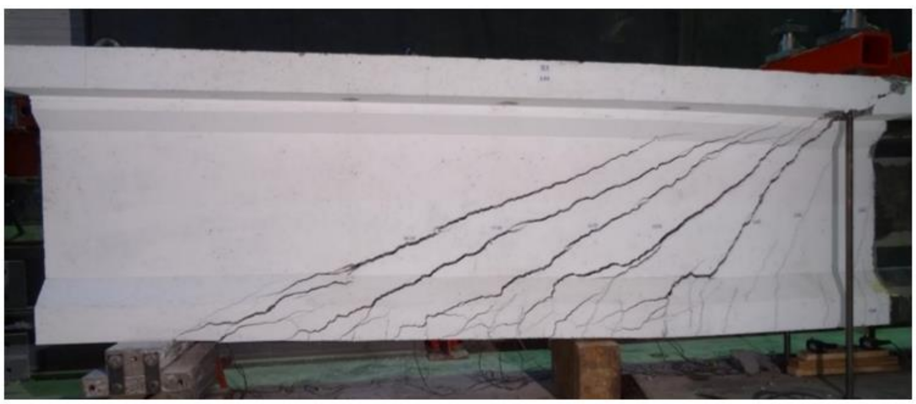

(a) Failure of specimen S1 at a shear of 660 kN

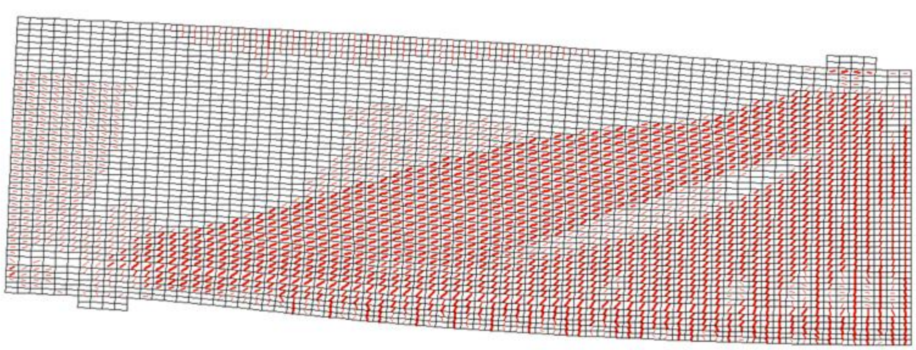

(b) Predicted deflected shape and crack pattern at a shear of 660 kN

Figure 4.7: Finite element prediction of the response of specimen S1

The shear-deflection responses predicted by the analysis follow the experimental results reasonably closely as can be seen in Figure 4.8. It is noted that the effective strain as determined using the CSA S6-14 code is for rectangular and T-shaped beams. For an I-girder this effective strain would be somewhat lower due to the shape of the cross-section and the debonding that would take place at the re-entrant corners. Hence, the maximum displacement would be somewhat less than that predicted as shown in Figure 4.8.

Prior to failure, the predictions closely match the experimental results, indicating that finite element analysis has the ability to accurately predict the response of I-girders strengthened in shear with externally bonded FRP. More work is needed in order to be able to accurately model the bond and to predict the debonding that occurs in I-girders. It is noted that there are two predicted shear-deflection curves for specimen S4 representing the original and shortened shear spans. The prediction using the long shear span is identical to that of specimen S3 as the horizontal anchorage strips which are the only difference between specimens S3 and S4 were not simulated in the finite element model.

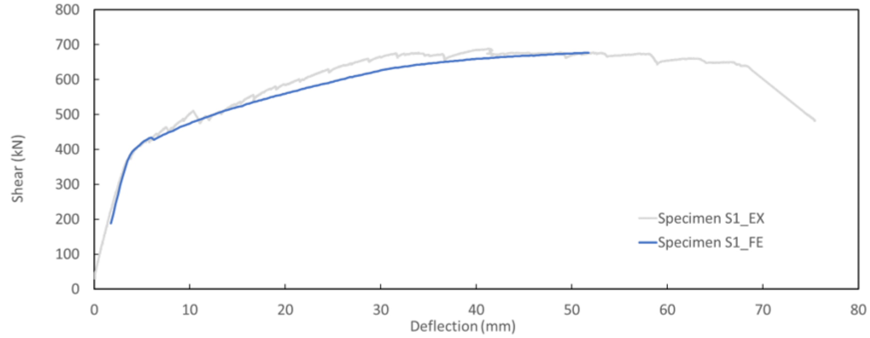

(a) Specimen S1

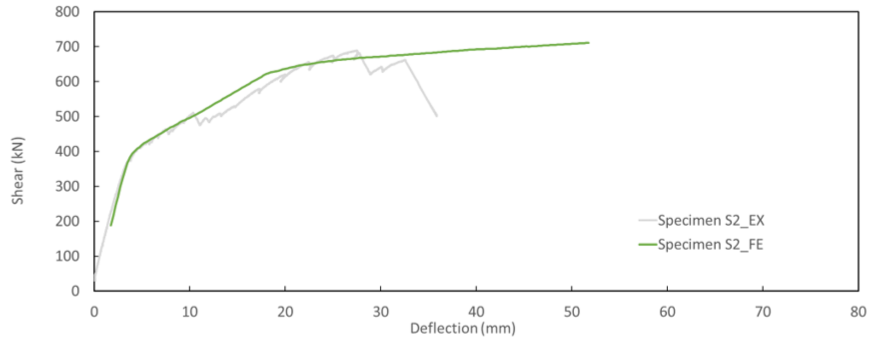

(b) Specimen S2

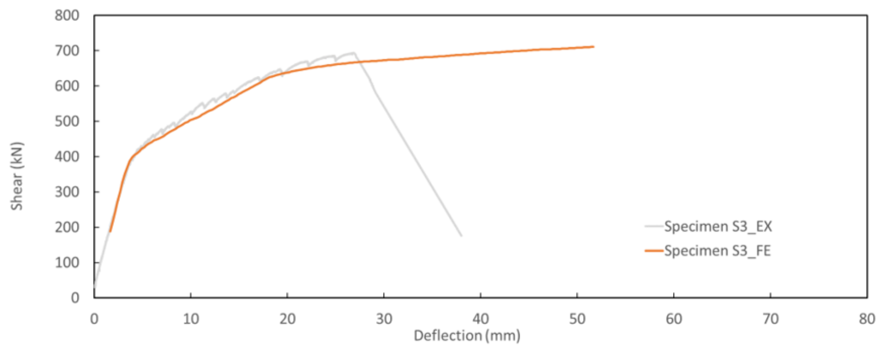

(c) Specimen S3

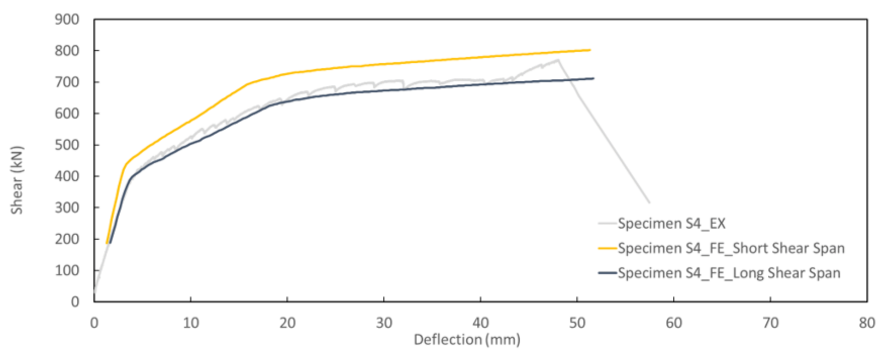

(d) Specimen S4

Figure 4.8: Comparison between finite element predictions and experimentally determined shear-displacement responses

4.3 Flexural Resistance Using Response 2000

The flexural resistance at midspan was determined using the Response 2000 (Bentz and Collins, 2015) sectional analysis program. This resulted in a predicted nominal flexural resistance of 2233 kN-m for girder 1. This corresponds to a maximum shear of 744 kN for a shear span of 3.0 m. Due to the higher concrete compressive strength, girder 2 had a predicted nominal flexural resistance of 2247 kN-m. In the testing of specimen S4, the shear span was reduced from 3.0 m to 2.7 m to avoid flexural failure. Recalculating to account for this reduced shear span, girder 2 had a maximum shear of 832 kN at flexural failure.

These values used a concrete compressive strength of 40.7 MPa and 44.2 MPa for girder 1 and 2, respectively and took into account the results of the material tests for the reinforcing steel and the prestressing steel material data provided by the manufacturer. The Response 2000 design input and analysis results for girder 1 are shown in Figure 4.9. Note that these results do not include the FRP shear strengthening. This type of analysis was also performed using assumed material properties at the girder design stage.

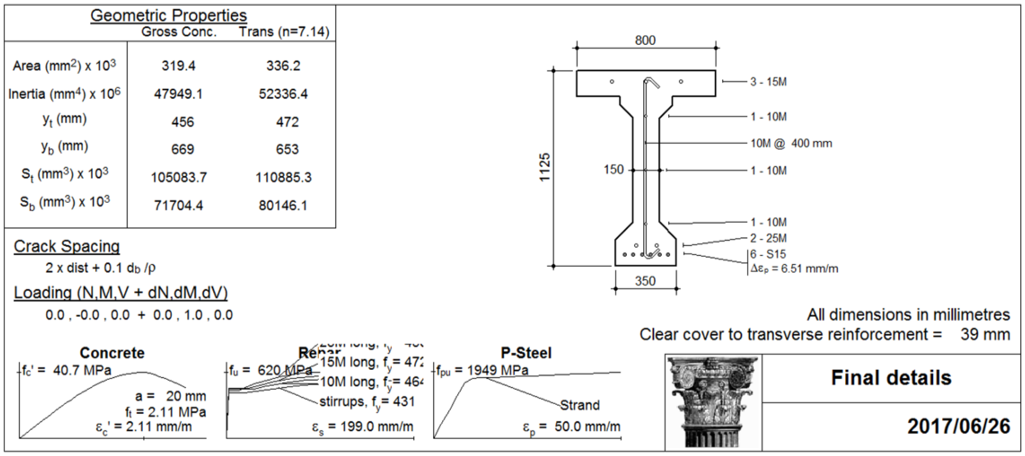

(a) Input data

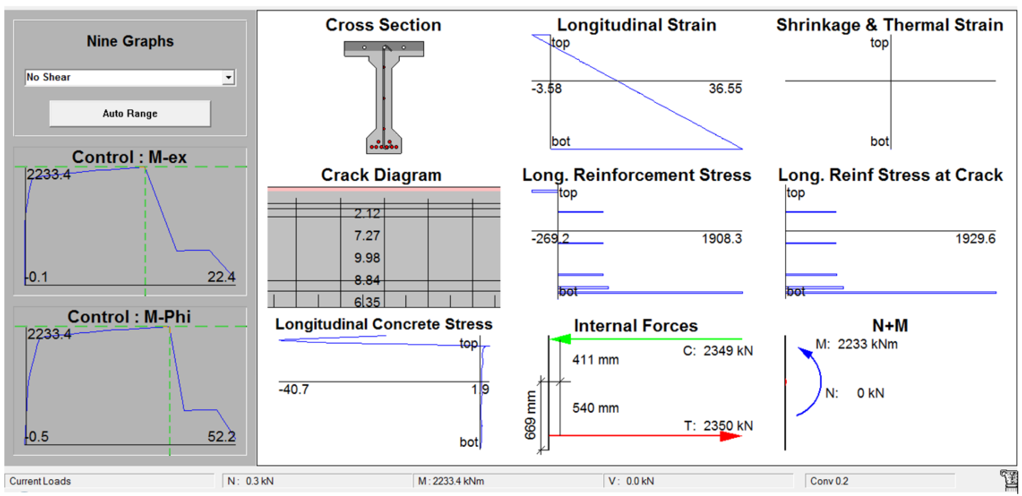

(b) Predicted response

Figure 4.9: Response 2000 predictions for girder 1

4.4 Analyzing the Effectiveness of External FRP Shear Strengthening

Table 4.1 below shows the predictions determined using the CHBDC (CSA S6-14, 2014) sectional analysis approach detailed in Section 4.1 and compares these values with the experimentally determined values. In this analysis, the critical section was taken at a distance from the inner edge of the support equal to the effective shear depth, d_v. The effective shear depth was taken as 0.9 times the effective depth, d of the tension reinforcement. Hence, $d_v = 0.9 \times 1025 = 922.5\ mm$. The effective shear depth of the FRP reinforcement, d_{FRP} was taken as the clear height of the web of the I-girder, 600 mm.

The predictions of the shear capacities, using the sectional design approach, are shown to be conservative. The design method as specified in the CSA S6-14 (2014) gives reasonable and conservative predictions of the shear components. It is apparent that for all the specimens and specimen S1 in particular, the concrete component is underestimated. A possible explanation for this is the significant role that the top and bottom flanges of the girder play in stiffening and restraining the web. This effect is not accounted for in the current shear design method. As shown in Figure 3.16 which shows the maximum shear crack width versus the applied shear, excessive web shear cracking began in specimen S1 at an applied shear of 458 kN, which is 10 % above the predicted nominal shear resistance of 418 kN. The sectional design approach can be said to provide a reasonable estimate for the load at which severe cracking and yielding of the stirrups occurs.

The shear strengthening of the I-girders with CFRP strips results in higher predicted shear capacities which in turn results in higher longitudinal strains, ε_x and therefore reduced concrete shear resistance components, V_c. The significant CFRP shear resistance component and energy stored in the CFRP strips before failure results in extremely brittle shear failures when anchorage of the strips is lost and debonding occurs. This is in contrast to conventional steel stirrups adequately anchored in the top and bottom flanges which are able to withstand extremely large strains before rupture.

4.4.1 Components of Shear Resistance

Table 4.1 compares the shear components at the maximum shear capacity. Specimen S2 with an FRP spacing of 150 mm and horizontal anchorage strips, has the highest V_{FRP} at 311 kN and the lowest values of V_s and V_c. It is noted that with the addition of FRP strips, the stirrups and concrete components are reduced. Specimen S4, when compared to specimen S2, has a lower value for V_{FRP} which is due to the larger FRP strip spacing at 200 mm, with both specimens having horizontal anchorage strips. The lowest V_{FRP} component of the three specimens that used FRP is specimen S3. Specimen S4, with its improved FRP anchorage due to the presence of horizontal anchorage strips has a higher V_{FRP} than specimen S3. This indicates that the horizontal anchorage improve the ability of the FRP to strengthen the girder in shear. Both specimen S3 and S4 had a 200 mm strip spacing.

Table 4.1 also shows the cracking shear for each of the specimens. The cracking shear is shown to increase as the amount of FRP is increased and the anchorage details are improved. Belarbi et al. (2011) and Kim et al. (2012) also observed this increase in cracking shear with the presence of FRP strips and with increasing amounts of FRP shear strips.

Table 4.1: Experimental and predicted shear resistance results

Specimen	Experimental Results					Predicted Results						
	V_{cr} kN	V_{test} kN	V_c kN	V_s kN	V_{FRP} kN	V_n kN	V_c kN	V_s kN	V_{FRP} kN	ε_x $\times 10^3$	θ deg.	β
S1	400	458* 660**	312* 465**	146* 195**	0	418	251	166	0	0.27	30.9	0.285
S2	415	661	212	138	311	592	142	137	312	0.991	35.9	0.161
S3	447	665	262	161	243	559	161	142	256	0.857	35	0.175
S4	467	742†	303	179	260	587	176	147	265	0.73	34.1	0.191

* Web general yielding due to development of significant inclined cracks in web

** Complete shear failure

† Shear span reduced to 2.7 m from 3.0 m

5 Conclusions

The following conclusions are based on the experimental results and predictions:

(1) The presence of externally bonded CFRP shear strips on the I-girder specimens significantly reduced the inclined crack widths and resulted in increased web shear strength.

(2) The experimentally and analytically determined components of shear resistance confirm that the shear carried by the CFRP shear strips is a significant portion of the total shear resistance.

(3) Complete loss of anchorage of the CFRP shear strips can result in an extremely brittle shear failure.

(4) The shape of the I-girders makes it difficult to properly anchor the vertical CFRP shear strips. The re-entrant corners in particular are a location where debonding is likely to occur.

(5) Curved epoxy putty transitions between the web and flanges at re-entrant corners, combined with the use of horizontal CFRP anchorage strips in these regions, helped to improve the anchorage of the CFRP shear strips.

(6) The I-girder webs are restrained by the stiffness of the top and bottom flanges after significant shear cracks develop. This restraint resulted in increased shear strength of the I-girders.

(7) Non-linear finite element analysis accounts for the beneficial effects of web restraint offered by the stiffness of the I-girder flanges. The sectional design approach is not capable of accounting for this restraint.

(8) The predictions using the CSA S6-14 design code provided conservative estimates of the shear strength of the I-girder webs with and without external CFRP strengthening.

(9) Pull-off strength of the FRP-concrete bond is not only dependent on the concrete tensile strength. Surface preparation has a significant role to play in bond strength.

References

ACI 440.2R-08. (2008). Guide for the Design and Construction of Externally Bonded FRP Systems for Strengthening Concrete Structures. American Concrete Institute Committee 440: Farmington Hills, MI, USA

ACI 440.R-07. (2007). Report on Fiber-Reinforced Polymer (FRP) Reinforcement for Concrete Structures. American Concrete Institute Committee 440: Farmington Hills, MI, USA

Alexander, J., & Cheng, J. J. R. (1998). *Shear Design Model of Concrete Girders Strengthened with Advanced Composite Materials.* Paper presented at the Proceedings of the Fifth International Conference on Short and Medium Span Bridges, Calgary, Canada.

Alzate, A., Arteaga, A., De Diego, A., Cisneros, D., & Perera, R. (2013). Shear strengthening of reinforced concrete members with CFRP sheets. Refuerzo externo a cortante con laminas de CFRP en elementos de hormigon armado. *Materiales de Construccion, 63*(310), 251-265. doi:10.3989/mc.2012.06611

ASTM A416/A416M-12. (2012). Standard Specification for Low-Relaxation, Seven-Wire Steel Strand for Prestressed Concrete. ASTM International: West Conshohocken, PA, USA

ASTM A615/A615M-16. (2016). Standard Specification for Deformed and Plain Carbon-Steel Bars for Concrete Reinforcement. ASTM International: West Conshohocken, PA, USA

ASTM D7522/D7522M-15. (2015). Standard Test Method for Pull-Off Strength for FRP Laminate Systems Bonded to Concrete Substrate. ASTM International: West Conshohocken, PA, USA

Belarbi, A., Ayoub, A., Kuchma, D., Mirmiran, A., & Okeil, A. (2011). *NCHRP Report 678 - Design of FRP Systems for Strengthening Concrete Girders in Shear*. Transportation Research Board: Washington D.C.

Bentz, E. C., & Collins, M. P. (2006). Development of the 2004 Canadian Standards Association (CSA) A23.3 shear provisions for reinforced concrete. *Canadian Journal of Civil Engineering, 33*(5), 521-534. doi:10.1139/L06-005

Bentz, E.C. and Collins, M.P. (2015). http://www.ecf.utoronto.ca/~bentz/r2k.htm. Response-2000 webpage. Last Accessed: 14/08/18.

Chen, J. F., & Teng, J. G. (2001). Anchorage strength models for FRP and steel plates bonded to concrete. *Journal of Structural Engineering, 127*(7), 784-791. doi:10.1061/(ASCE)0733-9445(2001)127:7(784)

CIRC. (2016). *Canadian Infrastructure Report Card*. http://www.canadianinfrastructure.ca. Last accessed: 14/08/18

Collins, M. P., Mitchell, D., Adebar, P., & Vecchio, F. J. (1996). General shear design method. *ACI Structural Journal, 93*(1), 36-45.

CSA A23.2-8C-14. (2014). Flexural Strength of Concrete (Using a Simple Beam with Third Point Loading). Canadian Standards Association: Rexdale, ON, Canada

CSA A23.2-9C-14. (2014). Compressive Strength of Cylindrical Concrete Specimens. Canadian Standards Association: Rexdale, ON, Canada

CSA A23.2-12C-14. (2014). Making, Curing and Testing Compressive Test Specimens. Canadian Standards Association: Rexdale, ON, Canada

CSA A23.2-13C-14. (2014). Splitting Tensile Strength of Cylindrical Concrete Specimens. Canadian Standards Association: Rexdale, ON, Canada

CSA A23.3-94. (1994). Design of Concrete Structures. Canadian Standards Association: Rexdale, ON, Canada

CSA G30.18-09. (2009). Billet-Steel Bars for Concrete Reinforcement. Canadian Standards Association: Mississauga, ON, Canada

CSA S6-14. (2014). Canadian Highway Bridge Design Code. Canadian Standards Association: Mississauga, ON, Canada

Deniaud, C., & Cheng, J. J. R. (2001). Shear behavior of reinforced concrete T-beams with externally bonded fiber-reinforced polymer sheets. *ACI Structural Journal, 98*(3), 386-394.

Deniaud, C., & Cheng, J. J. R. (2003). Reinforced concrete T-beams strengthened in shear with fiber reinforced polymer sheets. *Journal of Composites for Construction, 7*(4), 302-310. doi:10.1061/(ASCE)1090-0268(2003)7:4(302)

Deniaud, C., & Cheng, J. J. R. (2004). Simplified shear design method for concrete beams strengthened with fiber reinforced polymer sheets. *Journal of Composites for Construction, 8*(5), 425-433. doi:10.1061/(ASCE)1090-0268(2004)8:5(425)

fib Bulletin 14. (2001). Externally Bonded FRP Reinforcement for RC Structures. International Federation for Structural Concrete (*fib*) Task Group 9.3: Lausanne, Switzerland

Ghorbani, M., Mostofinejad, D., & Hosseini, A. (2017). Experimental investigation into bond behavior of FRP-to-concrete under mixed-mode I/II loading. *Construction and Building Materials, 132*, 303-312. doi:10.1016/j.conbuildmat.2016.11.057

Horiguchi, T., & Saeki, N. (1997). Effect of test methods and quality of concrete on bond strength of CFRP sheet. *Proceedings of the Third International Symposium on Non-Metallic (FRP) Reinforcement for Concrete Structures, 1*, 265-270.

Hutchinson, R., Tadros, G., Kroman, J., & Rizkalla, S. (2003). *Use of Externally Bonded FRP Systems for Rehabilitation of Bridges in Western Canada.* Paper presented at the Field Applications of FRP Reinforcement: Case Studies. Farmington Hills, MI, USA.

Iovinella, I., Prota, A., & Mazzotti, C. (2013). Influence of surface roughness on the bond of FRP laminates to concrete. *Construction and Building Materials, 40*, 533-542. doi:10.1016/j.conbuildmat.2012.09.112

Kamel, A. S., Elwi, A. E., & Cheng, R. J. J. (2006). Experimental study on the behavior of carbon fiber reinforced polymer sheets bonded to concrete. *Canadian Journal of Civil Engineering, 33*(11), 1438-1449. doi:10.1139/L06-039

Kang, T. H. K., & Ary, M. I. (2012). Shear-strengthening of reinforced prestressed concrete beams using FRP: Part II - Experimental investigation. *International Journal of Concrete Structures and Materials, 6*(1), 49-57. doi:10.1007/s40069-012-0005-0

Khalifa, A., Gold, W. J., Nanni, A., & Aziz, A. M. I. (1998). Contribution of externally bonded FRP to shear capacity of RC flexural members. *Journal of Composites for Construction, 2*(4), 195-202. doi:10.1061/(ASCE)1090-0268(1998)2:4(195)

Kim, Y., Quinn, K., Satrom, N., Garcia, J., Sun, W., Ghannoum, W. M., & Jirsa, J. O. (2012). Shear Strengthening of Reinforced and Prestressed Concrete Beams Using Carbon Fiber

Reinforced Polymer (CFRP) Sheets and Anchors. Technical Report No. FHWA/TX-12/0-6306-1. Center for Transportation Research, Austin, TX, USA

Labossière, P., Neale, K. W., Rochette, P., Demers, M., Lamothe, P., Lapierre, P., & Desgagné, G. (2000). Fibre reinforced polymer strengthening of the Sainte-Émélie-de-l'Énergie bridge: design, instrumentation, and field testing. *Canadian Journal of Civil Engineering, 27*(5), 916-927.

Liu, K. (2014). *Influence of surface preparation on bond performance of externally-bonded FRP to concrete interfaces.* Paper presented at the 3rd International Conference on Advanced Engineering Materials and Architecture Science, ICAEMAS 2014, July 26, 2014 - July 27, 2014, Huhhot, China.

Loov, R., & Peng, L. (1998). The influence of concrete strength on shear friction based design of reinforced concrete beams. *Proceedings of the International Conference on HPHSC*, Perth, Australia, 505-519

Loov, R. E. (1998). Review of A23.3-94 simplified method of shear design and comparison with results using shear friction. *Canadian Journal of Civil Engineering, 25*(3), 437-450.

Lu, X. Z., Teng, J. G., Ye, L. P., & Jiang, J. J. (2005a). Bond-slip models for FRP sheets/plates bonded to concrete. *Engineering Structures, 27*(6), 920-937. doi:10.1016/j.engstruct.2005.01.014

Lu, X. Z., Ye, L. P., Teng, J. G., & Jiang, J. J. (2005b). Meso-scale finite element model for FRP sheets/plates bonded to concrete. *Engineering Structures, 27*(4), 564-575. doi:10.1016/j.engstruct.2004.11.015

Maeda, T., Asano, Y., Sato, Y., Ueda, T., & Kakuta, Y. (1997). *A Study on Bond Mechanism of Carbon Fiber Sheet.* Paper presented at the Proceedings of the Third International Symposium on Non-Metallic (FRP) Reinforcement for Concrete Structures, Japan.

Mostofinejad, D., & Mahmoudabadi, E. (2010). Grooving as alternative method of surface preparation to postpone debonding of FRP laminates in concrete beams. *Journal of Composites for Construction, 14*(6), 804-811. doi:10.1061/(ASCE)CC.1943-5614.0000117

Murphy, M. S. (2010). *Behavior of externally bonded fiber reinforced polymer systems for strengthening concrete girders in shear.* Ph.D. Dissertation, Missouri University of Science and Technology.

Perera, R., & Ruiz, A. (2012). Design equations for reinforced concrete members strengthened in shear with external FRP reinforcement formulated in an evolutionary multi-objective framework. *Composites Part B: Engineering, 43*(2), 488-496. doi:10.1016/j.compositesb.2011.10.013

Pham, H. B., Al-Mahaidi, R., & Saouma, V. (2006). Modelling of CFRP-concrete bond using smeared and discrete cracks. *Composite Structures, 75*(1-4), 145-150. doi:10.1016/j.compstruct.2006.04.039

Priestley, M. J. N., Seible, F., & Calvi, G. M. (1996). *Seismic Design and Retrofit of Bridges*. John Wiley & Sons, Inc: New York, NY, USA

Sun, W., Peng, X., Liu, H., & Qi, H. (2017a). Numerical studies on the entire debonding propagation process of FRP strips externally bonded to the concrete substrate. *Construction and Building Materials, 149*, 218-235. doi:10.1016/j.conbuildmat.2017.05.117

Sun, W., Peng, X., & Yu, Y. (2017b). Development of a simplified bond model used for simulating FRP strips bonded to concrete. *Composite Structures, 171*, 462-472. doi:10.1016/j.compstruct.2017.03.066

Triantafillou, T. C. (1998). Shear strengthening of reinforced concrete beams using epoxy-bonded FRP composites. *ACI Structural Journal, 95*(2), 107-115.

Triantafillou, T. C., & Antonopoulos, C. P. (2000). Design of concrete flexural members strengthened in shear with FRP. *Journal of Composites for Construction, 4*(4), 198-205. doi:10.1061/(ASCE)1090-0268(2000)4:4(198)

Tudjono, S., Ay Lie, H., Hidayat, A., & Purwanto. (2017). *Experimental Study on the Concrete Surface Preparation Influence to the Tensile and Shear Bond Strength of Synthetic Wraps.* Paper presented at the 3rd International Conference on Sustainable Civil Engineering Structures and Construction Materials, SCESCM 2016, September 5, 2016 - September 7, 2016, Bali, Indonesia.

Ueda, T., & Dai, J. (2005). Interface bond between FRP sheets and concrete substrates: Properties, numerical modeling and roles in member behaviour. *Progress in Structural Engineering and Materials, 7*(1), 27-43. doi:10.1002/pse.187

Vecchio, F. J., & Collins, M. P. (1986). Modified compression-field theory for reinforced concrete elements subjected to shear. *Journal of the American Concrete Institute, 83*(2), 219-231.

Vecchio, F.J., 2017, http://www.civ.utoronto.ca/vector, VecTor2 webpage. Last accessed: 13/09/17

Wong, P. S., Vecchio, F. J., & Trommels, H. (2013). VecTor2 & FormWorks User's Manual, Second Edition

Wu, Z., Islam, S. M., & Said, H. (2009). A three-parameter bond strength model for FRP-concrete interface. *Journal of Reinforced Plastics and Composites, 28*(19), 2309-2323. doi:10.1177/0731684408091961

Yao, J., Teng, J. G., & Chen, J. F. (2005). Experimental study on FRP-to-concrete bonded joints. *Composites Part B: Engineering, 36*(2), 99-113. doi:10.1016/j.compositesb.2004.06.001

Yuan, H., Teng, J. G., Seracino, R., Wu, Z. S., & Yao, J. (2004). Full-range behavior of FRP-to-concrete bonded joints. *Engineering Structures, 26*(5), 553-565. doi:10.1016/j.engstruct.2003.11.006